THE DEPTH DISTRIBUTION OF ORGANIC CARBON IN MINERAL CRYOSOLS AT TWO SITES IN THE CANADIAN ARCTIC

A Thesis Submitted to the College of

Graduate Studies and Research

in Partial Fulfillment of the Requirements

for the degree of Master of Science

in the Department of Soil Science

University of Saskatchewan

Saskatoon

By

Marcus R Phillips

PERMISSION TO USE

In presenting this thesis in partial fulfillment of the requirements for a Postgraduate degree from the University of Saskatchewan, I agree that the Libraries of this University may make it freely available for inspection. I further agree that permission for copying of this thesis in any manner, in whole or in part, for scholarly purposes may be granted by the professor or professors who supervised my thesis work or, in their absence, by the Head of the Department or the Dean of the College in which my thesis work was done. It is understood that any copying or publication or use of this thesis or parts thereof for financial gain shall not be allowed without my written permission. It is also understood that due recognition shall be given to me and to the University of Saskatchewan in any scholarly use which may be made of any material in my thesis.

DISCLAIMER

Reference in this thesis to any specific commercial products, process, or service by trade name, trademark, manufacturer, or otherwise, does not constitute or imply its endorsement, recommendation, or favouring by the University of Saskatchewan. The views and opinions of the author expressed herein do not state or reflect those of the University of Saskatchewan, and shall not be used for advertising or product endorsement purposes.

Requests for permission to copy or to make other uses of materials in this thesis in whole or part should be addressed to:
Head of the Department of Soil Science
51 Campus Dr
University of Saskatchewan
Saskatoon, Saskatchewan, Canada
S7N 5A8

ABSTRACT

The northern circumpolar permafrost region covers over 15% of the earth's land surface, and contains about 50% of global belowground organic carbon (OC). There has been a great deal of recent interest in cataloguing the distribution of organic carbon in these soils, as the Arctic is expected to experience particularly large warming in the coming century, which has potential to cause a release of carbon to the atmosphere and lead to a substantial positive feedback to warming. Despite this concern, little work has been done to elucidate the depth distribution of organic carbon in mineral Cryosols (permafrost-affected soils).

In this study, selected mineral Cryosols at Truelove Lowland, Devon Island, Nunavut and near Wright Pass, Yukon were examined. The depth distribution of OC in soils affected by cryoturbation (Turbic Cryosols) and soils not affected by cryoturbation (Static Cryosols) was compared using high depth-resolution GIS-based methods. Density of OC at Truelove Lowland ranged from 185 g OC m^{-2} cm^{-1} (1 g OC m^{-2} cm^{-1} = 0.1 kg OC m^{-3}) near the surface to 28 g OC m^{-2} cm^{-1} at 90 cm depth in Turbic Cryosols and 178 g OC m^{-2} cm^{-1} near the surface to 11 g OC m^{-2} cm^{-1} at 25 cm depth in Static Cryosols. At Wright Pass, OC density ranged from 334 g OC m^{-2} cm^{-1} near the surface to 110 g OC m^{-2} cm^{-1} at 46 cm depth in Turbic Cryosols and 330 g OC m^{-2} cm^{-1} near the surface to 29 g OC m^{-2} cm^{-1} at 70 cm depth in Static Cryosols. When depth distribution was compared, it was found that Turbic Cryosols contain up to 125 g OC m^{-2} cm^{-1} more OC at depths of 20 to 45 cm at Truelove Lowland and up to 148 g OC m^{-2} cm^{-1} more OC at depths of 12 to 90 cm at Wright Pass. The high depth-resolution method employed in this study can determine OC content for any selected depth range, and could be employed with existing databases of OC to provide vertically-resolved measures of OC.

Several existing models of cryoturbation processes were evaluated using data from this study. Soil movement by diapirism or cryohydrostatic movement is an unlikely explanation for the development of cryoturbation features in examined soil. Cryostatic movement and differential frost heave processes, however, are possible explanations for the development of some cryoturbation features. Some evidence suggests that transport of OC in a dissolved state may be important in the genesis of cryoturbation forms.

Additionally, several Turbic Cryosol pedons were selected as representative with respect to soil morphology and presumed cryogenesis and were examined using carbon:nitrogen ratio and nuclear magnetic resonance spectroscopy to explore OC quality. In all near-surface samples from all pedons examined there was a high proportion of O-alkyl carbon (range from 58.5 to 60.2 %) and a high O-alkyl carbon to alkyl carbon ratio (range from 2.3 to 2.6). Near-surface OC in examined soils was labile compared to that of temperate ecosystems; however a high arctic nonsorted circle had similar OC lability and degree of humification at depth and near the soil surface (O-alkyl to alkyl carbon ratios of 3.0 and 2.6 and carbon to nitrogen ratios of 16.5 and 16.6, respectively), while a low arctic earth hummock had chemically transformed OC at depth (O-alkyl carbon contents of 39.0 and 60.2% and O-alkyl to alkyl carbon ratios of 0.8 and 2.4, respectively). These results are unreplicated, but highlight the need for further study of OC quality amongst different modes of cryoturbation and different cryoturbation-related landforms.

ACKNOWLEDGEMENTS

First and most importantly I thank my partner Tara, who has been with me every step of the way. She has demonstrated phenomenal patience and unrelenting support and dedication to me. To you, Tara, I owe everything.

Next, I thank my supervisor Dr. Angela Bedard-Haughn for her patience, flexibility, guidance, and support. She is the model of a superb supervisor, and I am proud to be associated with her.

My gratitude goes to the members my advisory committee, Drs. Darwin Anderson, Dan Pennock, and Steve Siciliano for the guidance they provided to me through the development of this thesis. My committee was an impressive repository of expertise, and I can think of few people who could have improved the committee beyond these respected experts. I also thank Dr. Alec Aitken for his contribution as external examiner.

I also wish to recognize the contributions of Drs. Carissa Brown and Eric Lamb, as well as Jayme Viglas and Martin Brummell, who helped me in the field even though the labour was difficult and they were not obligated to do so. Furthermore, these people helped to keep the fieldwork fun and entertaining; the importance of which cannot be overstated. Significant contributions were also provided by Heather Crossman and Larisa Barber who helped me in the lab. I gratefully acknowledge many members and hangers-on, both past and present, of the Applied Pedology Lab who provided comments on my written work for this thesis including Samiran Banerjee, Louis Comeau, Catlan Dallaire, Hannah Konschuh, Zaho Matheos, Amanda Mycock, Dr. Maxime Paré, Amy Sangster, Lori Truba, Dr. Valerie Viaud, and Brian Wallace.

I also wish to acknowledge the support of all of my friends and family whom I have not already mentioned, particularly Martin and Margaret Phillips, Nancy and Gordon Vaxvick, Sean Sinclair and Allison Fairbairn, and Corey Kalynuk. Without these people, the last few years would have been much more difficult.

Funding for this research was provided by the NSERC Discovery Program, the Canadian International Polar Year Program, the Northern Scientific Training Program, and the Polar Continental Shelf Project. Facilities for research were provided by the Department of Soil Science at the University of Saskatchewan and the Klondike Region branch of Yukon Parks. Marcus Phillips was supported by an NSERC CGS-M, a University of Saskatchewan College of Graduate Studies and Research Dean's Scholarship, a University of Saskatchewan Graduate Teaching Fellowship, a Department of Soil Science Scholarship, a Dollie Hantelman Scholarship, and a Pederson Family Scholarship. Additional financial support for professional development activities was provided by the United States National Science Foundation, the International Arctic Research Center, the University of Alaska Fairbanks, and the Association of Canadian Universities for Northern Studies.

CONTENTS

LIST OF TABLES

LIST OF FIGURES

LIST OF ABBREVIATIONS

AC ..... alkyl carbon
ACIA ..... Arctic Climate Impact Assessment
AroC ..... aromatic carbon
C ..... carbon
CbyC ..... carbonyl carbon
CSSC ..... Canadian System of Soil Classification
D_b ..... bulk density
DFH ..... differential frost heave
GIS ..... geographic information system
IC ..... inorganic carbon
IPCC ..... Intergovernmental Panel on Climate Change
NEP ..... net ecosystem productivity
NMR ..... nuclear magnetic resonance
NPP ..... net primary productivity
OAC ..... O-alkyl carbon
OC ..... organic carbon
R_H ..... heterotrophic respiration

1. INTRODUCTION

There is now little doubt that climate change is an extremely important issue facing humanity in the coming century. Greenhouse gas forcing by carbon dioxide (CO_2) and methane (CH_4) are the two largest terms in the Intergovernmental Panel on Climate Change's (IPCC, 2007) global radiative forcing budgets. Both of these gases contain carbon (C), and there is a great deal of work underway to determine the size and dynamics of the various global carbon pools.

Global soils are an important reservoir of organic carbon (OC), and arctic soils are a particularly large and important part of this reservoir. Globally, soils are the largest terrestrial OC pool. Permafrost affected soils cover over 18 million km^2, or over 15 % of the earth's land area (Tarnocai et al., 2009), including over 4 million km^2 in Canada (Tarnocai, 1999). The northern circumpolar permafrost region contains 1672 Pg of C, or about 50 % of global belowground C (Tarnocai et al., 2009). The Arctic is expected to experience particularly large warming in the coming century (ACIA, 2004; IPCC, 2007) and both net primary productivity and heterotrophic respiration are expected to increase (Euskirchen et al., 2009). The net effect of this remains unclear, but the mineralization of even a small amount of the immense northern C pool reported by Tarnocai et al. (2009) could result in a substantial positive feedback to warming. A more complete understanding of C cycling in permafrost soil environments is needed to better predict how arctic soil C will respond to climate warming.

Many mineral soils in the Arctic are affected by cryoturbation, the physical movement of soil due to frost action. Cryoturbation is often evidenced by deformation of soil horizon boundaries, translocation of material both vertically and laterally within the soil profile, and sorting based on particle size (Bockheim and Tarnocai, 1998). The implications of this process for C cycling are twofold: (1) existing OC-rich materials near the surface are moved downwards in the soil profile to areas where conditions are less favourable for heterotrophic respiration (i.e. cooler and more

likely to be saturated) (Bockheim, 2007; Davidson and Janssens, 2006), and (2) OC-poor mineral materials are moved towards the soil surface, resetting the OC equilibrium and leading to more rapid accumulation of soil OC (Kaiser et al., 2007).

Soils affected by cryoturbation fall within the Turbic Cryosol Great Group in the Canadian System of Soil Classification (CSSC; Soil Classification Working Group, 1998). Turbic Cryosols comprise about 80% of permafrost-affected soils in Canada (Tarnocai, 2004). Of an estimated total 1024 Pg of C in all soils of the northern circumpolar soil region, 581 Pg (57%) is in Turbic Cryosols; however, this estimate is based on a small number of pedons used to represent a vast and varied region (Tarnocai et al., 2009). If only a small amount of this C is mineralized and released to the atmosphere, it will have significant consequences for climate change.

Despite the apparent importance of soil OC redistributed by cryoturbation, little work has been done to quantify the depth distribution of OC in Turbic Cryosols or to compare the depth distribution of this OC to that of soils not affected by cryoturbation. Moreover, it is not clear how the process of cryoturbation operates in all cases, and whether differences in the process of cryoturbation will result in differences in the depth distribution of OC. Thus, the objectives of this study are: (1) to examine the depth distribution of soil OC content in Turbic Cryosols and Static Cryosols, and (2) to observe differences in depth distribution of OC and OC quality among different observed modes of cryoturbation. Soils examined in this study are restricted to high arctic soils of Truelove Lowland, Devon Island, Nunavut and low arctic soils near Wright Pass along the Dempster Highway, Yukon Territory.

2. LITERATURE REVIEW

2.1. Cryoturbation

The term cryoturbation refers to all soil movements due to frost action, and is manifested in the soil profile by broken and distorted horizons and the mixing of materials between horizons (Bockheim and Tarnocai, 1998). Cryoturbation is a dominant process in permafrost-affected soils, and as such, is recognized at the great group level in the Canadian Soil Classification System (Soil Classification Working Group, 1998). Cryoturbation is often expressed at the surface as patterned ground (Bockheim and Tarnocai, 1998): roughly symmetrical, sorted or nonsorted circles, polygons, nets, steps, stripes, hummocks, and mudboils (French, 2007; Washburn, 1980). Cryoturbation occurs preferentially in areas characterized by imperfect drainage, parent materials rich in silt, and permafrost within the uppermost meter (Bockheim and Tarnocai, 1998; French, 2007; Washburn, 1980).

2.2. Cryoturbation Mechanisms

In his classic review, Washburn (1956) noted 19 distinct hypotheses for the genesis of patterned ground features closely associated with cryoturbation including ice thrusting, colloid water absorption, desiccation contraction, and vibration. While there are considerably fewer hypotheses invoked in more recent literature (see Bockheim, 2007), there is still not clear consensus regarding the mechanism driving cryoturbation. Commonly cited theories to explain cryoturbation features in the recent literature include the diapiric model (Swanson et al., 1999), the cryostatic model (Van Vliet-Lanoe, 1991; Vandenberghe, 1988; 1992), the cryohydrostatic model (Vandenberghe, 1988; 1992), and the differential frost heave model (Daanen et al., 2008; Peterson, 2008).

2.2.1. Cryosuction

Understanding of the cryoturbation models to be discussed in the following paragraphs requires some knowledge of the process of cryosuction. In soils, physiochemical forces bind water to the soil matrix. These forces are stronger closer to pore walls, and thus water is more strongly bound to soil particles when it is close to pore walls. The more strongly that water is bound to soil particles, the more energy must be released when it freezes (Nicolsky et al., 2008). This means that water close to pore walls requires temperatures lower than 0 °C for freezing to occur, and a thin layer of liquid water separates pore ice from the soil matrix. The unfrozen layer is thinner in colder soils, and thicker in soils at or near 0 °C. The amount of liquid water in a freezing soil is independent of the total moisture content because ice is not bound to the soil matrix by physiochemical forces in the same way that liquid water is (Williams and Smith, 1991). The strength of those forces, however, is closely related to soil texture, and is highest in soil with high capillarity and high mineral surface area. Thus, liquid water content in cryotic soils is generally highest in clays and lowest in sands (Williams and Smith, 1991). Since there is less liquid water bound to the soil matrix in already frozen or actively freezing soils than in adjacent unfrozen soils, there is a potential gradient normal to the freezing front that attracts liquid water, moving in the unfrozen film, towards the location of ice formation (Brouchkov, 2000; Nicolsky et al., 2008; Peterson and Krantz, 2008). However, the movement of water through the soil depends not only on the potential gradient, but also on the ease with which water can move through the soil, or the hydraulic conductivity. For this reason, the transmission of liquid water through the soil is not greatest in clays, as might be expected based on potential gradient alone, because of their low hydraulic conductivity. All other factors being equal, silts have the greatest potential for the transmission of liquid water in unfrozen films because of the balance of a strong potential gradient and a high hydraulic conductivity (Williams and Smith,

1991). Cryosuction can draw liquid water upwards, downwards, or laterally within the soil profile, depending on the direction in which freezing is progressing.

2.2.2. Diapirism Model

In the diapirism model, invoked by numerous researchers to explain cryoturbation features (Bertran et al., 2009; Harris et al., 2000; Murton and French, 1993; Superson et al., 2010; among others), but best articulated by Swanson et al. (1999), soil near the permafrost table flows upward by viscous flow as the denser overburden sinks into it. The resulting forms are described herein as diapirs because of their resemblance, as recognized by Shilts (1978) and Swanson (1999) to the much larger tectonic plumes of low-density material that move upward through denser rocks driven by buoyancy. For diapirs to form, low density soil must exist near the permafrost table overlain by denser soil. This unstable density profile may occur as a result of parent material layering or by the release of meltwater from ice-rich permafrost into the lower active layer.

An unstable density profile is certainly possible due to parent material layering; however, this explanation only applies at local scales and cannot be extended to explain diapir-like features in soils throughout the northern permafrost region. Swanson et al. (1999) suggest that unstable bulk density profiles may be commonplace in permafrost soils because substantial water is released into the active layer from thawing of ice-rich upper permafrost. Extremely ice-rich upper permafrost is common throughout the northern permafrost region, especially in areas with silty textures (Shur, 1988). Swanson et al. (1999) indicate that the ice-rich upper permafrost layer forms over multiple years by downward migration and freezing of water under gravity and cryosuction when freezing is occurring upwards from the permafrost table during permafrost aggradation.

As the ice-rich upper permafrost thaws during warmer periods, large amounts of water are released into the lower active layer and it rapidly becomes saturated, as the water remains perched on the permafrost. If water is present in excess of pore space the density of the lower active layer is effectively lowered relative to that of the overburden. In this situation, the denser overburden will sink into the less dense soil below, while soil from the lower active layer moves into the overburden in diapirs (Harris et al., 2000; Swanson et al., 1999).

As the diapir moves upwards through the soil, water is exchanged with the surrounding overburden. This exchange of water reduces the density difference between the diapir and the surrounding soil, and diapir movement will cease as the density difference nears equilibrium. Upward diapir movement will also stop if the diapir encounters another layer of low density, such as an organic layer at or near the soil surface. In cases where diapirs continue and breach the surface of the soil, destabilizing any vegetative cover, they will alter the thermal regime of the soil and potentially initiate a positive feedback where reduced insulation from vegetation and organic matter causes a deeper thaw and a greater release of water from the ice-rich upper permafrost (Swanson et al., 1999).

2.2.2.1. Characteristic Soil Conditions and Forms

Swanson et al. (1999) use soils from a large bioclimatic gradient on the North Slope of Alaska to validate their model. While the typical conditions they observed may not be an exhaustive list of the potential conditions under which diapirism is possible, these conditions do represent a subset of conditions known to satisfy the requirements of their numerical model for diapirism. These conditions are a good starting point to determine whether or not diapirism is possible in other soils; that is, if conditions are similar to those observed by Swanson et al. (1999) it is likely that diapirism could occur.

Soils used by Swanson et al. (1999) to validate their model were typically loamy in texture, had redoximorphic features just above the permafrost table, and often had a granular or blocky structure. Visible ice often occupied more than 50 % of some Cf horizons (Cz horizons in the CSSC). These soils typically consisted of three distinct layers: (1) an organic layer at the surface with a high water content (> 1 kg water kg^{-1} soil) and a low field-moist bulk density (< 1.2 Mg m^{-3}), (2) mineral soil in the middle of the active layer with a lower water content (0.25 – 0.40 kg water kg^{-1} soil) and a higher field-moist bulk density (1.6 – 2.0 Mg m^{-3}), and (3) an ice-rich near-permafrost layer consisting of Cf, Bg, and Oaf horizons (Cz, Bg, and Ohf horizons in the CSSC) with a high water content (0.50 – 2.0 kg water kg^{-1} soil) and a low field-moist bulk density (0.90 – 1.3 Mg m^{-3}). Thawed bulk density estimates of the bottom of the three layers were 0.1 – 0.6 Mg m^{-3} lower than the overlying mineral layer. Parent material layering may contribute to the unstable bulk density profile, but it is not required for diapir initiation if there is ice-rich upper permafrost (Swanson et al., 1999).

Early diapirs appear as a simple upward bulge of the buoyant layer into the overburden. The size and spacing of diapirs is related to the thickness of the buoyant layer. Diapirs predicted by the model range in diameters from 1 to 13 times the thickness of the buoyant layer, though 3 to 4 times seems to be typical. More developed diapirs have a wide, mushroom shaped head and a more irregular shape. It should be noted, however, that simple diapiric forms may not always be distinguishable in the soil morphology as most soils subject to diapirism would probably have multiple diapiric forms superimposed. Simple diapiric forms, where present, may indicate rarer, episodic destabilizations. In cases where the overburden is too rigid or dry for viscous flow, diapirs may flow upwards in existing cracks or zones of mechanical weakness, more analogous to a dike than a diapir (Swanson et al., 1999).

2.2.3. Cryohydrostatic Model

In the cryohydrostatic model (Shilts, 1978; Van Vliet-Lanoe, 1991; others), best described in two reviews by Vandenberghe (1988; 1992), increasing amounts of water are trapped between an impermeable layer and the freezing front in a hydraulically closed system. Due to the volumetric expansion of freezing water in the surrounding soil, pore water pressure in the unfrozen pocket progressively increases. Eventually, liquefaction occurs in the unfrozen pocket and sediment laden water is squeezed, under pressure, into weak areas in the surrounding frozen soil. Cryohydrostatic movement occurs in a fluid state.

2.2.3.1. Characteristic Soil Conditions and Forms

An impermeable layer, permafrost or otherwise, is required to prevent water in the unfrozen pocket from escaping downwards. For regularly occurring patterns to occur, some existing heterogeneity is required; for example, an existing polygonal frost crack network. Characteristic forms expected from cryohydrostatic pressure are dike-like, irregularly shaped extrusion features oriented in all directions. Cryohydrostatic forms may cut across other soil features, and will occur preferentially at contacts, faults, and other zones of mechanical weakness (Vandenberghe, 1988; Vandenberghe, 1992).

2.2.4. Cryostatic Model

The cryostatic model (Superson et al., 2010; Tarnocai and Zoltai, 1978; Van Vliet-Lanoe, 1991; others), similar but distinct from the cryohydrostatic model, was also clearly explained in reviews by Vandenberghe (1988; 1992). In the cryostatic model, unfrozen soil is trapped below a frozen carapace at the soil surface. Ice growth at the downward moving freezing front causes heave and updoming of the soil surface. As the frozen carapace becomes thicker and heavier, additional pressure is exerted on the underlying unfrozen soil. Water expands as it turns to ice at

the freezing front, causing additional downward pressure on unfrozen soils. This cryostatic pressure is responsible for soil deformation. It is likely that the greatest pressures will be in a direction normal to the freezing front, but some lateral pressure will also exist. Substantial pressures can also exist in frozen or freezing areas of the soil as cryosuction draws additional unfrozen water into frozen areas, causing some plastic deformation in frozen soils as well. Cryostatic movement occurs in a plastic state, a key distinction from cryohydrostatic movement (described above), which occurs in a liquid state (Vandenberghe, 1988; 1992).

2.2.4.1. Characteristic Soil Conditions and Forms

In the cryostatic model, there is no explicit requirement for permafrost; thus, cryostatic deformations could occur in areas of seasonal frost as well as permafrost regions. Silty or clayey soils are particularly susceptible because of large amounts of capillary water present in unfrozen films at temperatures between 0 °C and -22 °C. However, regular patterning by cryostatic pressure would require some preexisting soil heterogeneity (Vandenberghe, 1988; 1992).

2.2.5. Differential Frost Heave Model

Differential frost heave (DFH) refers to a situation where there is laterally more frost heave in one area than in another (Nicolsky et al., 2008). Generally, greater heave occurs in the centre of the features than in the inter-centre regions. The laterally non-uniform heave of the ground surface is attributed to laterally non-uniform freezing of water within the patterned ground feature (Peterson and Krantz, 2008).

The heave of freezing soils that contain a large amount of pore water is well known, generally attributed to the approximately 9% volumetric expansion of water when its temperature drops from 4°C to 0°C. This expansion explains why water saturated soils heave upon freezing; however, surface heave in the centre of patterned ground features is often observed to be well in

excess of the heave expected from the expansion of water alone. Moreover, the observed heave is greater than expected in the centre of patterned ground features and less than expected in inter-centre regions (Nicolsky et al., 2008; Peterson and Krantz, 2008). For this DFH to occur, a mechanism is required to redistribute water from the inter-centre to the centre regions of patterned ground features.

A conceptual model for DFH is outlined in Figure 2.1. During freeze-up, the freezing front proceeds downwards from the ground surface. Freezing does not occur at a discrete plane, but rather in a region 0.1-1 cm thick known as the frozen fringe. In the frozen fringe of a saturated soil, pore ice grows until it is sufficient to support the overburden. Water migrating from the unfrozen soil into the frozen fringe by cryosuction will freeze into an ice lens. Continued cryosuction allows the lens of segregated ice to grow until the ice content below it is too great to allow water migration. This process then repeats itself, forming a series of ice lenses (Peterson and Krantz, 2008).

In a homogeneous landscape, the freezing front would be horizontal relative to the ground surface; however, heterogeneity in snow cover, vegetation cover, organic matter distribution, and soil properties causes perturbations in the freezing front. In the DFH model, frost propagation is more rapid in the centre relative to the inter-centre of patterned ground features because of a sparser cover of insulative vegetation in the centre (Nicolsky et al., 2008; Peterson and Krantz, 2008). The water flux (via cryosuction) and heat flux is roughly perpendicular to the freezing front. Water is supplied to the centre regions of patterned ground features from the surrounding tundra, and water is usually assumed to be abundant (near saturation) during the freezing period. The flux of water into the centre of the patterned ground feature causes a preferential formation of ice lenses in the centre relative to the inter-centre (Daanen et al., 2007). This creates a general

movement of soil upwards within the centre of the patterned ground feature. Preferential heave in the centre further exacerbates the perturbation in the freezing front, as snow cover will be thinner above the areas with maximum heave, increasing heat flux in these areas (Nicolsky et al., 2008).

In the spring and summer, the soil displaced by frost heave thaws and moves by viscous relaxation under the influence of gravity (Walker et al., 2004). During relaxation, particles move downward and radially outward near the surface of the centre (Mackay, 1980; Van Vliet-Lanoe, 1991), and downward and radially inward at greater depths (Mackay, 1980; Nicolsky et al., 2008). Though it is not incorporated into more recent models of DFH, Van Vliet-Lanoe (1991) suggests that another heave process, called secondary frost heave, is at work during the thaw period. Thawing proceeds from the ground surface downwards. This inversion of the thermal gradient causes ice lenses to thaw, then allows the movement of water downwards where it refreezes into underlying ice lenses. The net movement of soil particles when all components of the DFH model are included resembles a convection cell.

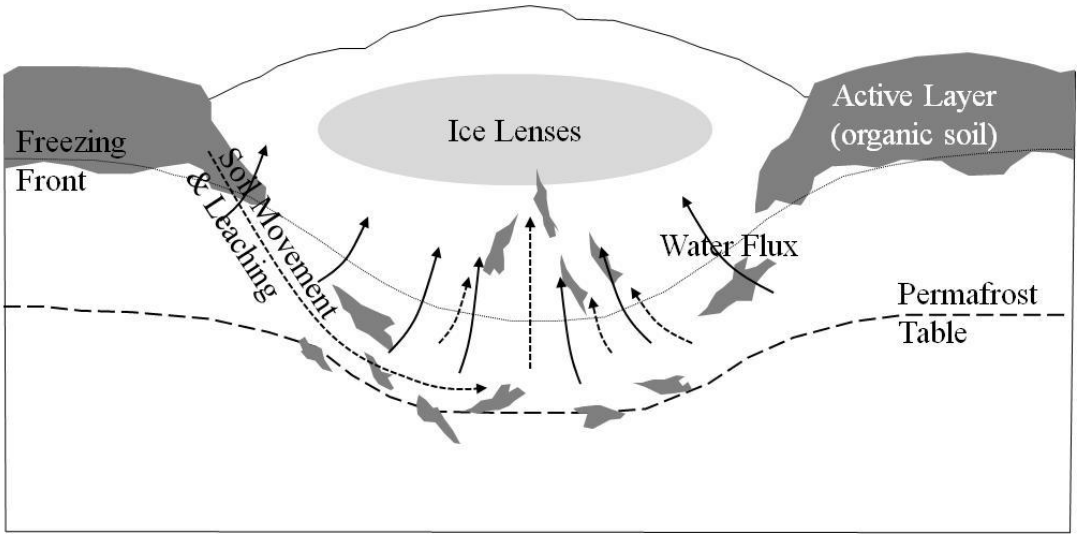

Figure 2.1 Modeled fluxes of water and soil during fall freezing of a nonsorted circle. Dashed arrows indicate direction of soil movement and leaching, which solid arrows indicate the direction of water movement during fall freezing. Adapted from Nicolsky et al. (2008).

2.2.5.1 Characteristic Soil Conditions and Forms

In the DFH model for cryoturbation outlined above, permafrost is not explicitly required (Peterson and Krantz, 2008), but saturated or near-saturated conditions are required. Permafrost is commonly found in association with patterned ground features because it acts as a barrier to water movement and helps to maintain saturated conditions in the active layer. Indeed, several researchers (Ballantyne, 1996; Van Vliet-Lanoe, 1991) have noted patterned ground features attributed to DFH in regions without permafrost.

The cryosuction required for DFH is sensitive to the soil texture. Sandy soils usually exhibit the smallest amount of DFH. This is attributed to the fact that the unfrozen water content is generally lowest in sandy soils, and highest in clayey soils (Nicolsky et al., 2008). However, the hydraulic conductivity is highest in sandy soils, and lowest in clayey soils. On balance, silty soils are generally the most frost-heave susceptible (Walker et al., 2004).

Several soil features are commonly attributed to DFH in the field (Walker et al., 2004) and in models (Nicolsky et al., 2008; Peterson and Krantz, 2008). A platy structure is common, crumbling to a granular structure in the centre. An extremely ice-rich upper permafrost layer is common, though not present in all cases. A bowl-shaped permafrost table is also common, though this is thought to be a consequence of the surface pattern caused by DFH, not a cause of it.

2.3. Typical Genesis of Nonsorted Circles and Earth Hummocks

While numerous models of cryoturbation exist, most cryoturbation features in the field are considered polygenetic, and similar features may form by different processes. A recent conceptual model (Figure 2.2), developed by Shur and Ping (2003) and Shur et al. (2005) and later described by Walker et al. (2008) and supported by models from Daanen et al. (2008),

Nicolsky et al. (2008), and Peterson and Krantz (2008), is a likely explanation for many nonsorted circles and earth hummocks. According to this model, the process begins with thermal contraction, producing cracks (Matsuoka, 2011) that are preferentially colonized by plants, eventually creating an organic-rich zone insulating soil under and around the crack (Kade et al., 2006). This causes cooler soil conditions under the organic-rich cracks than in other areas. The presence of thermal cracking without the development of ice wedges, upon initial consideration, seems to be at odds with current understanding of the development of thermal contraction cracking; however, field evidence indicates that shallow contraction cracks can form that close

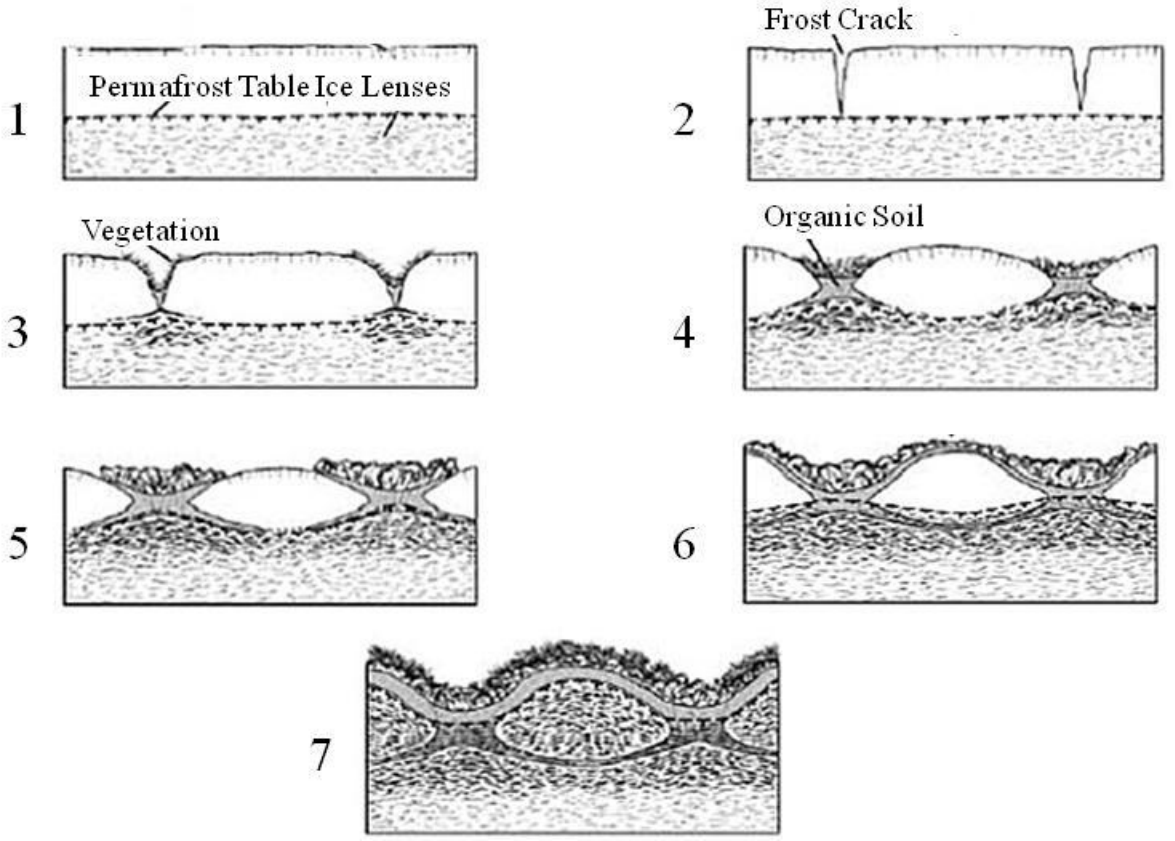

Figure 2.2 Conceptual model for nonsorted circle and earth hummock development. Stage 6 (nonsorted circles or mud hummocks) is the typical final stage of development, but stage 7 features (earth hummocks) may form under favourable conditions Adapted. from Walker et al. (2008)

by thermal expansion or infilling with mud before water trickles in to form wedge ice (Mackay, 1988; Mackay and Burn, 2002). Furthermore, Walker et al. (2008) suggest that cracking is overwhelmed by the influence of vegetation succession; a claim which appears to be supported by field evidence from the Illisarvik drained lake experiment, where cracking ceased within 10 years at several locations where vegetation growth and increased snow depth provided sufficient insulation to prevent cracking (Mackay and Burn, 2002).

Deeper summer thawing in the area between the cracks causes a bowl-shaped permafrost table beneath the features, and differential frost heave creates a barren nonsorted circle. Water high in dissolved OC flows into the bowl-shaped area and the OC precipitates upon freezing to create an organic-rich zone at the permafrost table. As conditions improve for plants growing in the cracks, vegetation may spread onto the centres of nonsorted circles. This increases the insulation over the feature and causes the permafrost table to aggrade, first at the edges of the patterned ground features and then in the centres, causing greater differential frost heave and the development of a hummock feature. As the permafrost table aggrades, the OC-rich material from the bottom of the bowl is incorporated into the permafrost. In the context of this document, the model described by Walker et al. (2008) is not intended to be used to describe all forms of patterned ground and all cryoturbation features, but it is a useful description of the probable genesis of many features considered in this study.

2.4. Arctic Soils and the Global Carbon Cycle

Most soils are close to equilibrium with respect to organic carbon stocks, but soils can act as either net sinks or net sources of the greenhouse gases CO_2 and CH_4 when conditions change, depending on the balance of net primary production (NPP), which adds OC to the soil, and heterotrophic respiration (R_H), which releases SOC to the atmosphere (Figure 2.3a). Net

ecosystem productivity (NEP) takes both NPP and R_H into account (NEP = NPP - R_H). A positive NEP means that there is a net flux of C from the atmosphere to the soil, and a negative NEP indicates that there is a net flux of C from the soil to the atmosphere. Permafrost-affected soils in the northern hemisphere (i.e. Cryosols in the CSSC) have had a small positive NEP through much of the Holocene, and have accumulated vast amounts of OC (Tarnocai et al., 2009). Much of this accumulation is likely due to the influence of cryoturbation, which redistributes OC to depth and slows R_H because of cooler and wetter conditions near the permafrost table (Bockheim, 2007; Kaiser et al., 2007), causing an accumulation of OC in Turbic Cryosols (Tarnocai et al., 2009). Warmer temperatures are expected to stimulate NPP in arctic ecosystems; however, R_H is likely to be more responsive to temperature than NPP (Euskirchen et al., 2009) and a negative NEP is possible. Given the large amounts of OC and vast area of Cryosols, a change to a negative NEP could have significant consequences for global climate.

2.5. Cryoturbation and Arctic Soil Organic Carbon

Cryoturbation has two apparent effects on the depth distribution of SOC: (1) soil material rich in OC is moved from near the soil surface toward the permafrost table (Bockheim, 2007; Bockheim and Tarnocai, 1998), and (2) soil material poor in OC is moved from near the permafrost table toward the soil surface (Kaiser et al., 2007) (Figure 2.3b). Both of these effects serve to increase the SOC stock in permafrost-affected mineral soils subject to cryoturbation.

When SOC is moved downwards in the soil profile, it is moved closer to the permafrost table. In permafrost-affected soils with a shallow active layer, conditions are cooler and more likely to be saturated, and therefore less favourable for R_H, near the permafrost (Bockheim, 2007; Davidson and Janssens, 2006). Thus, cryoturbation has a preserving effect on SOC. Once SOC begins to accumulate in the pedon, it serves to provide additional insulation above the

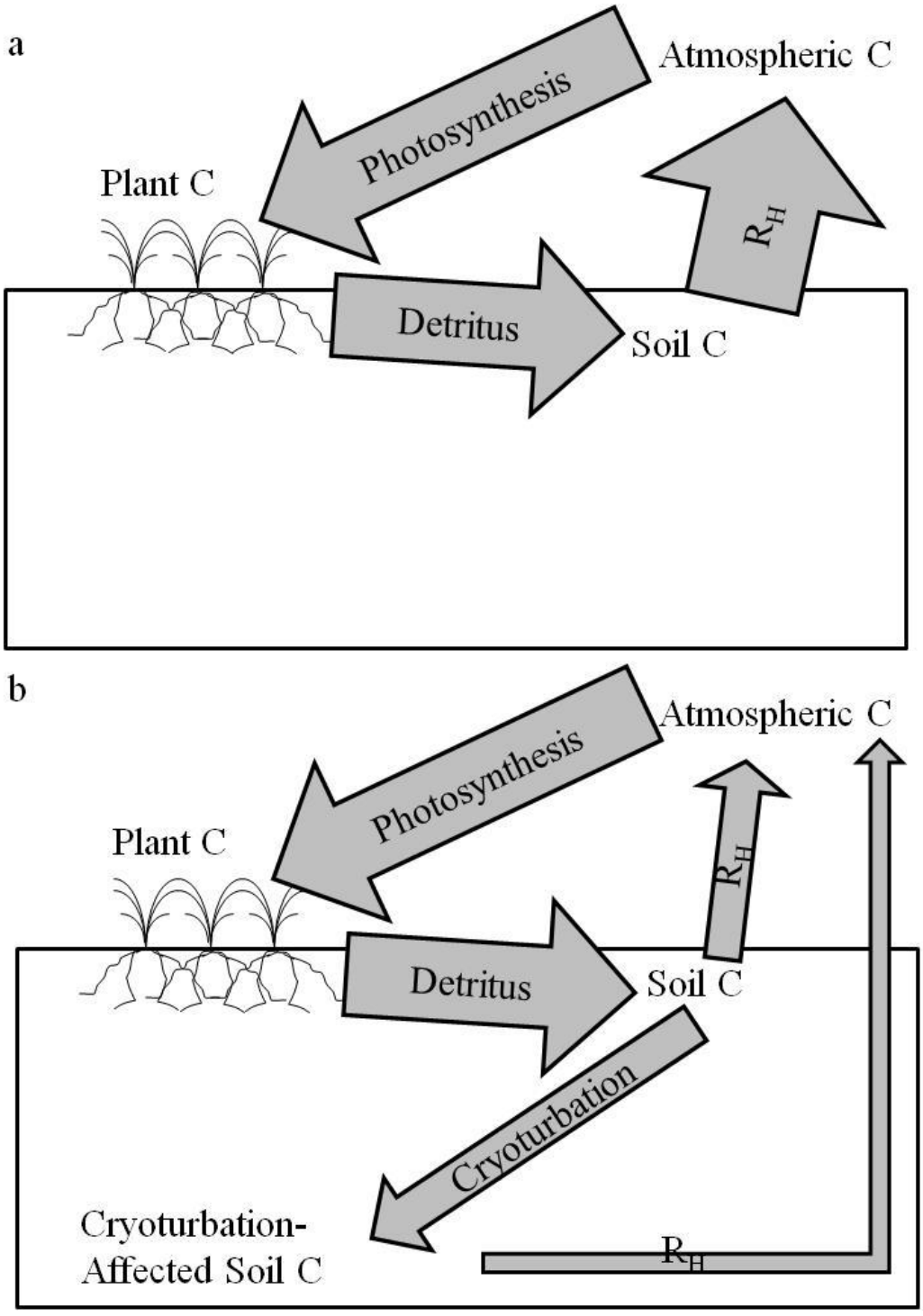

Figure 2.3 Simplified flow diagram of the relevant portions of the carbon cycle (a) without cryoturbation and (b) with cryoturbation. NPP refers to net primary productivity and R_H refers to heterotrophic respiration. Arrow sizes, while not quantitative, represent ranked sizes of carbon flows.

permafrost. This can lead to the upward migration of the permafrost table and consequent incorporation of buried SOC into the perennially frozen soil (Koven et al., 2009).

A supply of SOC-poor mineral material to the soil surface also increases the stock of OC in the soil. As previously explained, a positive NEP results when NPP is greater than R_H (NEP = NPP – R_H). Cryoturbation moves SOC-poor mineral material to the soil surface. There is little food available for decomposing microbes, so R_H is very small. However, plants grow in the SOC-poor mineral material and their detritus is added to the SOC pool. Thus NPP is much larger than R_H and there is a relatively rapid accumulation of SOC (Kaiser et al., 2007).

2.6. Other Processes Transporting SOC to Depth

There are other processes that can cause increase the amount of OC at depth in arctic soils. Burial of OC by alluvial aggradation (Tarnocai et al., 2009) is important in river deltas, and aeolian deposition has buried more than 400 Pg of OC in Siberia and central Alaska and Yukon (Tarnocai et al., 2009; Zimov et al., 2006). Mass wasting and slope processes such as solifluction (Matthews et al., 2005), and active layer detachments (Lewkowicz, 2007) can cause the burial of OC, but they can also expose buried OC in upslope positions. While these processes all depend on local geomorphic factors, the transport of OC in a dissolved state followed by cryochemical precipitation (Kowalkowski et al., 1986) may also be widespread in permafrost soils (Gundelwein et al., 2007), though little work has been done in this area.

2.7. The Use of NMR Spectroscopy and C:N Ratios to Evaluate Decomposition

In order to better interpret the role of cryoturbation in C cycling in mineral Cryosols, it is necessary to obtain some information about the degree of humification of OC at various depths. This can be accomplished with solid-state ^{13}C NMR spectroscopy, in which ^{13}C nuclei in different chemical structures can be sensed as different chemical shift values (usually reported in

parts per million) of the frequency of the NMR spectrometer's magnetic field from a reference value. The intensity for each chemical shift value is used to produce a spectrum, and the integrated area under the spectrum represents the total C content. The integrated area is divided into sections based on ranges of chemical shifts and the integrated areas of these sections are reported as proportions of the total C content (Baldock et al., 1997).

Table 2.1 Chemical shift ranges and types of chemical compounds for ^{13}C NMR spectroscopy categories used in this thesis†

Category	Chemical Shift Range (ppm)	Types of Compounds Included
alkyl C (AC)	0 - 45	lipids fatty acids plant polymers waxes resins side chains of amino acids
O-alkyl C (OAC)	45 - 100	polysaccharides (cellulose, hemicelluloses) carbohydrates methoxyls proteins side chains of lignins
aromatic C (AroC)	110 – 160	aromatics molecules derived from lignins molecules derived from proteins
carbonyl C (CbyC)	160 – 220	esters carboxyl groups amide carbonyls

† Chemical shift ranges and compound names and adapted and adopted from Baldock et al. (1992; 1997), Helfrich et al. (2006), Paré (2011), Parfitt and Newman (2000), and Schnitzer (2001).

There are four widely accepted categories of C types sensed in ^{13}C NMR spectroscopy (summarized in Table 2.1), though other categories using different chemical shift limits exist. Alkyl C (AC) is represented by the chemical shift range of 0 to 45 ppm and includes lipids, fatty acids, plant polymers, waxes, resins, and side chains of amino acids (Baldock et al., 1992; Helfrich et al., 2006; Paré, 2011; Parfitt and Newman, 2000). The chemical shift range from 45

to 110 ppm comprises the O-alkyl C (OAC) category which includes polysaccharides (cellulose and hemicelluloses), carbohydrates, methoxyls, proteins, and side chains of lignins (Baldock et al., 1992; Helfrich et al., 2006; Paré, 2011; Parfitt and Newman, 2000; Schnitzer, 2001). The aromatic C (aroC) category, which has a chemical shift range from 110 to 160 ppm, is made up of molecules derived from lignins and proteins (Baldock et al., 1992; Helfrich et al., 2006; Paré, 2011). Finally, the carbonyl C (CbyC) category includes esters, carboxyl groups, and amide carbonyls sensed in the shift range of 160 to 220 ppm (Helfrich et al., 2006; Paré, 2011).

OC in the OAC category contains compounds that are attractive to microbes and will be preferentially decomposed early. The proportion of OAC is usually greatest in fresh litter. OC in the AC, AroC, and CbyC categories is not preferred over OAC by microbes and will decompose more slowly (Baldock et al., 1992, 1997; Mathers et al., 2000). In particular, AC tends to accumulate in the later stages of humification (Baldock et al., 1992, 1997), and as such, the ratio of OAC and AC can be used as an indicator of degree of humification (Baldock et al., 1997; Mathers et al., 2000; Preston et al., 2009). The OAC:AC ratio will decrease as humification proceeds.

In this document, the term ‘labile’ is used to describe OC occurring dominantly in compounds that are preferred by microbes (i.e. OAC), and the term ‘recalcitrant’ describes OC occurring dominantly in compounds that are less preferred by microbes (i.e. AroC, CbyC, and AC). Thus, as humification of OC proceeds and the proportion of OAC decreases while the proportions of AroC, CbyC, and AC increase, the OC is becoming less labile (or more recalcitrant).

In some circumstances, the C:N ratio can also be used as a basic indicator of the degree of humification and relative lability or recalcitrance of OC. When different residues are compared,

the residue with the lowest C:N is likely to be the most attractive to microbes because it best satisfies their N requirements. In this situation, the residue with the C:N closest to that of the microbes, usually about 8, will be preferentially consumed first (Brady and Weil, 2002). However, when there is only one residue present, microbes will tend to choose less humified OC with a higher C:N (i.e. higher in OAC) over more humified OC with a lower C:N (i.e. higher in AroC, CbyC, and AC) (Baldock et al., 1992; Brady and Weil, 2002). Assuming that N limitation is not a substantial problem for microbes (i.e. C:N less than ~25), there will be an initial rapid drop in C:N as the most labile OC is decomposed. With additional time the rate of C:N change decreases and eventually approaches an asymptote at approximately the C:N of the microbial biomass (Baldock et al., 1992; Brady and Weil, 2002). Numerous researchers (Baldock et al., 1992, 1997; Kuhry and Vitt, 1996; Parfitt and Newman, 2000; Quideau et al., 2000) have noted a narrowing C:N ratio with increasing degree of humification. Thus, when a single plant association at a single pedon is considered, a decreasing C:N ratio can be taken to indicate an increasing degree of humification and an increasing decree of recalcitrance of OC.

2.8. Current State of Cryoturbation-Carbon Interaction Science

2.8.1 Existing Studies

Bockheim (2007) examined cryoturbation-affected pedons in Alaska and found that an average of 55 % of SOC density in the active layer had been affected by cryoturbation. He further noted that this SOC was frequently of mid-Holocene age. Furthermore, the age of subducted SOC often indicated that burial was coincident with periods of warming, indicating that cryoturbation may become more important as a C sequestration process as the Arctic warms in the coming century.

A study of cryoturbation-affected soils in northern Siberia (Kaiser et al., 2007) found that the total amount of C in horizons buried through cryoturbation is more than double the amount of C in surface horizons. Additionally, the mean age of buried C was three times greater than that of C in the surface layer (~1300 and ~400 yr BP, respectively), indicating that C translocated downwards in the soil profile is protected against decomposition. The researchers concluded that long term SOC storage occurs in cryoturbation-affected soils by burying C and slowing its decomposition.

A study of a nonsorted stripe complex in northwest Greenland (Horwath et al., 2008) also noted the role of cryoturbation in SOC distribution. In this complex, the distribution of SOC was highly variable; however, 62 % of the total SOC was found below 25 cm depth which was attributed to a combination of burial by glacial drift and cryoturbation. Buried SOC was found to have radiocarbon ages of 27,480 – 31,900 yr BP.

A study along a large bioclimatic gradient in Alaska and the western Canadian Arctic Archipelago (Michaelson et al., 2008) examined soil properties in frost boil ecosystems. A strong relationship ($R^2 = 0.89$, $p < 0.01$) was observed between the amount of frost heave and SOC stocks in the active layer. The authors also noted soil morphology evidence that indicated that much of the SOC was moved to the lower active layer by cryoturbation.

In a study in the central Canadian Arctic, Hugelius et al. (2010) found that 17% of the total landscape SOC mass is in pockets of soil redistributed by cryoturbation. Of this SOC, 80% was in the active layer. Cryoturbated soil pockets accounted for 51% of the total SOC mass in Turbic Cryosols. Radiocarbon dates indicate that cryoturbated SOC is older than surface SOC; however, C:N ratios suggest that the degree of humification is similar in cryoturbated and surface SOC, indicating that decomposition of cryoturbated SOC is slower.

Koven et al. (2009) modeled the role of cryoturbation in C stocks at high latitudes. They found that including redistribution of SOC by cryoturbation and insulation of soils from organic matter led to a 30% higher SOC stock in the upper 1 m of soil after 10,000 years. They also noted that cryoturbation had a larger effect on total C content than insulation by organic matter. Moreover, they found that the system had not reached equilibrium with respect to C stocks after a 10,000 year model run, suggesting that many northern soils have not yet reached equilibrium state.

2.8.2 Knowledge Gaps

Previous studies have recognized the role of cryoturbation in SOC storage; however, much of this work has been either anecdotal in nature or has used low resolution measures of depth distribution. Heretofore, no study has explicitly compared soils affected by cryoturbation to soils not affected by cryoturbation, and no study has closely examined the depth distribution of SOC in the Static and Turbic great groups of the Cryosolic soil order in the CSSC.

3. MATERIALS AND METHODS

3.1. Study Sites

Three study sites were included in this research (Figure 3.1). In 2008, 10 pedons at Truelove Lowland, Devon, Island, Nunavut (75.67°N, 84.58°W; hereafter referred to as Truelove Lowland) were examined. In 2009, 18 pedons were investigated in the foothills of the Richardson Mountains near Wright Pass, northern Yukon (67.01°N, 136.21°W; hereafter referred to as Wright Pass), as well as two pedons near the point where the Dempster Highway crosses the Arctic Circle north of Eagle Plains Lodge, northern Yukon (66.58°N, 136.31°W; hereafter referred to as Eagle Plains)

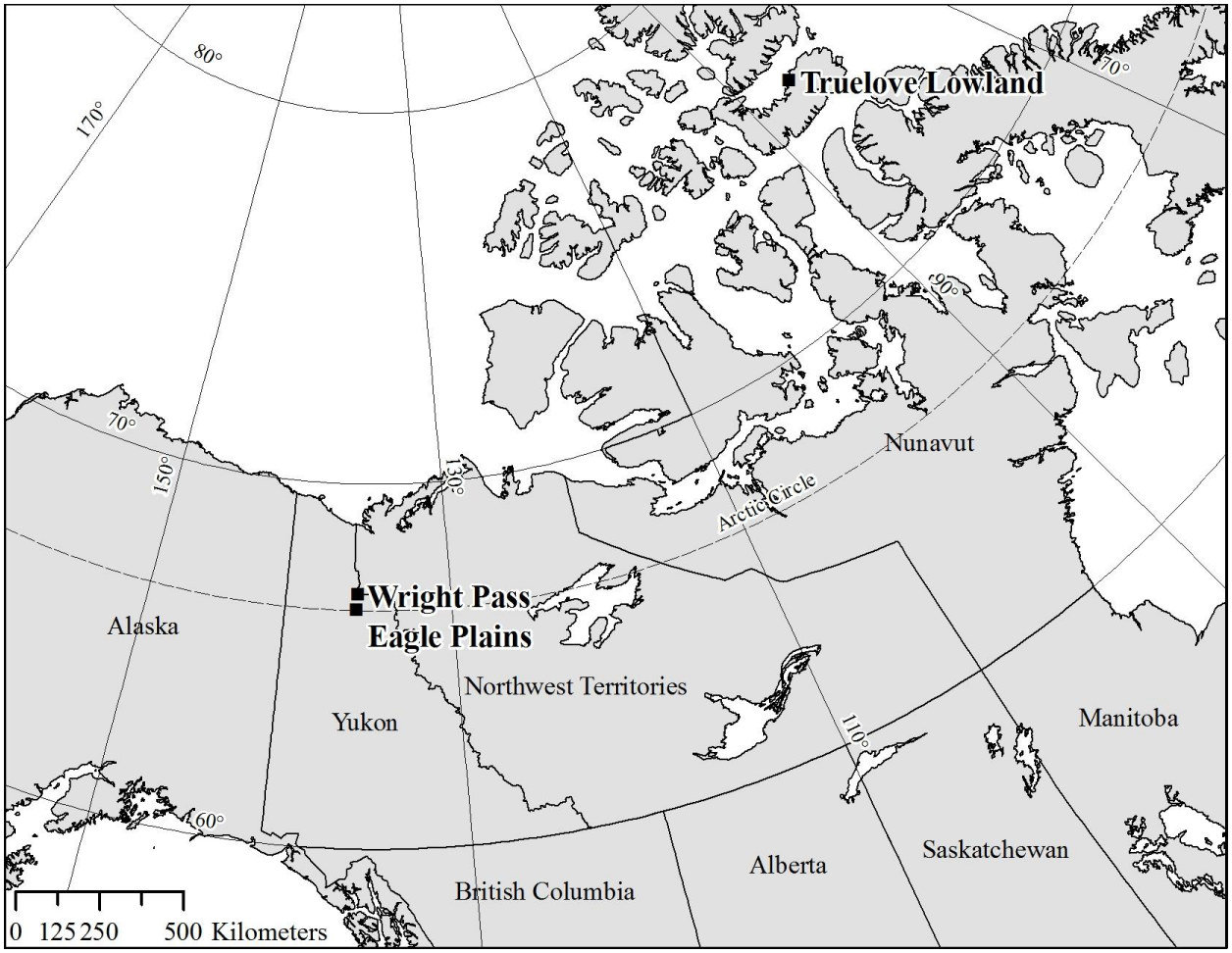

Figure 3.1 Study sites included for this research.

3.1.1. Truelove Lowland, Devon Island, Nunavut, Canada

Truelove Lowland is a 43 km^2 emerged coastal shelf located on the northeastern coast of Devon Island in the Canadian Arctic Archipelago (Lat. 75°40'N, Long. 84°35'W; Figure 3.1). Truelove Lowland is bordered by steep, 300 m high cliffs, the waters of Jones Sound and the Truelove River. This is a high arctic ecosystem, characterized by low temperatures, low insolation, low precipitation, and large seasonal variation; however, in several ways Truelove Lowland has more in common with low arctic sites than with the surrounding high arctic areas. There is greater diversity of vegetation and wildlife in this polar oasis than on the polar desert of the adjacent plateau (Bliss, 1977). About 22% of the area is covered by surface water (Krupicka, 1977), and Truelove Lowland's appearance and vegetation characteristics, and, to a lesser extent, climate, resemble low arctic sites of the Arctic Coastal Plain of Alaska, the Taimyr Peninsula of Russia, and the Mackenzie Delta of Canada (Bliss, 1977; King, 1991; Krupicka, 1977).

3.1.1.1. Geology and Physiographic Setting

The bedrock of Truelove Lowland consists of granulites and granitic gneisses of the Canadian Shield unconformably overlain by dolomitic sandstones and shales of the Arctic Platform. The crystalline rocks of the shield frequently outcrop in the Lowland (Krupicka, 1977). The bedrock is mantled by late Pleistocene and early Holocene glacial, glacio-marine, and fluvial deposits subsequently reworked by wave action, weathering, frost action, cryoturbation, deflation, aeolian deposition, and solifluction (Lev and King, 1999; Walker and Peters, 1977). Regional ice cap thinning and deglaciation began approximately 11,000 yr BP. A marine transgression covered the Lowland up to a current altitude of 86 m asl as a result of rising sea level and glacio-isostatic depression. Emergence began about 9700 yr BP, slowing substantially after 6700 yr BP. During emergence shallow coastal lagoons were isolated by

emerging sandbars, creating many small lakes. Some lakes subsequently filled with sediment and organic material, creating level meadows at topographic lows (King, 1991).

3.1.1.2. Climate

Devon Island has the macroclimate of a high latitude continental landmass. Sea ice surrounds the island for 10 months of the year, suppressing maritime influences. During the thawing months, the lakes of Truelove Lowland have a thermal reservoir effect, decreasing the local amplitude of regional temperature fluctuations. Snowmelt from Truelove Lowland usually begins in late May or early June and finishes by early July. The meltwater that interacts with the Truelove Lowland originates on the Lowland itself, as meltwater from the adjacent plateau bypasses the Lowland by travelling down the Truelove River and into Jones Sound (Courtin and Labine, 1977).

Temperature and precipitation data from Truelove Lowland are limited. Measurements from 1961-62 indicate that Truelove Lowland has a mean annual air temperature of -16 °C (King, 1969). In 1961, 95 days had a temperature above 0 °C. Measurements taken from 1970-73 indicate that total annual precipitation for Truelove Lowland is about 185 mm, of which 36 mm is wet precipitation (Ryden, 1977). Measurements from the nearby weather station at Grise Fiord, Nunavut (82.90°W, 76.42°N; Environment Canada, 2011) show a mean annual temperature of -14.4°C and a mean annual precipitation of about 180 mm for the period from 1993 to 2006.

3.1.1.3. Permafrost

Truelove Lowland lies within the continuous permafrost zone (Brown, 1977). Active layer depth varies with topography (approximate range from 30 to 100 cm), soil texture, soil moisture, and vegetation characteristics: on coarser-textured beach ridges with little vegetation the active

layer is thicker, gradually thinning under the insulating conditions of the organic mat of meadows with finer textured, moister soils (Lev and King, 1999). Overall, permafrost condition at Truelove Lowland is typical of a high arctic site (Walker and Peters, 1977).

3.1.1.4. Vegetation

Truelove Lowland possesses rich species diversity and a mosaic of plant communities. Lev and King (1999) identified several dominant plant associations that tend to vary with slope (Figure 3.2). The vegetation gradually shifts from a cushion-plant-lichen association on raised beach crests and upper foreslopes, increasing in vascular plant cover with distance downslope, to a cushion-plant-lichen mixed with cushion-plant-moss association on lower foreslopes.

3.1.1.5 Soils

Soils of Truelove Lowland follow a catena related to topography, drainage, and vegetation (Figure 3.2). On raised beach crests poorly developed Regosolic Static Cryosols underlie aeolian-deflated surficial deposits. Brunisolic Eutric Turbic Cryosols dominate soils on upper slope positions. Brunisolic Eutric Turbic Cryosols with discontinuous lenses of organic matter and hummocky surface relief are found at lower slope positions. Flat meadow sites, where anaerobic conditions often persist for much of the year, usually contain Gleysolic Turbic Cryosols subject to lensing and convolutions caused by cryoturbation (Lev and King, 1999; Walker and Peters, 1977).

Lev and King (1999) found that cation exchange capacity, OC, total nitrogen, moisture content, and % silt increased from the raised beach crest to the wet sedge meadow, while inorganic carbon (IC), bulk density (D_b) and % sand decreased along the same transect (Figure 3.2). They also found that cation exchange capacity, OC, and total nitrogen decreased with depth while IC, and D_b increased with depth, regardless of slope position.

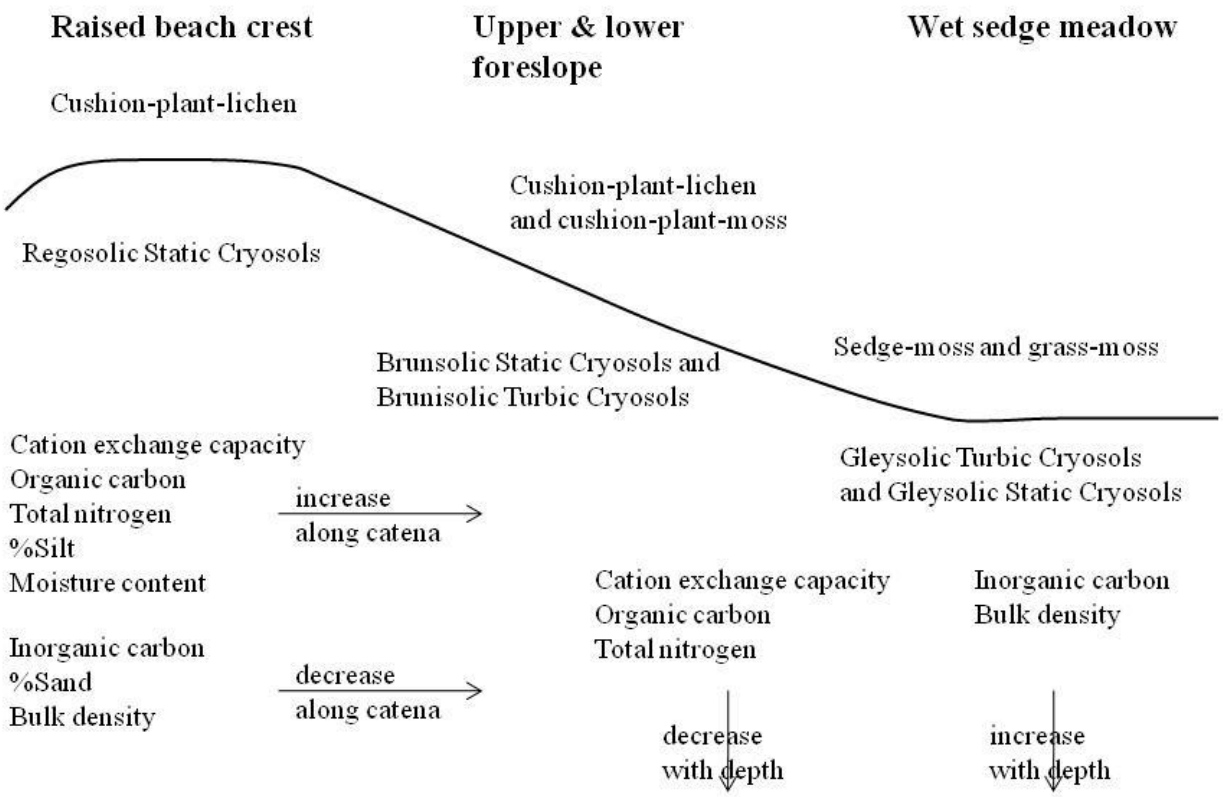

Figure 3.2 Catenary relationships at Truelove Lowland, derived from Lev and King (1999).

3.1.2. Wright Pass, Richardson Mountains, Yukon, Canada

Eighteen pedons were examined at Wright Pass (Figure 3.1) in 3 groups, each consisting of 3 Turbic Cryosol pedons and 3 Static Cryosol pedons. In this region, the Porcupine Plain is west, and the foothills of the Richardson Mountains are east, of the Dempster Highway. The three clusters of pedons were on the east side of the highway, near kilometers 469 (67.03°N, 136.20°W), 466 (67.01°N, 136.21°W), and 434 (66.87°N, 136.32°W). Two additional pedons were studied on the west side of the highway at Eagle Plains (Figure 3.1) near kilometer 403 (66.58°N, 136.31°W).

3.1.2.1 Geology and Physiographic Setting

The southern Richardson Mountains are a north-south barrier which separates the Mackenzie Delta to the east and the intermontane plateau of the northern Yukon interior to the

west (Duk-Rodkin, 1993). These mountains were a barrier to glaciation, and were not overridden by the Laurentide or Cordilleran ice sheets during the Pleistocene (Duk-Rodkin, 1999; Smith et al., 2004; Smith et al., 1990). As such, the southern Richardson Mountains make up the easternmost edge of Beringia, a vast, unglaciated region extending westward through Alaska (Hughes et al., 1993).

The southern Richardson Mountains rise to elevations of over 1700 m. They are composed primarily of Palaeozoic sedimentary rocks that were folded and uplifted in late Cretaceous or early Tertiary time (Hughes et al., 1993; Smith et al., 1990; Yukon Ecoregions Working Group, 2004). At Wright Pass, bedrock is noncalcareous black marine shale of the Road River Formation. At Eagle Plains, bedrock is noncalcareous siltstone and sandstone of the Imperial Formation (Gordey and Makepeace, 1999; Norris, 1997). Surface deposits are generally residiuum (comprised of locally derived bedrock which has been weathered *in situ*).

3.1.2.2. Climate

Data from July 1995 – June 2011 from the nearby Environment Canada Rock River weather station (66.98°N, 136.22°W) indicate that the mean annual temperature is about -5 °C; however, many data are missing, and the number should be regarded as an estimate. There are no precipitation data available from near the study site, but the Environment Canada weather station at Old Crow, Yukon (67.57°N, 139.84°W) records an annual precipitation of 266 mm, of which 144 mm falls as rain (Environment Canada, 2011).

3.1.2.3. Permafrost

The entire Wright Pass and Eagle Plains region is underlain by continuous permafrost (Burn, 1993; Yukon Ecoregions Working Group, 2004). The active layer is usually 40 – 80 cm thick,

and was about twice as thick near the end of the early Holocene warm period (10,000 – 8,000 yr BP) (Burn, 1993).

3.1.2.4. Vegetation

A complete vegetation survey was not completed, but vegetation at Wright Pass sites commonly included Labrador tea **(***Ledum* spp.), *Carex* spp., crowberry **(***Empetrum* spp.), arctic willow **(***Salix arctica*), dwarf birch **(***Betula nana*), lingonberry (*Vaccinium vitis-adaea*), bearberry **(***Arctostaphylos* spp.), *Dryas octopetala*, *Cassiope tetragona*, fruticose lichens, and acrocarpous mosses. Vegetation cover is largely continuous, except in the centres of nonsorted circles. Vegetation at Eagle Plains was similar, but somewhat more productive, with increased woody plant cover. Additional vegetation included coltsfoot **(***Tussilago farfara*), *Eriophorum vaginatum*, additional sedges, and tussock grasses at Eagle Plains. There were also several isolated stands of stunted black spruce (*Picea mariana*) near the examined pedons at Eagle Plains. Plant cover at Eagle Plains was continuous, except for isolated bare patches on some earth hummock tops.

3.1.2.5. Soils

Soils at Wright Pass are dominantly Regosolic Turbic Cryosols and Orthic Dystric Turbic Cryosols along with Brunisolic Dystric Static Cryosols and Regosolic Static Cryosols. Soils at Eagle Plains are dominantly Gleysolic Turbic Cryosols (Soil Classification Working Group, 1998).

3.2. Pedon Selection and Description

Sampling locations were judgment-based, selected using surface characteristics. Static Cryosol pedons were selected at sites where there was no evidence of patterned ground and relatively little variation in vegetation cover. Turbic Cryosols were located in sites where there

was evidence of patterned ground, either in patterning of vegetation cover or microtopography (Figure 3.3). Upon excavation, four pedons selected as Static Cryosols were found to be in other orders (two Melanic Brunisols, one Dystric Brunisol, and one Regosol); however, this was not because of significant genetic differences in these pedons compared to Static Cryosols, but rather a permafrost depth greater than the 1 m requirement in the CSSC, or a lithic contact before permafrost was reached. Given the similarity of the sola of these pedons to those of surrounding Static Cryosol pedons, they were included as reasonable analogs for Static Cryosols.

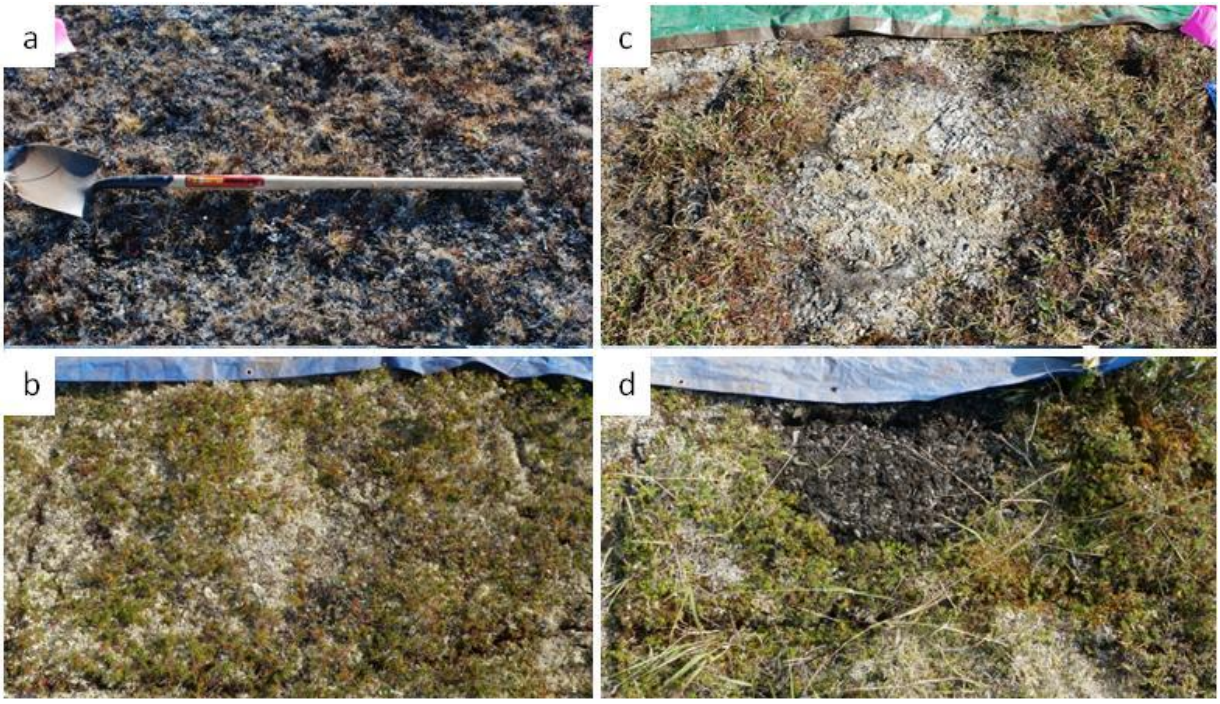

Figure 3.3 – Surface conditions typical of sampled Static Cryosols (a & b) and Turbic Cryosols (c & d). Note the relative uniformity of vegetation cover in (a & b) compared to the heterogeneous vegetation cover in (c & d)

The lateral dimension of examined Static Cryosol pedons was approximately 100 cm. For Turbic Cryosols, the lateral dimension was large enough to include one full cycle of variation in surface characteristics, which generally corresponded to one full cycle of variation in soil characteristics. The patterned ground features were not of uniform size and the lateral dimension of examined Turbic Cryosol pedons varied from 100 to 190 cm, measured from the midpoint of

the intercircle or interhummock region, through the centre of the circle or hummock region, to the midpoint of the next intercircle or interhummock region (Soil Classification Working Group, 1998). This pedon description scheme gives only a two dimensional representation of soil variability; however, given the regularity with which surface patterns occur, it is reasonable to assume a similar degree of variation in other directions as well (Kimble et al., 1993). The vertical dimension examined for pedons from both the Static and Turbic Great Groups was from the highest point of the soil surface to 10 to 15 cm beyond the permafrost table, except where field conditions prohibited excavation into the frozen soil due to high water table or excessive stoniness. Excavation was done by hand to the top of the frozen layer, and beyond the permafrost table using an impact hammer (Tarnocai, 1993). Profiles were described according to the CSSC (Soil Classification Working Group, 1998). A flexible grid with cells 20 cm x 20 cm was overlaid on the profiles and exposed profiles were drawn to scale using the techniques of Kimble et al (Kimble et al., 1993).

3.3. Laboratory and Analytical Methods

Cores of known volume (100 cm^3) were collected from each unfrozen horizon and used to determine volumetric water content and bulk density (Hao et al., 2008). In frozen horizons, the clod method was used (Blake and Hartge, 1986). In a few instances horizons were too rocky to allow for the collection of an intact core or clod. To obtain the best estimate possible for horizons where it was impossible to collect a sample for bulk density (D_b) measurement an empirical equation was developed from a regression of measured properties in horizons from this study for which it was possible to obtain a sample for D_b measurement. Missing D_b values were then interpolated using the regression equation. This model was developed by fitting all

available terms without interactions, then simplifying the model by manual stepwise deletion until all remaining terms were significant ($p<0.05$). The relationship is:

$$D_b = 1.13497 - 0.27406 * ln(OC) - 0.30128 * CF_s + 0.18495 * y \quad (3.1)$$

where D_b is the bulk density (g cm^{-3}), OC is the organic carbon content (%), CF_s is the volumetric proportion of coarse fragments sized between 0.475 cm and 10 cm, and y is a binary variable indicating the presence or absence of cryoturbation ('1' for horizons with a 'y' subscript; '0' for all other horizons). All included terms are highly significant ($p<0.001$), and the R^2 value is 0.63. This regression was developed using horizons for which all data was available, then used to estimate D_b for horizons where it was not possible to obtain a sample for measurement.

Based on soil morphology, Turbic Cryosol pedons were grouped according to similar distribution and shape of horizons and surface forms. For each group, a representative pedon was selected for more intensive study and additional analyses.

Total C, total OC, and total inorganic carbon were determined for all pedons by dry combustion using a LECO C632 Total Carbon Analyzer (LECO Corporation, St. Joseph, MI) after pretreatments according to the methods outlined by Skjemstad and Baldock (2008). Total nitrogen (N) was determined for representative pedons by dry combustion using a LECO Truspec CN Analyzer (LECO Corporation, St. Joseph, MI). Soil pH was determined for representative pedons using a 2:1 water:soil ratio for most samples, and a 5:1 ratio for samples very high in organic matter (Hendershot and Lalande, 2008). Particle size distribution was determined for IS pedons using a Horiba LA-950 Laser Diffraction Particle Size Distribution Analyzer (Horiba Scientific, Edison, NJ) following treatment to remove carbonates and organic matter according to the methods outlined in Kroetsch and Wang (2008).

Whole-soil solid state cross-polarization magic-angle spinning ^{13}C nuclear magnetic resonance (NMR) spectroscopy was performed at the Canada Plant Biotechnology Institute in Saskatoon. Spectra were obtained on a Bruker DRX-400 NMR spectrometer (Bruker BioSpin Ltd, Milton, ON) (B_0 = 8.46 T; $v_L(^1H)$ = 360.119 MHz; $v_L(^{13}C)$ = 90.563 MHz). A solid sample of adamantane with a spinning rate of 2.3 kHz was used for chemical shift referencing and ^1H pulse width calibration. A ^1H π / 2 pulse width of 5.0 ms was found and the adamantane chemical shift of the high frequency ^{13}C NMR signal was set to 38.56 ppm. A 7 mm double-resonance magic-angle spinning probe was used, and the magic angle was set by observing the ^{79}Br free-induction decay signal and maximizing the number of rotational echoes for solid KBr while using a spinning rate of 2.3 kHz. All samples were packed in 7 mm (o.d.) zirconia rotors and spun at 5.0 kHz. A $^1H \rightarrow {}^{13}C$ cross-polarization pulse sequence with a spectral width of 300 ppm, acquisition time of 18.96 ms, contact time of 1.0μs, and pulse delay of 1 s was used to collect data. For each sample, 6144 acquisitions were summed and processed with a 30 Hz exponential multiplication factor. Relative proportions of selected functional groups were determined by chemical shift regions using Bruker Topspin software v. 1.3 (Bruker BioSpin Ltd, Milton, ON). Selected spectral ranges were 0 to 45 ppm to represent AC, 45 to 110 ppm to represent OAC, 110 to 160 to represent AroC, and 160 to 220 to represent CbyC (Baldock et al., 1997; Paré, 2011).

3.4 Carbon Density Calculations

Horizon OC density was calculated for all pedons by:

$$\text{OC Density } (kg\ OC\ m^{-3}) = D_b(g\ cm^{-3}) \times OC(\%) \times 10 \quad (3.2)$$

(Bockheim, 2007). Horizon bulk densities were adjusted for coarse fragments by multiplying by the volumetric proportion of the horizon occupied by particles smaller than 2 mm in diameter.

The volume of particles larger than 4.75 mm in diameter was estimated visually, and the volume of particles 2 – 4.75 mm in diameter was determined gravimetrically. Scale drawings were digitized (Figure 3.4) using ArcGIS (ESRI, 2008) and horizon OC densities were used to create OC density diagrams. Horizon OC densities were multiplied by horizon areas to determine horizon OC content, and these products were summed to determine pedon OC content. Pedon OC content was normalized by the pedon width to calculate OC content on a m^2 basis, assuming similar variation in all lateral directions (Kimble et al., 1993). To calculate OC content for portions of pedons, only the portions of each horizon falling within the depth increment of interest were included.

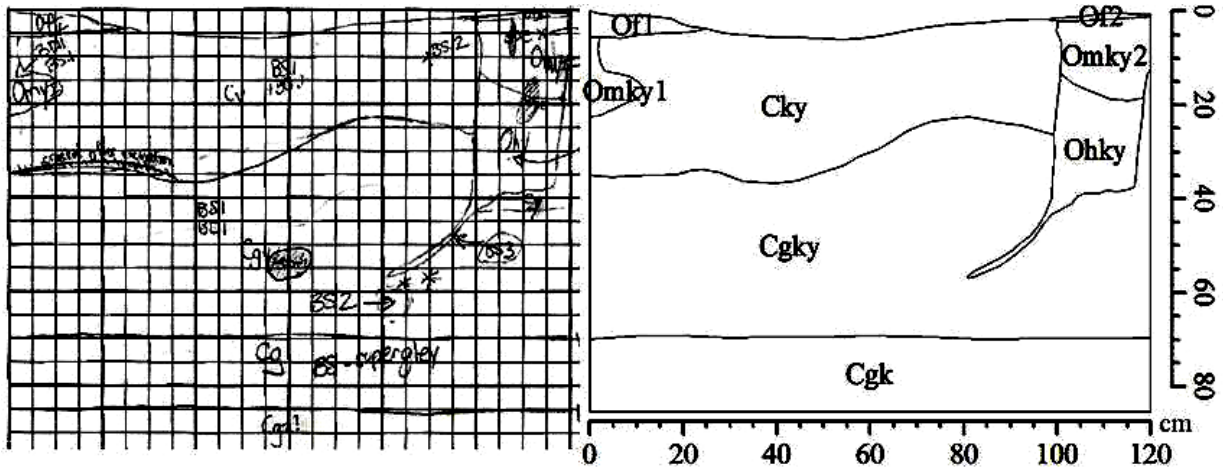

Figure 3.4 Scale drawing created in the field (left) and digitized into a GIS (right)

Organic carbon density profiles (Figure 4.1) were constructed for all pedons by summing the OC content for the portions of horizons present within 1 cm depth intervals. This interval was chosen to reflect the approximate maximum resolution available in scale drawings. Larger increments would have ignored small, but important horizons. To simplify the creation of these high-resolution depth increments, OC density diagrams were rasterized using maximum area cell assignment and 1 cm^2 cell size (ESRI, 2008). These rasters were then imported into a spreadsheet for simple graphing and calculations. Profiles of OC density are presented in

g OC m^{-2} cm^{-1}, which should be interpreted as the amount of OC in an average square meter of surface area for one-centimeter depth increments.

4. RESULTS

4.1. Organic Carbon Mass

Organic carbon masses for several depth increments were calculated for all pedons at Truelove Lowland and Wright Pass. A summary of these results is presented in the following section; for a detailed table of OC masses for each pedon, see Appendix 8.2.

4.1.1. Truelove Lowland

Mean OC masses and p-values from t-test comparisons of Static Cryosols and Turbic Cryosols for Truelove Lowland are presented in Tables 4.1 and 4.2. There was no significant difference in OC mass between Static Cryosols and Turbic Cryosols for any of the cumulative depth increments considered.

Table 4.1 Mean OC masses for Truelove Lowland for cumulative depth increments.

depth range (cm)	Static Cryosols		Turbic Cryosols		p†
	mean OC mass (SE) (kg OC m^{-2})	n	mean OC mass (SE) (kg OC m^{-2})	n	
0 to 25	2.7 (0.9)	5	2.9 (0.6)	5	0.861
0 to 50	3.3 (1.0)	5	4.7 (0.9)	5	0.319
0 to 75	4.3 (1.5)	4	5.3 (1.5)	3	0.671
0 to 100	5.5 (2.3)	3	4.5 (1.0)	2	-

† p-values are the result of a t-test comparison

The lack of significant differences for comparisons of mean OC mass of cumulative depths suggests that there is no difference in the depth distribution of OC in mineral Cryosols at Truelove Lowland; however, a significant difference emerges when comparisons are made on the basis of discrete depth increments rather than cumulative depths (Table 4.2). There is no significant difference in the OC mass of Static Cryosols and Turbic Cryosols for the 0-to-25- and

50-to-75-cm depth increments, but Turbic Cryosols have approximately double the OC mass of Static Cryosols in the 25-to-50-cm increment.

Table 4.2 Mean OC Masses for Truelove Lowland for discrete depth increments.

depth range (cm)	Static Cryosols		Turbic Cryosols		p†
	mean OC mass (SE) (kg OC m^{-2})	n	mean OC mass (SE) (kg OC m^{-2})	n	
0 to 25	2.7 (0.9)	5	2.9 (0.6)	5	0.861
25 to 50	0.6 (0.1)	5	1.8 (0.4)	5	**0.035**
50 to 75	0.9 (0.2)	4	1.1 (0.3)	3	0.713
75 to 100	0.9 (0.2)	3	0.6 (0.1)	2	-

† p-values are the result of a t-test comparison. Significant values ($p < 0.1$) are bolded

4.1.2. Wright Pass

Significant differences ($p < 0.1$) in OC mass between Static Cryosols and Turbic Cryosols were detected for the 0-to-75- and 0-to-100-cm depth increments, but not for the 0-to-25- or 0-to-50-cm depth increments (Table 4.3).

Table 4.3 Mean OC masses for Wright Pass for cumulative depths increments.

depth range (cm)	Static Cryosols			Turbic Cryosols		p‡	p†‡
	mean OC mass (SE) (kg OC m^{-2})	n	mean OC mass (SE)† (kg OC m^{-2})	mean OC mass (SE) (kg OC m^{-2})	n		
0 to 25	5.8 (1.8)	9	4.1 (0.8)	4.2 (0.8)	9	0.438	0.950
0 to 50	7.6 (2.7)	9	5.1 (0.9)	7.5 (1.3)	9	0.965	0.150
0 to 75	6.4 (1.2)	6		10.4 (1.8)	9	**0.095**	
0 to 100	7.6 (1.8)	5		17.6 (2.0)	3	**0.014**	

†Calculated with outlier pedon WPSC14 excluded

‡ p-values are the result of a t-test comparison. Significant ($p < 0.1$) values are bolded.

Table 4.4 Mean OC masses for Wright Pass soils for discrete depth increments

depth range (cm)	Static Cryosols			Turbic Cryosols		p‡	p†‡
	mean OC mass (SE) (kg OC m^{-2})	n	mean OC mass (SE)† (kg OC m^{-2})	mean OC mass (SE) (kg OC m^{-2})	n		
0 to 25	5.8 (1.8)	9	4.1 (0.8)	4.2 (0.8)	9	0.438	0.950
25 to 50	1.8 (0.9)	9	0.9 (0.2)	3.3 (0.6)	9	0.209	**0.006**
50 to 75	0.9 (0.2)	6		2.9 (0.8)	9	**0.032**	
75 to 100	1.1 (0.3)	5		4.7 (1.0)	3	**0.056**	

†Calculated with outlier pedon WPSC14 excluded
‡ p-values are the result of a t-test comparison. Significant ($p < 0.1$) values are bolded.

Among the Wright Pass pedons, the WPSC14 pedon had OC masses 4.7 times greater and 10 times greater than the means for the other Static Cryosols for the 0-to-25- and 25-to-50-cm depth increments, respectively (see Appendix 8.2 for details for each pedon). Field observations indicate that this pedon had thicker O and A horizons than other pedons; however, there was no reason observed for why these thick horizons occurred at this pedon and not others. Comparisons were also performed without this pedon included. When pedon WPSC14 was removed from the analysis the comparisons for the 0-to-25- and 0-to-50-cm depth increments changed substantially (Table 4.3); however, statistical comparisons for these depth increments were still not significant, though the p-value dropped to 0.150 for the 0-to-50-cm depth increment. For discrete depth increments, the 25-to-50-cm depth increment changed substantially when pedon WPSC14 was excluded (Table 4.4). The 25-to-50-cm depth increment comparison showed a significant difference ($p = 0.006$), indicating that the high OC content of the WPSC14 pedon was likely masking a significantly higher OC content in Turbic Cryosols at this depth. These results show that, generally, there is a similar amount of OC near the surface in Static Cryosols and Turbic Cryosols at Wright Pass, but there is significantly more OC in Turbic Cryosols at depths greater than 25 cm within the active layer.

4.2. Representative Pedons

Based on the characteristics of Turbic Cryosol pedons examined, it was possible to create categories of pedons based on similar subsurface and surface features and similar OC density profile shapes. A typical pedon was selected from each group for additional analyses. A typical Static Cryosol is also discussed below.

4.2.1. Turbic Cryosols With Inward Curving Vertical Horizons (TLTC03)

A group of 3 pedons (TLTC02, TLTC03, and TLTC04) found at Truelove Lowland can be described as Turbic Cryosols with inward curving vertical horizons (see Figure 4.1 for TLTC03, Appendix 8.1 for others). On the surface, these pedons are all nonsorted circles. In cross-section, OC-rich horizons occur underneath the vegetated edges of nonsorted circles, while OC-poor horizons are found below the barren centres of nonsorted circles. These OC-rich horizons extend downwards to depths of about 55 cm, eventually curving inwards toward the centre of the pedon. OC-rich horizons do not extend completely through the active layer and into the permafrost, though they do extend to the perched water table at a depth of 55 cm in pedon TLTC04. The OC density profiles have an OC density of 150 to 250 g OC m^{-2} cm^{-1} at 10 cm depth. The OC density remains approximately at this level until about 40 cm depth, at which point it rapidly drops to 35 g OC m^{-2} cm^{-1} in pedon TLTC02, and about 70 g OC m^{-2} cm^{-1} in pedons TLTC03 and TLTC04. Pedons TLTC03 and TLTC04 had gleyed horizons and standing water at depths below 40 cm, whereas the TLTC02 pedon did not.

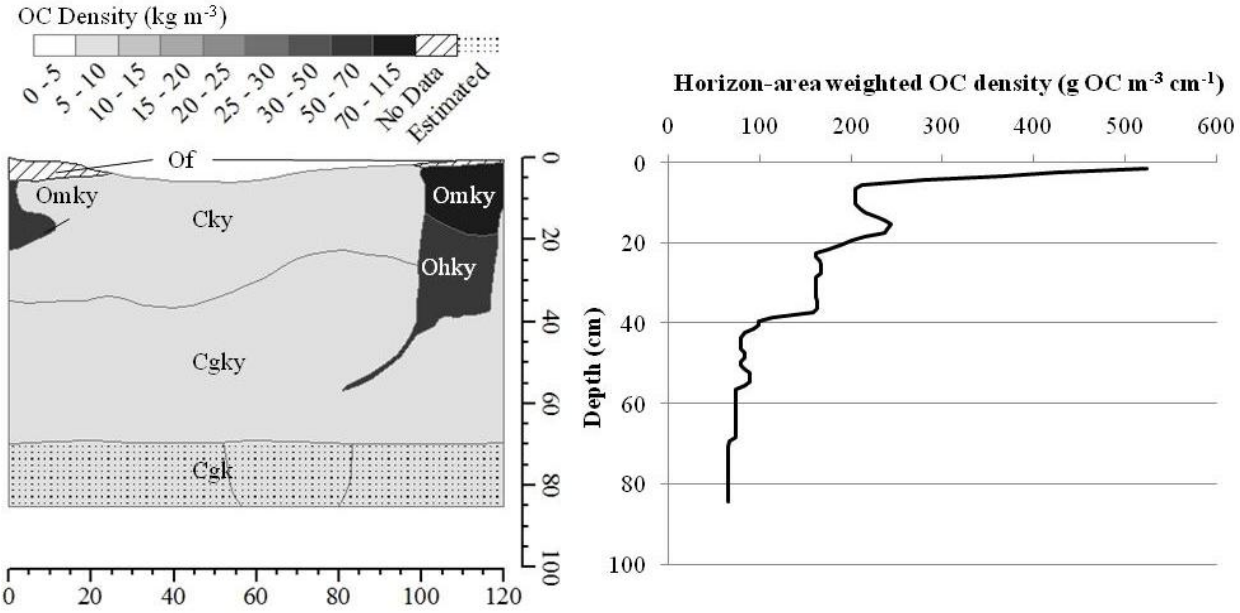

Figure 4.1 OC Density diagram (left) and profile (right) for the TLTC03 pedon at Truelove Lowland, representative of the 'Turbic Cryosols with inward curving vertical horizons' group. The profile is created by aggregating the OC densities in the diagram in 1 cm depth increments. Horizon OC densities are weighted by horizon areas falling within the depth increment when performing the aggregation calculation.

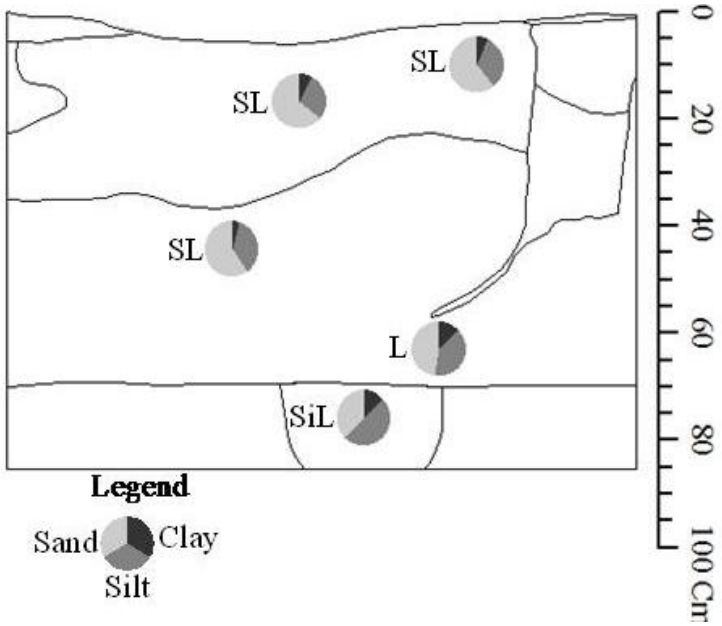

Figure 4.2 Particle size distributions of selected samples from the TLTC03 pedon. Charts are placed on the pedon diagram according to the location of sampling. Labels give textural class: SiL = silt loam, L = loam, SL = sandy loam

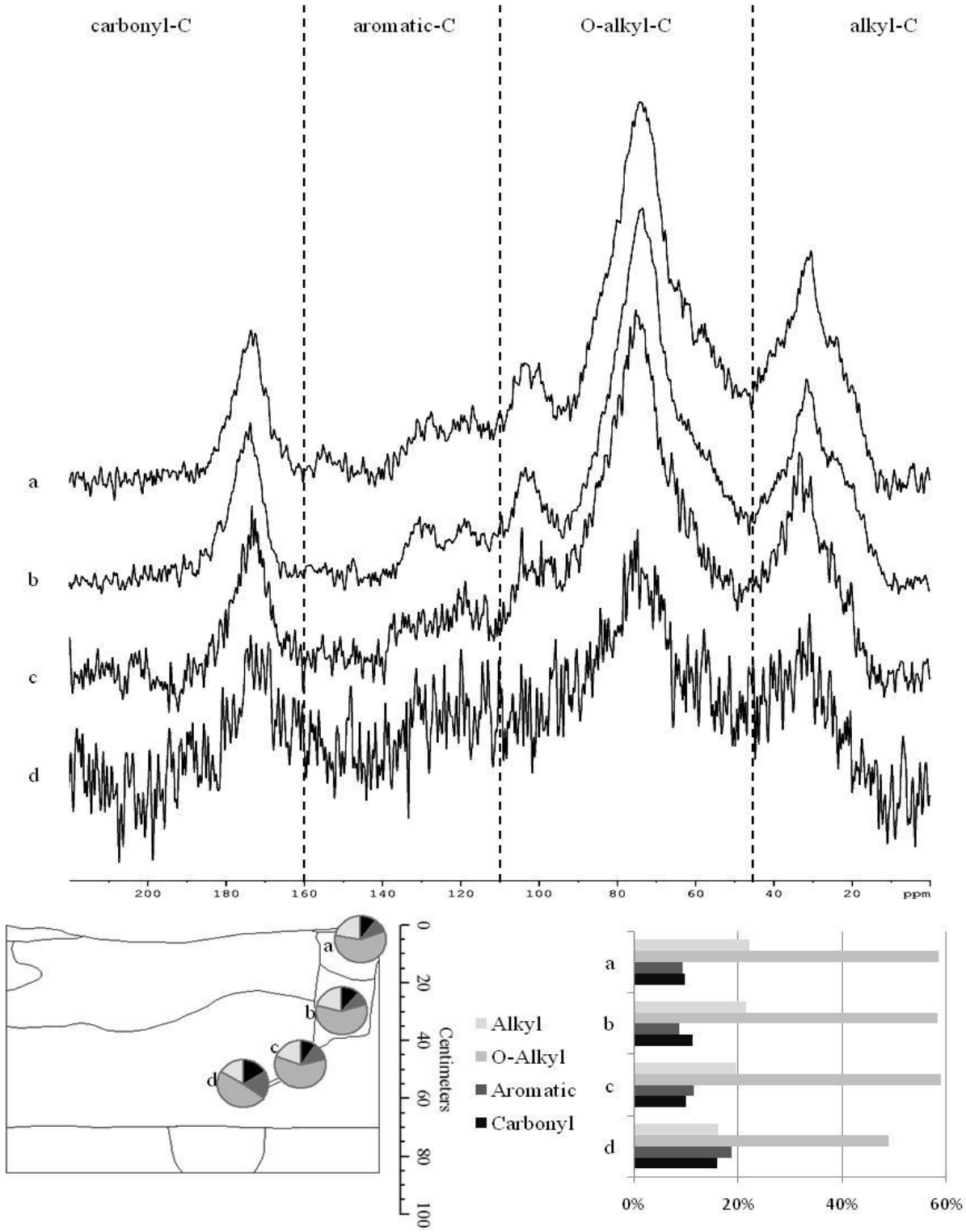

Figure 4.3 Spectra (top) and C category proportions (bottom) for NMR analyses for selected samples in the TLTC03 pedon. Pie charts are placed on the pedon diagram according to the location of sampling. Lowercase letters refer to samples labeled in the diagram at the lower left and given in text as TLTC03a, TLTC03b, TLTC03c, and TLTC03d.

There is little difference in the proportions of CbyC, AroC, OAC, and AC in samples TLTC03a and TLTC03b (Figure 4.3, Table 4.5). Samples TLTC03c and TLTC03d have a slightly higher OAC:AC than samples TLTC03a and TLTC03b. C:N ratios were relatively consistent at ~16.5 in the OC-rich horizons. There is a slight increase in AroC and AC in samples TLTC03c and TLTC03d; however, this may be partly due to a reduced signal:noise ratio in the deeper samples containing less OC (Figure 4.3).

The texture of pedons in this category was generally sandy. In pedon TLTC03, the proportion of fines increased with depth, and texture ranged from sandy loam at the soil surface to silt loam in the upper permafrost (Figure 4.2).

Table 4.5 NMR and C:N results for TLTC03 pedon. †

	CbyC	AroC	OAC	AC	OC	OAC:AC	C:N
			%				
a	9.9	9.4	58.5	22.2	30.9	2.6	16.6
b	11.3	8.8	58.3	21.6	30.4	2.7	15.9
c	9.9	11.6	58.9	19.6	14.9	3.0	16.3
d	16.1	18.9	48.9	16.2	7.9	3.0	16.5

† Lowercase letters at left refer to samples labeled in Figure 4.3 and given in text as TLTC03a, TLTC03b, TLTC03c, and TLTC03d. Categories are carbonyl C (CbyC), aromatic C (AroC), O-alkyl C (OAC), and alkyl C (AC)

4.2.2. Turbic Cryosols With Highly Mixed Horizons (TLTC05)

Two pedons, TLTC05 and WPTC09 (see Figure 4.4 for TLTC05, Appendix 8.1 for WPTC09) had OC-rich horizons that were highly mixed and streaked with material from other horizons. Pedons within this category did not have similar textures. The WPTC09 pedon had high silt content, and a texture of approximately silt loam. The texture of pedon TLTC05 is generally sandy and ranges from sandy loam to sand (Figure 4.5). There was no clear depth pattern to the particle size distribution in TLTC05; however, the areas of the pedon with the highest proportions of silts and clays tended to be the portions of the pedon that were most

highly mixed, while the areas with the highest proportions of sand tended to be the less thoroughly mixed C horizons.

In Turbic Cryosols with highly mixed horizons, OC-rich horizons were preferentially located under the areas with the densest plant growth (i.e. the areas between nonsorted circles); however, they were not confined to these areas. In both pedons the OC-rich horizons were confined to the top 30-40 cm of the pedon (Figure 4.4). In pedon TLTC05, this was the top of the permafrost, whereas in pedon WPTC09 this included only the top half of the active layer. The OC density profiles for these pedons are similar, showing an OC density of 350 to 400 g OC m^{-2} cm^{-1} in the first 5 cm of the soil. The OC density is steady or gradually dropping to 30 to 40 cm depth, at which point it drops rapidly to about 40 g OC m^{-2} cm^{-1} for the remainder of the pedon.

The C:N ratios are highly variable in the OC-rich horizons of pedon TLTC05. The surface Of horizon had a C:N of 15, and the C:N of cryoturbation-affected A and B horizons varied from 7.4 to 22.3, reflecting the highly mixed and streaked appearance of the horizons in this pedon that situates high-OC content soil immediately adjacent to low-OC content soil in the same horizon. The mean coefficient of variation of OC content in cryoturbation-affected A and B horizons of pedons in this category was 0.55, compared with 0.23 in other Turbic Cryosols. Because of the complex mixture of various types of OC in this pedon, and the analytical cost involved, NMR spectra were not obtained for this pedon.

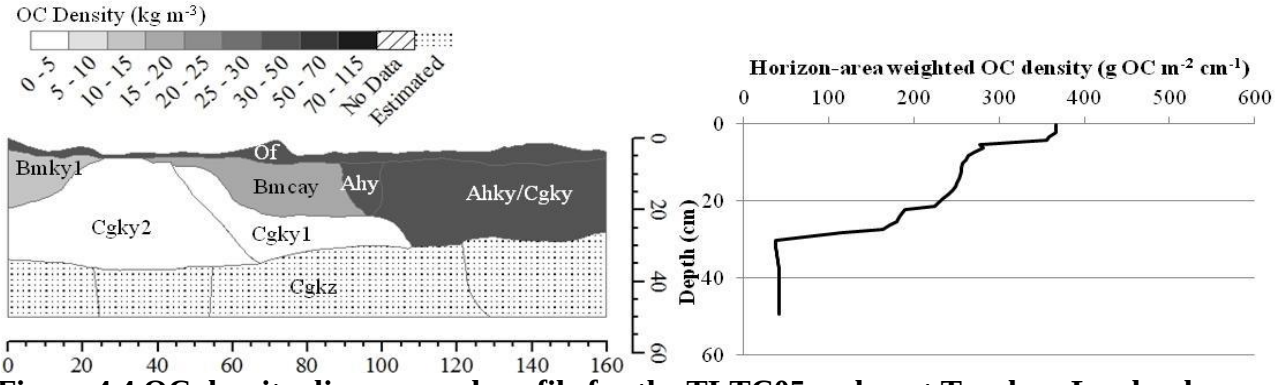

Figure 4.4 OC density diagram and profile for the TLTC05 pedon at Truelove Lowland, representative of the 'Turbic Cryosols with highly mixed horizons' group. The profile is created by aggregating the OC densities in the diagram in 1 cm depth increments. Horizon OC densities are weighted by horizon areas falling within the depth increment when performing the aggregation calculation.

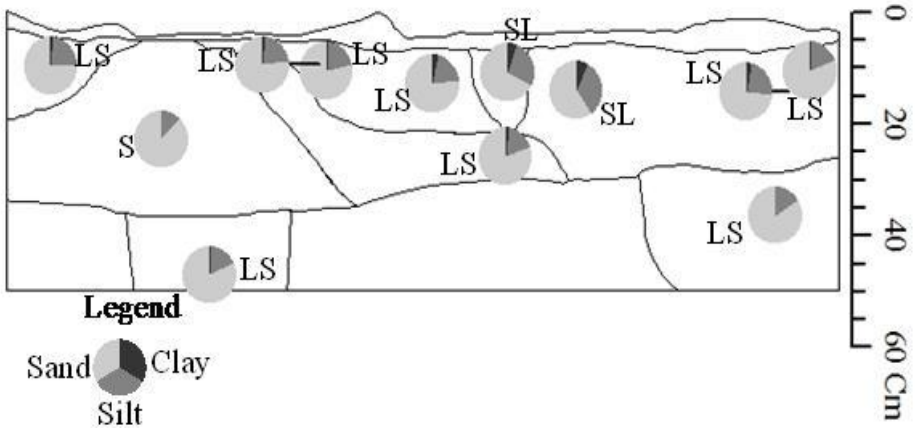

Figure 4.5 Particle size distributions of selected samples from the TLTC05 pedon. Charts are placed on the pedon diagram according to the location of sampling. Labels give textural class: SL = sandy loam, LS = loamy sand, S = sand

4.2.3. Turbic Cryosols With Dominantly Vertical Horizons (WPTC11)

Several pedons (TLTC01, WPTC06, WPTC07, WPTC10, and WPTC11) had OC-rich horizons that were dominantly vertical in cross-section (see Figure 4.6 for WPTC11, Appendix 8.1 for others). These OC-rich horizons were aligned with vegetated areas at the edges of nonsorted circles. The vegetated inter-circle areas had relatively uniform vegetation cover, but often appeared to be less productive at pedons in this group than at other nearby Turbic Cryosol pedons. These pedons are distinct from the TLTC03 group because OC-rich horizons in the

WPTC11 group do not curve inwards with depth, but rather are oriented vertically through the entire pedon. The OC-rich horizons may become wider or narrower with depth, and do not show streaking like that of pedons in the TLTC05 group. Most pedons in this group had more than 10 cm of standing water in the bottom of the soil pit or strongly gleyed features near the permafrost table. The OC-rich horizons generally extended to the saturated or gleyed layer, but in the instances where it was possible to excavate and observe beyond this point the OC-rich horizons did not appear to continue much deeper. The OC density profile of these pedons shows high variability near the soil surface; at 3 cm depth pedons WPTC06, WPTC07 and WPTC11 had 180 to 380 g OC m^{-2} cm^{-1} while pedons TLTC01 and WPTC10 both had less than 100 g OC m^{-2} cm^{-1}. This difference was caused by a decreased prevalence (i.e. smaller cross-sectional area) of surface O and A horizons in pedons TLTC01 and WPTC10 relative to the rest of the pedons in the group. By 20 cm depth, all pedons in this category had less than 85 g OC m^{-2} cm^{-1} with the exception of WPTC07 which had 111 g OC m^{-2} cm^{-1}, again caused by the thicker O and A horizons. OC Densities for all pedons remain between 25 and 110 g OC m^{-2} cm^{-1} for the remainder of the examined depth. The horizontal 'band' of low OC density near the surface in pedon WPTC11 (Figure 4.6) is not due to exceptionally low OC content in the fine fraction, but rather to an exceptionally high coarse fragment content in this layer and thus a low D_b and a low OC density as calculated by Equation 3.2. Indeed, high coarse fragment content seems to be a unifying characteristic in this group, as Turbic Cryosols in this category contained a mean of 65% coarse fragments by volume in each horizon, while other Turbic Cryosol pedons from Truelove Lowland and Wright Pass contained 35% coarse fragments by volume in each horizon.

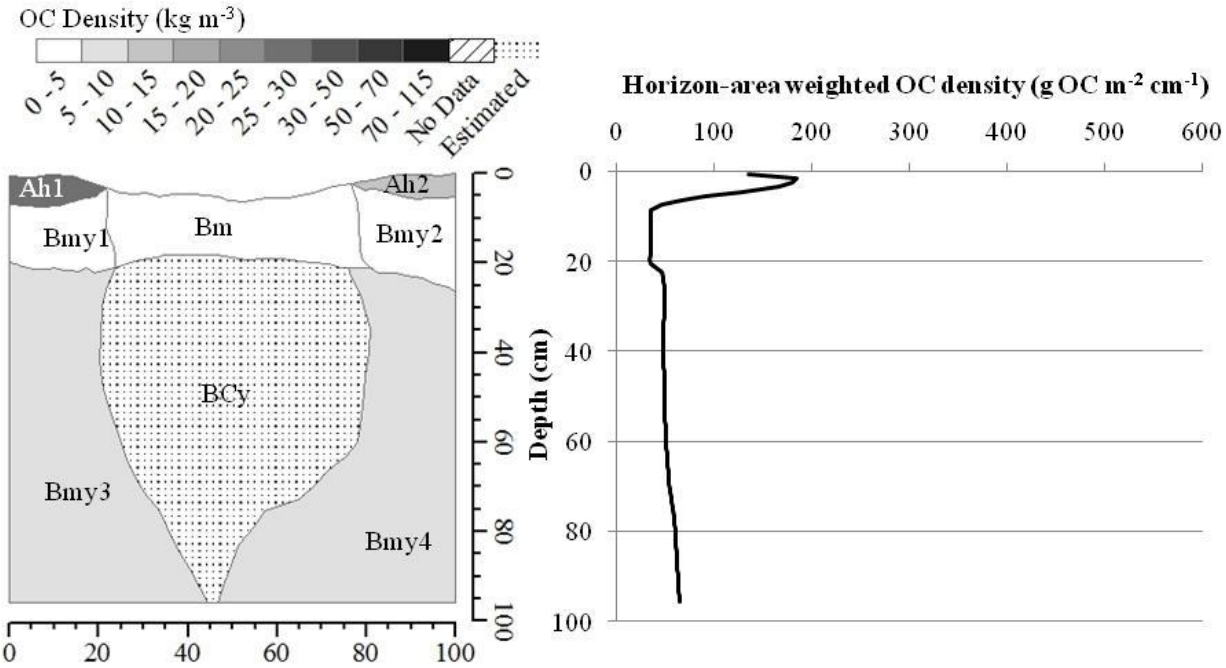

Figure 4.6 OC density diagram and profile for the WPTC11 pedon at Wright Pass, representative of the 'Turbic Cryosols with dominantly vertical horizons' group. The profile is created by aggregating the OC densities in the diagram in 1 cm depth increments. Horizon OC densities are weighted by horizon areas falling within the depth increment when performing the aggregation calculation.

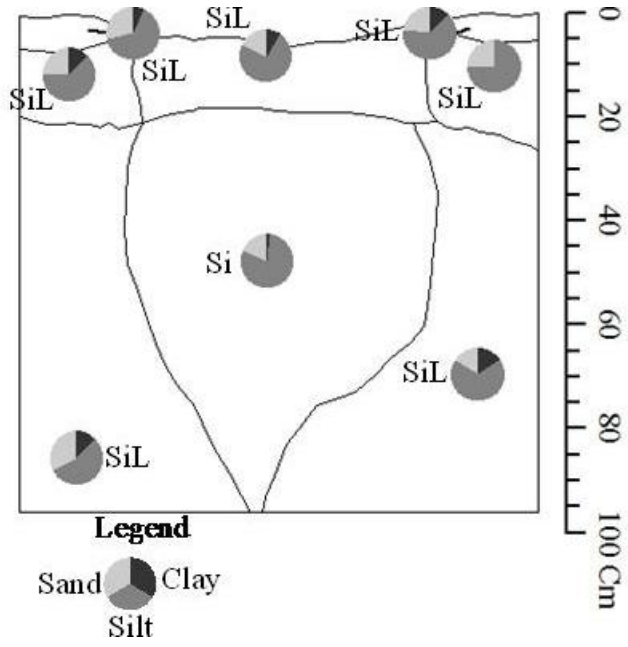

Figure 4.7 Particle size distributions of selected samples from the WPTC11 pedon. Charts are placed on the pedon diagram according to the location of sampling. Labels give textural class: SiL = silt loam, Si = silt

The WPTC11 pedon was very silty, with textures ranging from silt to silt loam (Figure 4.7). The areas of the pedon with highest proportions of silt were in the centre of the pedon under the barren nonsorted circle.

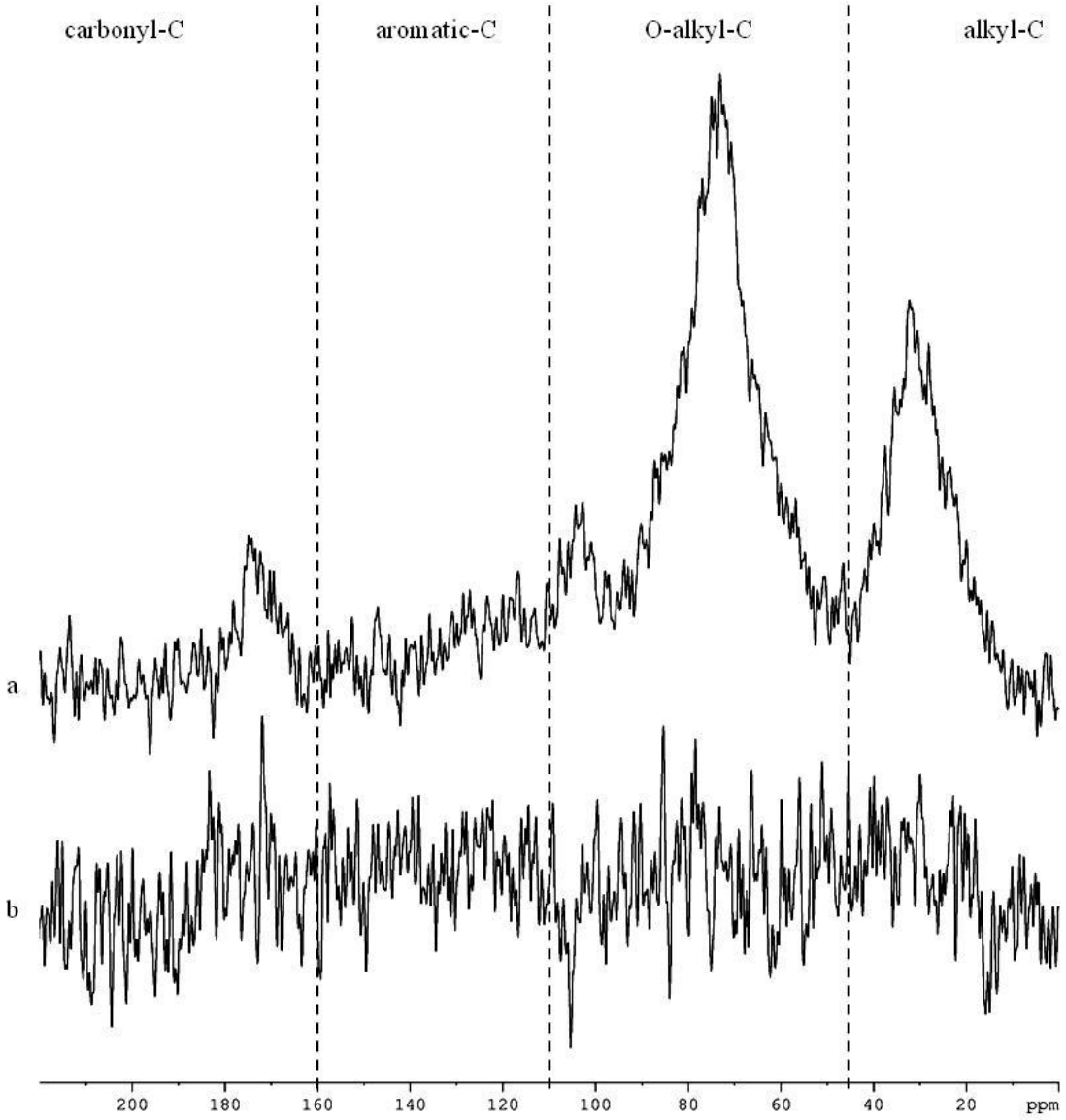

Figure 4.8 Spectra for NMR analyses for selected samples in the WPTC11 pedon. Spectrum a was obtained using a sample from 5 cm depth in the Ah1 horizon and spectrum b was obtained using a sample from 85 cm depth in the Bmy3 horizon (see Figure 4.6).

Soil NMR results were obtained for samples in the Ah1 and Bmy3 horizons (top and bottom of Figure 4.8, repectively); unfortunately, the signal:noise ratio was too poor in the deeper

sample to provide useful data, and it was thus discarded. The near-surface sample from the Ah1 horizon had a much higher proportion of OAC (60.2%) than AC (25.0%), and relatively low proportions of AroC (8.5%) and CbyC (6.34%), suggesting that relatively undecomposed OC is present in this horizon. Surface A horizons in the WPTC11 pedon had C:N ratios of 17.6 and 12.4, while the C:N ratios of B horizons ranged from 4.5 to 7.8, with a mean value of 6.4.

4.2.4. Turbic Cryosols With Hummock Surface Forms (EPTC15)

Pedons EPTC15 and EPTC16 (see Figure 4.9 for EPTC15, Appendix 8.1 for EPTC16) had a hummock surface form, not a nonsorted circle form as Turbic Cryosols at Truelove Lowland and Wright Pass had. The pedons had nearly continuous vegetative cover over the entire feature, though the EPTC16 pedon had a small barren patch near the top of the hummock. In cross section, thin OC-rich horizons occur on the sides of the hummocks, while thick OC-rich horizons occur in the depressions between hummocks and a thick OC-rich horizon is found along the permafrost boundary. The pedon was excavated as deeply as time and logistical constraints allowed, but the C horizon was not reached below the thick OC-rich horizon at the base of the active layer. It is clear that the Bmyz horizons continued at least a few centimeters past the depth of excavation, but the total depth is not known. Horizons relatively poor in OC (1.8 to 2.4 % OC) were found in the middle of the hummock, though this soil was generally higher in OC than OC poor horizons in representative pedons from Truelove Lowland (0.4 to 0.7 % OC) and Wright Pass (0.7 % OC).

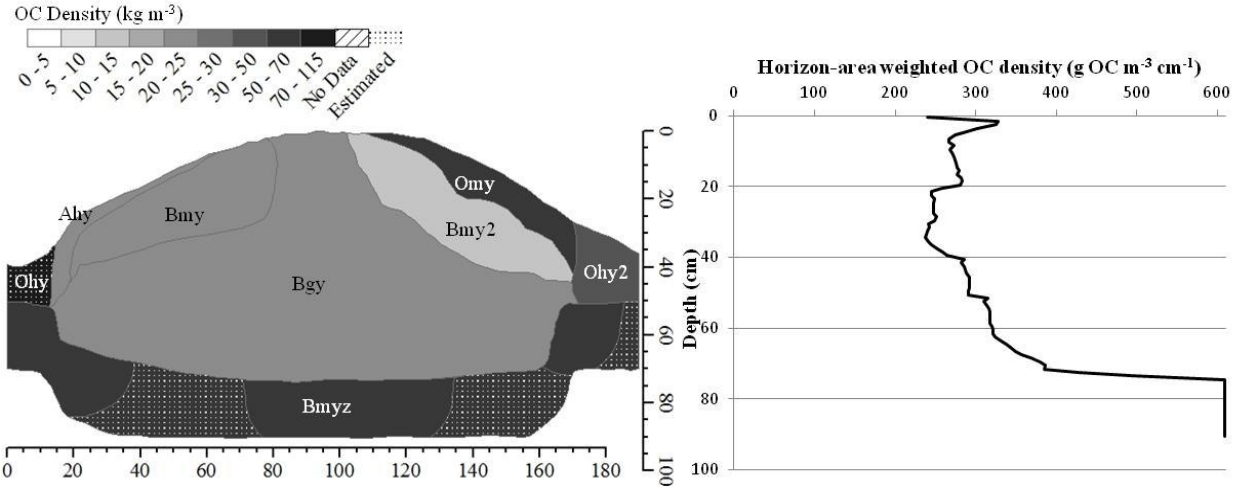

Figure 4.9 OC density diagram and profile for the EPTC15 pedon at Eagle Plains, representative of the 'Turbic Cryosols with hummock surface forms' group. The profile is created by aggregating the OC densities in the diagram in 1 cm depth increments. Horizon OC densities are weighted by horizon areas falling within the depth increment when performing the aggregation calculation.

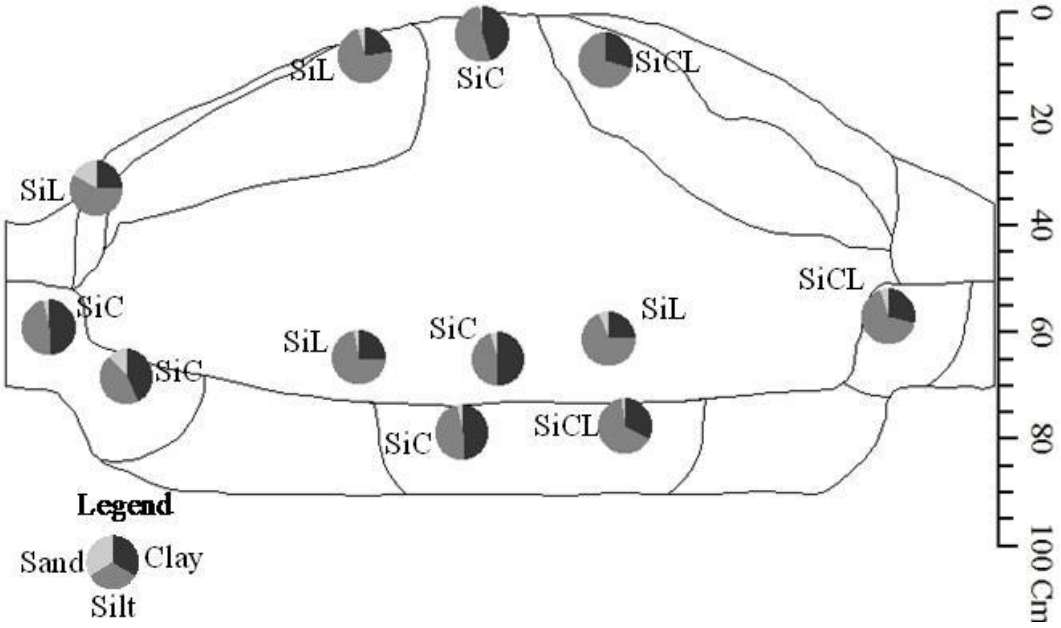

Figure 4.10 Particle size distributions of selected samples from the EPTC15 pedon. Charts are placed on the pedon diagram according to the location of sampling. Labels give textural class: SiC = silty clay, SiCL = silty clay loam, SiL = silt loam

Interpretation of the OC density profiles from hummock pedons such as EPTC15 (Figure 4.9) is less straightforward than others in this study. The goal of these diagrams is to evaluate the depth distribution of OC; however, depth in these pedons is measured from the top of the

hummock, not the soil surface at other points across the pedon. An alternative would be to adjust the OC density profile so that distance from the permafrost table is used instead of depth, as this would represent similar soil conditions in various parts of the pedon in terms of soil temperature and degree of water saturation. Calculations based on distance from the permafrost table altered the shape of the OC density profile little, and the OC density diagram and profile were left in their original forms to allow easier comparison with other pedons included in the study. It should also be noted that OC density profiles for these pedons show an area weighted average of OC density, and the total OC density for a given depth will also depend on the width of the pedon within that depth increment. Nonetheless, the key feature is immediately evident in the OC density diagram and profile: OC density is relatively high through much of the depth range examined, and stays high or increases in the upper permafrost. The EPTC15 pedon was dominated by silt-sized particles, along with substantial amounts of clay. Texture ranged from silt loam to silty clay (Figure 4.10). The areas with the largest proportion of clay (i.e. the silty clays) were along the top of the permafrost in the Bmyz horizon and in a channel extending up the middle of the pedon.

Results from NMR analysis and C:N determination are presented in Figure 4.11 and Table 4.5. The near surface sample EPTC15a is high in OAC and relatively low in AC. Samples EPTC15b, EPTC15c, and EPTC15d still have a large proportion of OAC, but AC is also high.

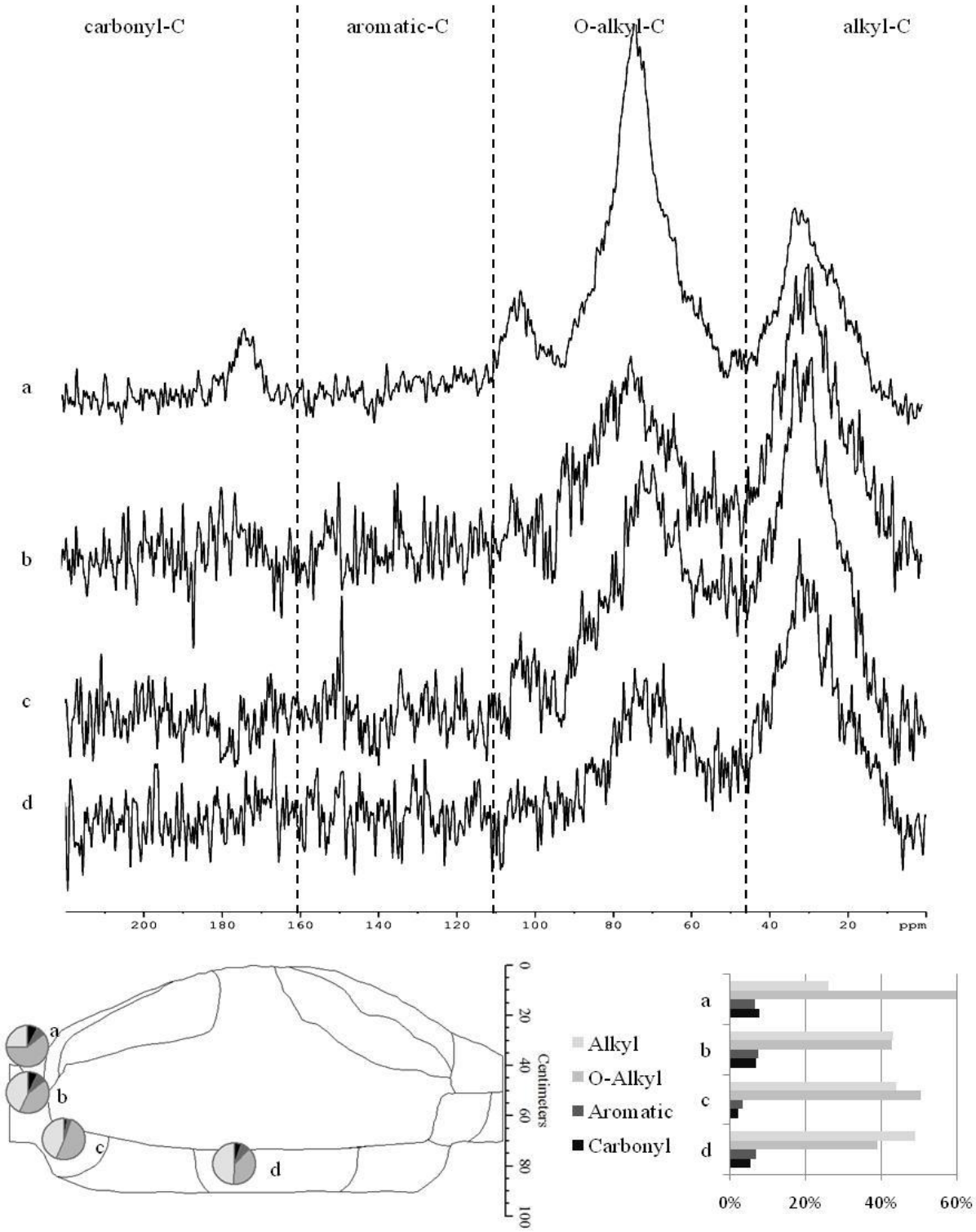

Figure 4.11 Spectra (top) and C category proportions (bottom) for NMR analyses for selected samples in the EPTC15 pedon. Pie charts are placed on the pedon diagram according to the location of sampling. Lowercase letters refer to samples labeled in the diagram at the lower left and given in text as EPTC15a, EPTC15b, EPTC15c, and EPTC15d.

Table 4.6 NMR and C:N results for EPTC15 pedon†

	CbyC	AroC	OAC	AC	OC	OAC:AC	C:N
			%				
a	7.6	6.6	59.9	25.9	18.0	2.3	25.1
b	6.9	7.3	42.8	43.0	6.2	1.0	14.7
c	2.1	3.3	50.5	44.0	7.3	1.2	17.9
d	5.3	6.7	39.0	49.0	5.8	.8	15.3

† Lowercase letters at left refer to samples labelled in Figure 4.11 and given in text as EPTC15a, EPTC15b, EPTC15c, and EPTC15d. Categories are carbonyl C (CbyC), aromatic C (AroC), O-alkyl C (OAC), and alkyl C (AC)

4.2.5. A Typical Static Cryosol (WPSC07)

Pedon WPSC07 (Figure 4.12) is a Static Cryosol typical of those seen at Truelove Lowland and Wright Pass. Static Cryosols were generally drier, and often stonier than nearby Turbic Cryosols. Plant cover at a typical Static Cryosol was homogeneous (i.e. there were no large barren patches). The mean depth to frozen soil was only marginally greater in Static Cryosols (86 cm) than Turbic Cryosols (79 cm), though it was highly variable depending on local moisture, organic matter, and coarse fragment conditions. The highest OC density in Static Cryosols occurs at and near the soil surface in O and/or A horizons. The OC density quickly drops with depth, usually dropping to 20 to 60 g OC m^{-2} cm^{-1}) by 10 to 30 cm depth. This OC density profile shape of a high (~175 g OC m^{-2} cm^{-1} at Truelove Lowland, ~325 g OC m^{-2} cm^{-1} at Wright Pass) start followed by a rapid drop within the first few decimeters was typical of nearly all Static Cryosols examined in this study.

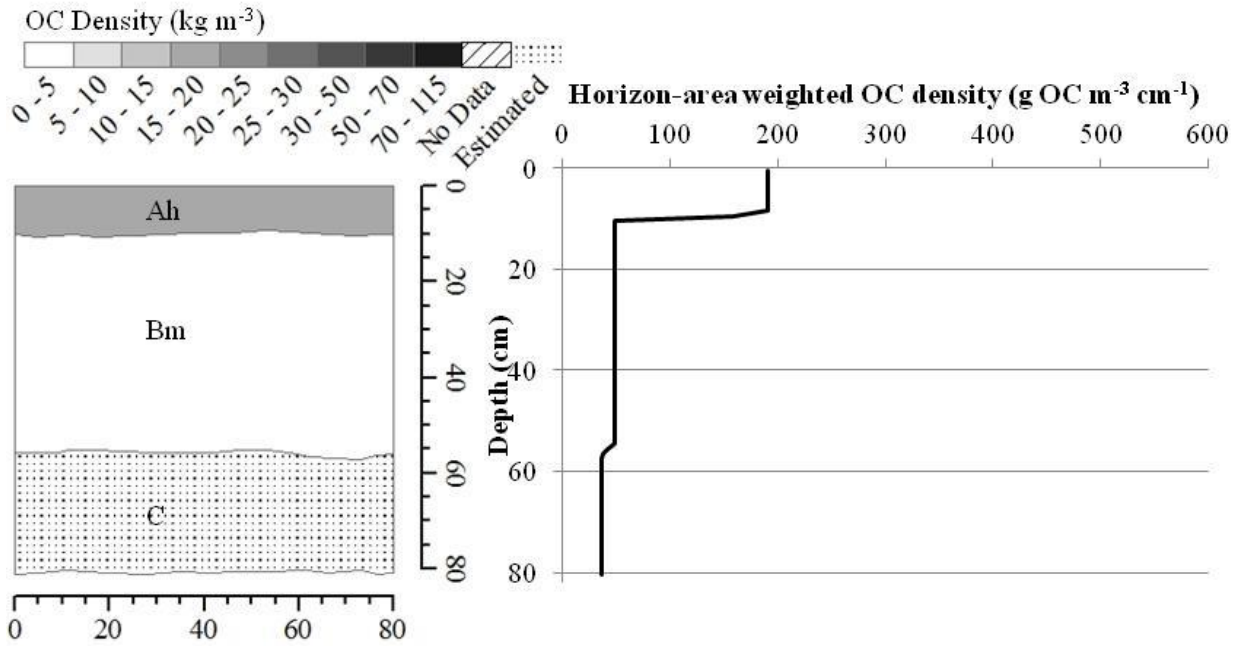

Figure 4.12 OC density diagram and profile for the WPSC07 pedon at Truelove Lowland, representative of the 'Static Cryosols' group. The profile is created by aggregating the OC densities in the diagram in 1 cm depth increments. Horizon OC densities are weighted by horizon areas falling within the depth increment when performing the aggregation calculation.

4.3. Organic Carbon Density Profiles

When conventional cumulative depths were used for OC comparisons, no significant differences were detected between Static Cryosols and Turbic Cryosols at Truelove Lowland, and significant differences ($p<0.1$) were detected at Wright Pass when depths greater than 50 cm were included in the comparison (Tables 4.1 and 4.3). When discrete depth increments of 25 cm thickness were considered (Tables 4.2 and 4.4), significant differences were detected for 25 to 50 cm at Truelove Lowland, and 50 to 100 cm at Wright Pass (25 to 100 cm when an outlier pedon was excluded from analysis). When GIS-based high depth-resolution techniques were used (Figures 4.13 and 4.14), however, differences between Static Cryosols and Turbic Cryosols were observed for depth ranges of 20 to 45 cm at Truelove Lowland, and 49 to 90 cm depth at Wright Pass (12 to 90 cm when an outlier pedon was excluded from the analysis).

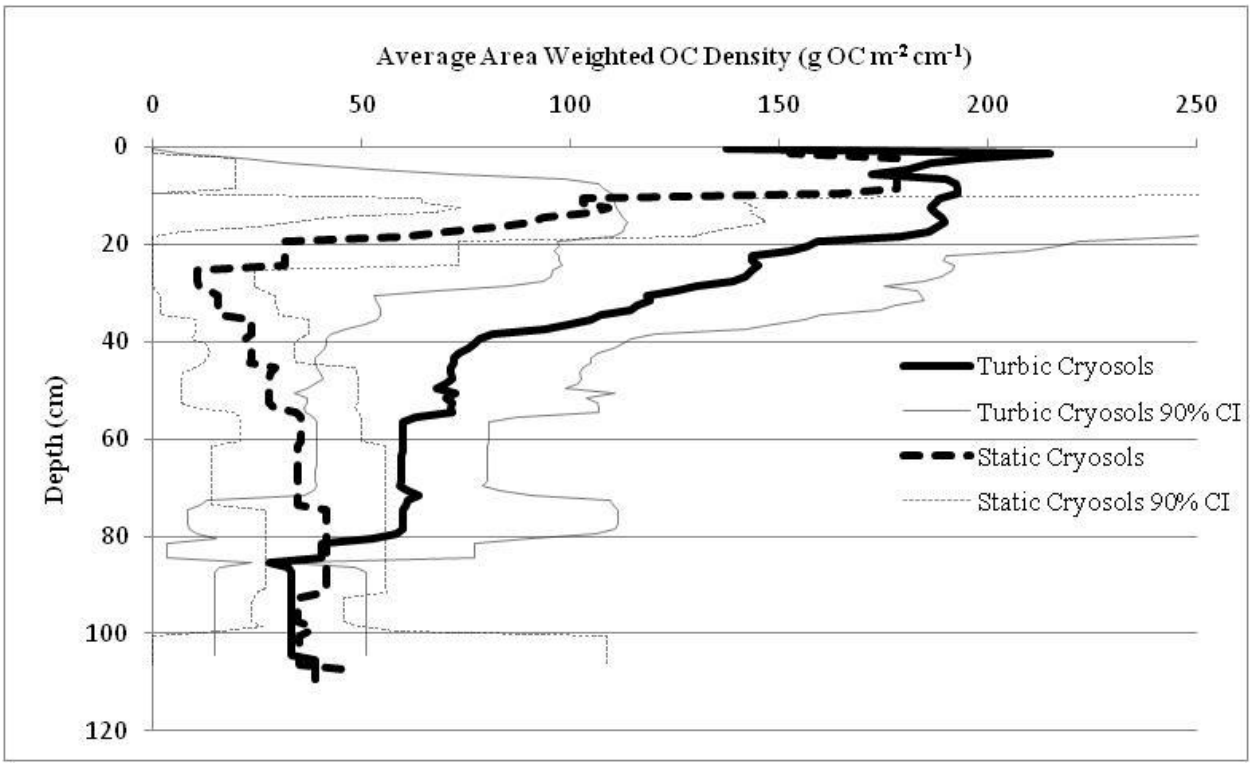

Figure 4.13 Average OC density profiles from Truelove Lowland. Thick lines represent the average profile, while thin lines are 90% confidence intervals of the mean

Using the pedon OC density profiles developed for this study, it is possible to create aggregate OC density profiles that represent the mean OC density profiles for Turbic Cryosols and Static Cryosols for Truelove Lowland and Wright Pass (Figures 4.13 and 4.14). Using 90% confidence intervals to quantify uncertainty surrounding these estimates, differences can be identified in the depth distribution of OC in these soils with high depth-resolution.

Static Cryosols at Truelove Lowland have a near-surface (0 to 10 cm) OC density of ~175 g OC m^{-2} cm^{-1} that quickly drops to ~30 g OC m^{-2} cm^{-1} by 20 cm depth. Following this rapid drop, the OC densities of Static Cryosols remain low (15 to 45 g OC m^{-2} cm^{-1}) for the remaining depth of the examined pedons. Turbic Cryosols also start with ~175 g OC m^{-2} cm^{-1} at 0 to 10 cm depth, but instead of a rapid drop it gradually decreases to low ~30 g OC m^{-2} cm^{-1} by 80 cm depth. There is a clear difference in the OC densities of Static Cryosols and Turbic Cryosols between 20 and 45 cm. Throughout this depth range Turbic Cryosols have a higher OC density.

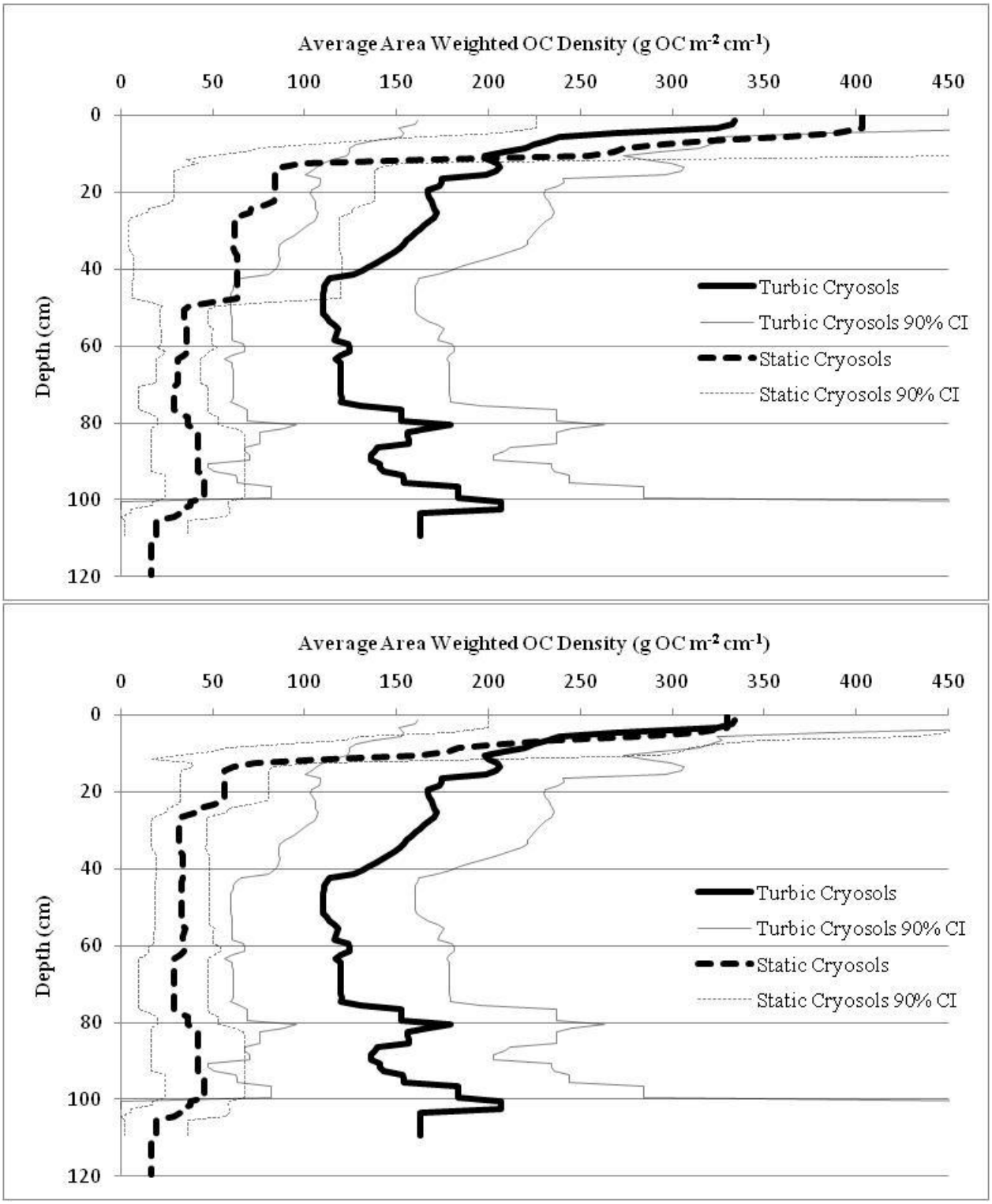

Figure 4.14 Average OC density profiles from Wright Pass with all pedons included (top) and with pedon WPSC14 excluded (bottom). Thin lines mark 90% confidence intervals around the average OC density profiles.

The difference is large near 20 cm (~80 g OC m^{-2} cm^{-1}), and gradually shrinks until it disappears at about 45 cm depth.

Static Cryosols at Wright Pass have a high OC density at 0 to 5 cm (~400 g OC m^{-2} cm^{-1}) which rapidly drops to ~80 g OC m^{-2} cm^{-1} by 15 cm depth, then drops further to low OC density (~35 g OC m^{-2} cm^{-1}) by 50 cm depth. Turbic Cryosols also have a relatively high OC density in the top centimeters (~340 g OC m^{-2} cm^{-1}) which quickly drops to ~175 g OC m^{-2} cm^{-1} by about 15 cm depth, and remains between 110 and 150 g OC m^{-2} cm^{-1} for most of the remainder of the depths examined. However, when pedon WPSC14 is excluded from the average (see section 4.1.2) the Static Cryosol OC density profile changes substantially above 50 cm depth (Figure 4.14). With pedon WPSC14 excluded, the average Static Cryosol OC density profile is now about the same as the Turbic Cryosol OC density in the top centimeters (~340 g OC m^{-2} cm^{-1}) and rapidly drops to less than 50 g OC m^{-2} cm^{-1} by about 25 cm depth. There is no difference between the OC density profiles of Static Cryosols and Turbic Cryosols from 0 to 49 cm depth; however, from 49 to 90 cm depth Turbic Cryosols have a consistently higher mean OC density by ~90 g OC m^{-2} cm^{-1}. When pedon WPSC14 is excluded this difference becomes more evident, and Turbic Cryosols have a higher OC density from 12 to 90 cm by an average of ~100 g OC m^{-2} cm^{-1}.

5. DISCUSSION

5.1. Depth Distribution of Organic Carbon

The OC contents of Turbic Cryosols were greater than Static Cryosols at depths of 20 to 45 cm for Truelove Lowland and 12 to 90 cm for Wright Pass (Figures 4.8 and 4.9). This suggests that either OC inputs are larger or there is greater preservation of OC in Turbic Cryosols, or both. In either case, assuming a similar rooting depth, movement of OC from near the surface to greater depth in Turbic Cryosols is necessary to explain the different depth distributions. This mechanism is generally assumed to be cryoturbation in Turbic Cryosols, but some recent work (Gundelwein et al., 2007; Michaelson et al., 1996; Walker et al., 2008) indicates that transportation of OC in a dissolved state and precipitation upon freezing is also important. Irrespective of the transport mechanism, the movement of OC to deeper in the soil profile observed in this study may have consequences for the climate system. The OC pool deeper in Turbic Cryosols tends to be preserved, as indicated by isotopic, NMR, and radiocarbon dating studies (Gundelwein et al., 2007; Horwath et al., 2008; Kaiser et al., 2007), because cold temperatures slow microbial decomposition (Fang et al., 2005). The data from this study support the assertion that OC deeper in Turbic Cryosols is preserved, as shown by the higher OC content at depth than in Static Cryosols. Moreover, the NMR and C:N data from the TLTC03 pedon at Truelove Lowland show that the OC at depth is not substantially more humified than that near the surface; however, C:N and OAC:AC data from the EPTC15 pedon at Eagle Plains indicate that OC subducted by cryoturbation is substantially more humified and recalcitrant than surface OC. A key feature of the EPTC15 pedon is the relatively high OC density in the frozen soil (Figure 4.9), apparently composed of more recalcitrant material than that encountered in other pedons, indicating that this OC is not only frozen, but will be more difficult to decompose upon thawing. More study is required to determine whether this is a unique property of these pedons

or a larger trend across the regions. There is some evidence that OC continues to decompose at cool, even subzero temperatures; however, C fluxes from frozen soils are small compared to unfrozen soils (~10 to 20 % smaller at -2°C than at 4°C) (Michaelson and Ping, 2003). While deeper OC currently has a slow turnover rate, experimental evidence indicates that expected warming will likely cause decomposition of this deeper OC as soils warm. For example, when increased snow depth caused deeper thaw in Alaskan soils, the age of respired C increased from ~100 yr BP to a range of 1525 to 8300 yr BP (Nowinski et al., 2010).

There are no available estimates of OC contents to 1 m depth for the areas studied to compare with the results of this study. However, the OC contents found in this study are reasonable given existing databases of soil OC for the entire circumpolar permafrost region. Soils examined in this study had OC contents of 5.5 and 4.5 kg OC m^{-2} to a depth of 100 cm for Static Cryosols and Turbic Cryosols at Truelove Lowland, and OC contents of 7.6 and 17.6 kg OC m^{-2} for Static Cryosols and Turbic Cryosols at Wright Pass (Tables 4.1 and 4.3). These are lower than the mean values of 22.6 and 32.2 kg OC m^{-2} for Orthels (Static Cryosols) and Turbels (Turbic Cryosols) in the Northern Circumpolar Permafrost Region, but are well within the ranges of 0.1 to 65 kg OC m^{-2} for Orthels and 1 to 126 kg OC m^{-2} for Turbels (Tarnocai et al., 2009).

5.2. Between Site Differences in Organic Carbon Depth Distribution

The OC contents of Turbic Cryosols and Static Cryosols are different at Truelove Lowland over a smaller depth range than at Wright Pass; that is, the OC profile is generally shallower in Turbic Cryosols at Truelove Lowland than in Turbic Cryosols at Wright Pass (Figures 4.8 and 4.9), indicating that cryoturbation may operate more shallowly at Truelove Lowland than at Wright Pass. This does not appear to be related to active layer depth, as the OC profiles of

several of the Turbic Cryosols at Truelove Lowland terminated a few cm to more than 2 decimeters above the bottom of the active layer. However, this could be related to a textural difference, as soil texture was dominantly sandy loam to loamy sand in Turbic Cryosols of Truelove Lowland, while soil texture was dominantly silt loam at Wright Pass. Previous work has indicated that silty textures are the most conducive to cryoturbation (Walker et al., 2008; Washburn, 1980; Williams and Smith, 1991). It may also be possible that the OC profiles of Turbic Cryosols at Truelove Lowland will deepen with time to become more similar to those of Wright Pass. The Wright Pass soils are all on the western side of the Richardson Mountains, and as such were not overridden by ice during the most recent glaciations (Duk-Rodkin, 1999), so soil formation has been operating here for more than 10,000 years. Recent soil OC modeling for soils north of 60° latitude (Koven et al., 2009) indicates that it may take more than 10,000 years for Turbic Cryosols to reach equilibrium with respect to OC. Truelove Lowland soils included in this study, on the other hand, were covered by a marine transgression until at least 4000 to 5000 years ago (King, 1991), and may not have reached OC equilibrium in that short time.

There may be other implications of the shallower OC profile in Turbic Cryosols at Truelove Lowland than at Wright Pass. For example, one expected consequence of warming is greater vegetation encroachment onto the barren centres of patterned ground features (Walker et al., 2008). This will cause a shallower thaw in many Turbic Cryosols as a consequence of the increased insulative effect of denser vegetation cover (Kade and Walker, 2008). In the case of Wright Pass, this will likely lead to much more OC being incorporated into the frozen soil. In Turbic Cryosols at Truelove Lowland, however, the OC profile is much shallower and it is unlikely that substantial OC will be incorporated into the permafrost in most pedons.

5.3. Decomposition, Recalcitrance, and the Depth Distribution of Organic Carbon

Baldock et al. (1997) indicate that OAC is a preferred substrate for many microbes, and will typically be consumed first during humification. Results of NMR analysis (Figures 4.3, 4.8, and 4.11) from some pedons in this study indicate that there is little difference in the degree of humification of surface OC, as evidenced by high OAC content. At Truelove Lowland, Wright Pass, and Eagle Plains, OAC content for surface organic horizons is ~60%, similar to the ~63% found in some arctic soils by Paré (2011), who concluded that this indicated that OC in these soils in generally more labile (i.e. more readily decomposable) than those in several other ecosystems, including a northern hardwood forest, a spruce forest, and a prairie soil.

Decreasing OAC content and OAC:AC ratios indicate increasing degree of OC humification (Baldock et al., 1997). Similarly, decreasing C:N ratios indicate increasing degree of OC humification as C is preferentially lost during decomposition (Kuhry and Vitt, 1996). The representative earth hummock pedon examined at Eagle Plains (Figure 4.6 and Table 4.5) showed generally decreasing OAC, OAC:AC, and C:N with increasing depth, whereas the representative nonsorted circle with inward curving vertical horizons (Figure 4.3 and Table 4.5) showed nearly constant OAC, OAC:AC, and C:N with increasing depth. This suggests that in the earth hummocks at Eagle Plains more decomposition is taking place at depth or prior to movement than in nonsorted circles with inward curving vertical horizons at Truelove Lowland.

Samples from the frozen earth hummock soil (EP pedon) examined using NMR analysis indicated a lower proportion of OAC (as low as 39%, see Figure 4.11 and Table 4.5) and higher proportion of AC than surface horizons. Similarly, the C:N ratio in the representative earth hummock pedon is lower in the frozen soil than at the surface, indicating that the OC is more humified than that at the surface. This indicates a higher degree of recalcitrance, and a lower

temperature sensitivity of decomposition in this soil (Davidson and Janssens, 2006). This is similar to the result reported by Gundelwein et al. (2007), who found that the OAC signal weakened with increasing depth in soils from the Taimyr Peninsula in Siberia. Based on this finding, warming of this pedon is likely to accelerate decomposition of OC in surface horizons more than in currently frozen horizons, even when thawed.

There are some key differences in the depth distribution of OC qualities in samples examined by NMR spectroscopy. There is little difference in the chemical form of OC in the near surface samples in the examined pedon from Truelove Lowland (TLTC03a in Figure 4.3) and near surface sample in the pedon from Eagle Plains (EPTC15a in Figure 4.11). Plant residues are different at these sites so a direct comparison is not possible, but this similarity suggests a similar degree of humification of this near surface OC. The differences begin as we look deeper into the pedon. The proportions of the different OC categories and C:N ratios in deeper samples from the Truelove Lowland pedon with inward curving vertical horizons (TLTC03b, TLTC03c, and TLTC03d in Figure 4.3; Table 4.5) are similar to the near surface sample, suggesting that humification occurs only slowly after subduction by cryoturbation has occurred. In contrast, the deeper samples from the Eagle Plains pedon with a hummock form (EPTC15b, EPTC15c, and EPTC15d in Figure 4.11; Table 4.6) are similar to each other, but different from the near surface sample. This indicates that the OC in this pedon has been transformed into different chemical forms, perhaps by transport in a dissolved state and precipitation upon freezing, discussed further in the following section.

5.4. Explanatory Power of Cryoturbation Mechanism Models

There is little evidence for diapirism as described in section 2.2.2 in soils examined in this study. No forms resembling diapirs were observed and unstable bulk density profiles were rare,

existing only where the underlying low density layer was in a frozen state with high ice content. Furthermore, the ice-rich permafrost that Swanson et al. (1999) indicate is a probable source of water to create an unstable bulk density profile was observed only in the earth hummock pedons (EPTC15 and EPTC16) and one Static Cryosol where diapirism cannot explain the forms observed. Diapirism is an unlikely process for the genesis of Turbic Cryosols in this study.

The cryohydrostatic model discussed in section 2.2.3 is also an improbable genetic process for cryoturbation forms observed in this thesis. No injection- or extrustion-like features were observed in the field. In this model the last unfrozen area would likely be near the permafrost table rather than near the soil surface, yet cryoturbated horizons were most common near the soil surface, especially at Truelove Lowland.

There is some evidence which suggests that the earth hummock pedons at Eagle Plains may have evolved in a manner similar to that outlined by Walker et al. (2008; see section 2.3). As discussed above, the quality of OC in the Bmyz horizon of EPTC15 (Figures 4.9 and 4.11) indicates that it may have been transported in a dissolved state and precipitated by cryochemical precipitation (Gundelwein et al., 2007; Kowalkowski et al., 1986). The ice-rich character of this horizon suggests that cryosuction in a roughly downward direction creating ice lenses is probable, and the generally high silt and clay content of this pedon supports this line of reasoning. Furthermore, the shape of the permafrost table is similar to that indicated in the Walker et al. (2008) model, allowing some gravity drainage of OC-rich water from the vegetatively-productive margins of the hummock toward the middle of the bowl-shaped permafrost table. While draining, some of this water is likely to be intercepted by cryosuction and drawn towards the permafrost, leaving a continuous horizon of OC-rich mineral material along the bottom margin of the active layer.

While it is difficult to link other specific pedons to a specific cryoturbation mechanism, there are a few features in the TLTC05 pedon that allow some speculation. In the representative pedon with highly mixed horizons (Figures 4.4 and 4.5) the horizons with the greatest amount of mixing, as evidenced by streaked colours, generally had the lowest proportions of sand and the highest proportions of silt. As high silt contents are conducive to cryosuction (Williams and Smith, 1991), this suggests that cryosuction may have played an important part in the genesis of these horizons. Cryosuction is an integral part of the DFH model (Daanen et al., 2007; Peterson and Krantz, 2008), and is also important in the cyrostatic model, suggesting that these mechanisms may have some importance here. There is no obvious explanation in either of these models, however, for the presence of a nonsorted circle and low-OC content horizons in the portions of the pedon that are highest in sand content.

5.5. High Depth-Resolution GIS Methods

The GIS methods used in this study allow determination of the amount of organic carbon for any selected depth range with a high depth-resolution. Ping et al. (2008) note that the location of OC in the soil profile is important for assessing the effect of climate warming on OC, and that surface measurements or whole pedon measurements alone are insufficient for modeling soil C processes where temperature and depth are important controls, such as decomposition. For example, the permafrost soil C POPCARN model (Khvorostyanov et al., 2008) is capable of calculating decomposition in vertically-resolved pools of soil C and Koven (2009) has successfully linked mixing by cryoturbation to this model; however, this model is poorly constrained due to a general lack of vertically-resolved observations of OC in permafrost soils. The GIS-based high depth-resolution techniques employed in this study are a promising step towards improving our knowledge of the depth distribution of OC in the soil profile. This

technique allows determination of precise depth ranges above threshold values of OC density, with potential for improved determination of the depth of OC mixing and better directed sampling regimes to determine OC content of Turbic Cryosols. It is probable that much of the data in existing databases such as the Northern Circumpolar Soil Carbon Database (Tarnocai et al., 2009) could easily be reanalyzed with no additional field sampling required.

6. CONCLUSIONS

There is a greater amount of OC in Turbic Cryosols than Static Cryosols from 20 to 45 cm depth at Truelove Lowland, Devon Island, Nunavut, and from 12 to 90 cm depth near Wright Pass, Yukon. Given the cooler temperatures and less favourable conditions for decomposition at depth in permafrost soils, this reaffirms existing assertions (Bockheim, 2007; Horwath et al., 2008; Hugelius et al., 2010; Kaiser et al., 2007; Koven et al., 2009; Michaelson et al., 2008) that Turbic Cryosols contain significant amounts of OC that have been preserved by translocation to greater depth. This subducted OC is of great importance to the climate system. Furthermore, the results of this study define a clear depth range where translocation of OC is most important at each study site. An examination of this difference at other sites in the Arctic will elucidate the depth ranges where this translocation is most important in other arctic regions.

The categories of Turbic Cryosols identified in this study may correspond to different varieties of cryoturbation. The cryoturbation model described by Walker et al. (2008) involving cracking and DFH is a probable explanation for the genesis of earth hummocks observed at Eagle Plains, the DFH and cryostatic models are possible explanations for other pedons observed at Truelove Lowland especially those with highly mixed horizons, and the diapirism and cryohydrostatic models are unlikely explanations for the development of Turbic Cryosols in this study. The pedons within the same category tended to have similar OC profiles. There are no published quantitative data indicating a relationship between the depth distribution of OC and different types of cryoturbation, but the results of this study suggest that there may be a link, as pedons with similar subsurface morphology had similar OC density profiles. Most noteworthy is the difference in the shape of the OC profiles for the category including the earth hummock pedons from the other categories containing nonsorted circles, which show a high OC density to the base of the active layer and into the upper permafrost. This evidence may mean that earth

hummocks transport OC to depth more efficiently than the varieties of nonsorted circles examined in this study. Further study is required to determine whether or not different cryoturbation processes lead to significantly different OC depth distributions.

Previous work has indicated that arctic OC is relatively labile near the soil surface (Gundelwein et al., 2007; Paré, 2011), and more humified and recalcitrant deeper in the soil (Gundelwein et al., 2007). Based on exploratory OC quality results, near-surface OC was labile compared to temperate ecosystems, similar to previous results. However, OC quality at greater depth in two Turbic Cryosol pedons with different cryoturbation forms, and from different arctic ecosystems, was not similar. A high arctic nonsorted circle with vertically-oriented OC-rich horizons that curve inwards towards the pedon centre had remarkably similar OC lability and degree of humification at depth and near the soil surface, while a low arctic earth hummock had significantly transformed OC in deep horizons that could be the result of transport in a soluble state. It is proposed that there may be substantial variation in deep OC characteristics in different parts of the Arctic, potentially leading to substantial variation in responses to climate warming; organic matter studies in other portions of the Arctic are required to test this hypothesis.

The high depth-resolution GIS method employed in this study improves our ability to vertically discretize OC distribution in Turbic Cryosols. This method can quantitatively determine the depth range of a pedon that is above or below a threshold value for OC density or clearly define depth ranges where differences or similarities are present between different classes of pedons. There is great potential for this method to be applied to existing databases of OC density in the northern permafrost regions to provide better estimates of OC distribution with depth in cryoturbated soils and, therefore, better baseline estimates of OC stocks, resulting in

more realistic predictions by OC models in the future. Moreover, this technique can be applied to properties other than OC in the future, allowing study of the relationship between depth and many soil properties in highly mixed Turbic Cryosols.

7. REFERENCES

ACIA. 2004. Impacts of a warming Arctic: Climate impact assessment. Cambridge University Press, Cambridge, UK.

Baldock, J.A., J.M. Oades, A.G. Waters, X. Peng, A.M. Vassallo, and M.A. Wilson. 1992. Aspects of the chemical structure of soil organic materials as revealed by solid-state ^{13}C NMR spectroscopy. Biogeochemistry 16:1-42.

Baldock, J.A., J.M. Oades, P.N. Nelson, T.M. Skene, A. Golchin, and P. Clarke. 1997. Assessing the extent of decomposition of natural organic materials using solid-state C-13 NMR spectroscopy. Australian Journal of Soil Research 35:1061-1083.

Ballantyne, C.K. 1996. Formation of Miniature Sorted Patterns by Shallow Ground Freezing: a Field Experiment. Permafrost and Periglacial Processes 7:409-424.

Bertran, P., G. Allenet, T. Ge, F. Naughton, P. Poirier, and M.F.S. Goni. 2009. Coversand and Pleistocene palaeosols in the Landes region, southwestern France. Journal of Quaternary Science 24:259-269.

Blake, G.R., and K.H. Hartge. 1986. Bulk Density, p. 363-375, *In* A. Klute, ed. Methods of Soil Analysis, Part 1. Physical and Mineralogical Methods, 2nd ed. Soil Science Society of America, Inc., Madison, Wisconsin.

Bliss, L.C. 1977. Introduction, p. 1-11, *In* L. C. Bliss, ed. Truelove Lowland, Devon Island, Canada: a high arctic ecosystem. University of Alberta Press, Edmonton.

Bockheim, J.G. 2007. Importance of cryoturbation in redistributing organic carbon in permafrost-affected soils. Soil Science Society of America Journal 71:1335-1342.

Bockheim, J.G., and C. Tarnocai. 1998. Recognition of cryoturbation for classifying permafrost-affected soils. Geoderma 81:281-293.

Brady, N.C., and R.R. Weil. 2002. The nature and properties of soils. 13 ed. Prentice Hall, Upper Saddle River, NJ.

Brouchkov, A. 2000. Salt and water transfer in frozen soils induced by gradients of temperature and salt content. Permafrost and Periglacial Processes 11:153-160.

Brown, R.J.E. 1977. Permafrost investigations on Truelove Lowland, *In* L. C. Bliss, ed. Truelove Lowland, Devon Island, Canada: a high arctic ecosystem. University of Alberta Press, Edmonton.

Burn, C.R. 1993. Permafrost, p. 16-19, *In* C. Tarnocai, et al., eds. International Tour of Permafrost Affected Soils: The Yukon and Northwest Territories of Canada. Centre for Land and Biological Resources Research, Ottawa.

Courtin, G.M., and C.L. Labine. 1977. Microclimatological studies on Truelove Lowland, p. 73-106, *In* L. C. Bliss, ed. Treulove Lowland, Devon Island, Canada: a high arctic ecosystem. University of Alberta Press, Edmonton, AB.

Daanen, R.P., M. Debasmita, and H. Epstein. 2007. Active-Layer Hydrology in Nonsorted Circle Ecosystems of the Arctic Tundra. Vadose Zone Journal 6:694-704.

Daanen, R.P., D. Misra, H. Epstein, D. Walker, and V. Romanovsky. 2008. Simulating nonsorted circle development in arctic tundra ecosystems. Journal of Geophysical Research-Biogeosciences 113:10.

Davidson, E.A., and I.A. Janssens. 2006. Temperature sensitivity of soil carbon decomposition and feedbacks to climate change. Nature 440:165-173.

Duk-Rodkin, A. 1993. Site 5, KM 30: Richardson Mountains and glacial limit, p. 66, *In* C. Tarnocai, et al., eds. International Tour of Permafrost Affected Soils: The Yukon and

Northwest Territories of Canada. Centre for Land and Biological Resources Research, Ottawa.

Duk-Rodkin, A. 1999. Glacial limits map of Yukon Territory. Geological Survey of Canada Open File 3288 and Yukon Geological Survey Open File 1999-2.

Environment Canada. 2011. Canada's National Climate Archive [Online] http://www.climate.weatheroffice.gc.ca (verified July 11, 2011).

ESRI. 2008. ArcGIS. Release ArcMap 9.3. ESRI.

Euskirchen, E.S., A.D. McGuire, F.S. Chapin, S. Yi, and C.C. Thompson. 2009. Changes in vegetation in northern Alaska under scenarios of climate change, 2003-2100: implications for climate feedbacks. Ecological Applications 19:1022-1043.

Fang, C.M., P. Smith, J.B. Moncrieff, and J.U. Smith. 2005. Similar response of labile and resistant soil organic matter pools to changes in temperature. Nature 433:57-59.

French, H.M. 2007. The Periglacial Environment. 3rd ed. John Wiley & Sons, West Sussex, England.

Gordey, S.P., and A.J. Makepeace. 1999. Yukon bedrock geology *in* Yukon digital geology, S.P. Gordey and A.J. Makepeace (compilers); Geological Survey of Canada open file D3826. Exploration and Geological Services Division, Yukon Region, Indian and Northern Affairs Canada, Whitehorse, Yukon.

Gundelwein, A., T. Muller-Lupp, M. Sommerkorn, E.T.K. Haupt, E.M. Pfeiffer, and H. Wiechmann. 2007. Carbon in tundra soils in the Lake Labaz region of arctic Siberia. European Journal of Soil Science 58:1164-1174.

Hao, X., B.C. Ball, J.L.B. Culley, M.R. Carter, and G.W. Parkin. 2008. Soil density and porosity, p. 743-759, *In* M. R. Carter and E. G. Gregorich, eds. Soil sampling and methods of analysis. CRC Press, Boca Raton, FL.

Harris, C., J. Murton, and M.C.R. Davies. 2000. Soft-sediment deformation during thawing of ice-rich frozen soils: results of scaled centrifuge modelling experiments. Sedimentology 47:687-700.

Helfrich, M., B. Ludwig, P. Buurman, and H. Flessa. 2006. Effect of land use of the composition of soil organic matter in density and aggregate fractions as revealed by solid-state ^{13}C NMR spectroscopy. Geoderma 136:331-341.

Hendershot, W.H., and H. Lalande. 2008. Soil reaction and exchangeable acidity, p. 173-178, *In* M. R. Carter and E. G. Gregorich, eds. Soil sampling and methods of analysis. CRC Press, Boca Raton, FL.

Horwath, J.L., R.S. Sletten, B. Hagedorn, and B. Hallet. 2008. Spatial and temporal distribution of soil organic carbon in nonsorted striped patterned ground of the High Arctic. Journal of Geophysical Research-Biogeosciences 113:16.

Hugelius, G., P. Kuhry, C. Tarnocai, and T. Virtanen. 2010. Soil Organic Carbon Pools in a Periglacial Landscape: a Case Study from the Central Canadian Arctic. Permafrost and Periglacial Processes 21:16-29.

Hughes, O.L., A. Duk-Rodkin, and L. Jackson. 1993. Physiography and Geology, p. 2-7, *In* C. Tarnocai, et al., eds. International Tour of Permafrost Affected Soils: The Yukon and Northwest Territories of Canada. Centre for Land and Biological Resources Research, Ottawa.

IPCC. 2007. Climate Change 2007: The Physical Science Basis. Contribution of Working Group I to the Fourth Assessment Report of the Intergovernmental Panel on Climate Change, Cambridge, United Kingdom and New York, NY, USA.

Kade, A., and D.A. Walker. 2008. Experimental alteration of vegetation on nonsorted circles: Effects on cryogenic activity and implications for climate change in the arctic. Arctic Antarctic and Alpine Research 40:96-103.

Kade, A., V.E. Romanovsky, and D.A. Walker. 2006. The N-factor of nonsorted circles along a climate gradient in Arctic Alaska. Permafrost and Periglacial Processes 17:279-289.

Kaiser, C., H. Meyer, C. Biasi, O. Rusalimova, P. Barsukov, and A. Richter. 2007. Conservation of soil organic matter through cryoturbation in arctic soils in Siberia. Journal of Geophysical Research-Biogeosciences 112.

Khvorostyanov, D.V., G. Krinner, P. Ciais, M. Heimann, and S.A. Zimov. 2008. Vulnerability of permafrost carbon to global warming. Part I: model description and role of heat generated by organic matter decomposition. Tellus Series B-Chemical and Physical Meteorology 60:250-264.

Kimble, J.M., C. Tarnocai, C.L. Ping, R. Ahrens, C.A.S. Smith, J. Moore, and W. Lynn. 1993. Determination of the Amount of Carbon in Highly Cryoturbated Soils, pp. 277-291, *In* D. A. Gilichinski, (ed.) International Conference on Cryopedology. Russian Academy of Sciences, Pushchino, Russia.

King, R.H. 1969. Periglaciation on Devon Island, N.W.T. PhD thesis, University of Saskatchewan, Saskatoon, Canada.

King, R.H. 1991. Paleolimnology of a Polar Oasis, Truelove Lowland, Devon Island, NWT, Canada. Hydrobiologia 214:317-325.

Koven, C., P. Friedlingstein, P. Ciais, D. Khvorostyanov, G. Krinner, and C. Tarnocai. 2009. On the formation of high-latitude soil carbon stocks: Effects of cryoturbation and insulation by organic matter in a land surface model. Geophysical Research Letters 36:5.

Kowalkowski, A., Z. Brogowski, and J. Kocon. 1986. Properties of cryogenic horizons in the profile of rusty soil. Quaternary Studies in Poland 7:25-37.

Kroetsch, D., and C. Wang. 2008. Particle Size Distribution, p. 713-725, *In* M. R. Carter and E. G. Gregorich, eds. Soil Sampling and Methods of Analysis. CRC Press, Boca Raton, FL.

Krupicka, J. 1977. Bedrock geology of the Truelove River area, p. 63-72, *In* L. C. Bliss, ed. Truelove Lowland, Devon Island, Canada: a high arctic ecosystem. University of Alberta Press, Edmonton.

Kuhry, P., and D.H. Vitt. 1996. Fossil carbon/nitrogen ratios as a measure of peat decomposition. Ecology 77:271-275.

Lev, A., and R.H. King. 1999. Spatial variation of soil development in a high Arctic soil landscape: Truelove Lowland, Devon Island, Nunavut, Canada. Permafrost and Periglacial Processes 10:289-307.

Lewkowicz, A.G. 2007. Dynamics of active-layer detachment failures, Fosheim Peninsula, Ellesmere Island, Nunavut, Canada. Permafrost and Periglacial Processes 18:89-103.

Mackay, J.R. 1980. The Origin of Hummocks, Western Arctic Coast, Canada. Canadian Journal of Earth Sciences 17:996-1006.

Mackay, J.R. 1988. Ice wedge growth in newly aggrading permafrost, Western Arctic Coast, Canada, pp. 809-814, *In* K. Senneset, (ed.) Fifth International Conference on Permafrost, Vol. 1. Tapir Publishers, Trondheim, Norway.

Mackay, J.R., and C.R. Burn. 2002. The first 20 years (1978-1979 to 1998-1999) of ice-wedge growth at the Illisarvik experimental drained lake site, western Arctic coast, Canada. Canadian Journal of Earth Sciences 39:95-111.

Mathers, N.J., X.A. Mao, Z.H. Xu, P.G. Saffigna, S.J. Berners-Price, and M.C.S. Perera. 2000. Recent advances in the application of ^{13}C and ^{15}N NMR spectroscopy to soil organic matter studies. Australian Journal of Soil Research 38:769-787.

Matsuoka, N. 2011. Climate and material controls on periglacial soil processes: Toward improving periglacial climate indicators. Quaternary Research 75:356-365.

Matthews, J.A., M. Seppala, and P.Q. Dresser. 2005. Holocene solifluction, climate variation and fire in a subarctic landscape at Pippokangas, Finnish Lapland, based on radiocarbon-dated buried charcoal. Journal of Quaternary Science 20:533-548.

Michaelson, G.J., and C.L. Ping. 2003. Soil organic carbon and CO2 respiration at subzero temperature in soils of Arctic Alaska. Journal of Geophysical Research-Atmospheres 108:10.

Michaelson, G.J., C.L. Ping, and J.M. Kimble. 1996. Carbon storage and distribution in tundra soils of Arctic Alaska, USA. Arctic and Alpine Research 28:414-424.

Michaelson, G.J., C.L. Ping, H. Epstein, J.M. Kimble, and D.A. Walker. 2008. Soils and frost boil ecosystems across the North American Arctic Transect. Journal of Geophysical Research-Biogeosciences 113:11.

Murton, J.B., and H.M. French. 1993. Thaw modification of frost-fissure wedges, Richards Island, Pleistocene Mackenzie Delta, Western Arctic, Canada. Journal of Quaternary Science 8:185-196.

Nicolsky, D.J., V.E. Romanovsky, G.S. Tipenko, and D.A. Walker. 2008. Modeling biogeophysical interactions in nonsorted circles in the Low Arctic. Journal of Geophysical Research-Biogeosciences 113:17.

Norris, A.W. 1997. Devonian, p. 163-200, *In* D. K. Norris, ed. The geology, mineral and hydrocarbon potential of northern Yukon Territory and northwestern District of Mackenzie. Geological Survey of Canada Bulletin 422, Ottawa.

Nowinski, N.S., L. Taneva, S.E. Trumbore, and J.M. Welker. 2010. Decomposition of old organic matter as a result of deeper active layers in a snow depth manipulation experiment. Oecologia 163:785-792.

Paré, M. 2011. PhD Thesis, University of Saskatchewan, Saskatoon.

Parfitt, R.L., and R.H. Newman. 2000. ^{13}C NMR study of pine needle decomposition. Plant Soil 219:273-278.

Peterson, R.A. 2008. Stability analysis and numerical simulation of differential frost heave. Mathematical Geosciences 40:277-298.

Peterson, R.A., and W.B. Krantz. 2008. Differential frost heave model for patterned ground formation: Corroboration with observations along a North American arctic transect. Journal of Geophysical Research-Biogeosciences 113:17.

Ping, C.L., G.J. Michaelson, M.T. Jorgenson, J.M. Kimble, H. Epstein, V.E. Romanovsky, and D.A. Walker. 2008. High stocks of soil organic carbon in the North American Arctic region. Nature Geoscience 1:615-619.

Preston, C.M., J.R. Nault, and J.A. Trofymow. 2009. Chemical changes during 6 years of decomposition of 11 litters in some Canadian forest sites. Part 2. ^{13}C abundance, solid-state ^{13}C NMR spectroscopy and the meaning of lignin. Ecosystems 12:1078-1102.

Quideau, S.A., M.A. Anderson, R.C. Graham, O.A. Chadwick, and S.E. Trumbore. 2000. Soil organic matter processes: characterization by ^{13}C NMR and ^{14}C measurements. Forest Ecology and Management 138:19-27.

Ryden, B.E. 1977. Hydrology of Truelove Lowland, p. 107-136, *In* L. C. Bliss, ed. Truelove Lowland, Devon Island, Canada: a high arctic ecosystem. University of Alberta Press, Edmonton.

Schnitzer, M. 2001. The *in situ* analysis of organic matter in soils. Canadian Journal of Soil Science 81:249-254.

Shilts, W.W. 1978. Nature and genesis of mudboils, Central Keewatin, Canada. Canadian Journal of Earth Sciences 15:1053-1068.

Shur, Y. 1988. The Upper Horizon of Permafrost Soils, pp. 867-871, *In* K. Senneset, (ed.) Fifth International Conference on Permafrost, Vol. 1. Tapir Publishers, Trondheim, Norway.

Shur, Y., and C.L. Ping. 2003. The driving force of frost boils and hummocks formation. Eos Transactions American Geophysical Union 84:Fall Meeting Supplement, Abstract C21B-0823.

Shur, Y., C.L. Ping, and D.A. Walker. 2005. Comprehensive model of frost boils and earth hummocks formation 2nd European Conference on Permafrost, 12-16 June, Potsdam, Germany.

Skjemstad, J.O., and J.A. Baldock. 2008. Total and Organic Carbon, *In* M. R. Carter and E. G. Gregorich, eds. Soil Sampling and Methods of Analysis, 2 ed. CRC Press, Boca Raton, FL.

Smith, C.A.S., J.C. Meikle, and C.F. Roots, (eds.) 2004. Ecoregions of the Yukon Territory: biophysical properties of Yukon landscapes. Agriculture and Agri-Food Canada, PARC Technical Bulletin No. 04-01, Summerland, British Columbia.

Smith, C.A.S., A.D. Tomlin, J.J. Miller, L.V. Moore, M.J. Tynen, and K.A. Coates. 1990. Large enchytraeid (Annelida: Oligochaeta) worms and associated fauna from unglaciated soils of the northern Yukon, Canada. Geoderma 47:17-32.

Soil Classification Working Group. 1998. The Canadian System of Soil Classification. Agriculture and Agri-food Canada Publication 1646 (Revised).

Superson, J., P. Gebica, and T. Brzezinska-Wojcik. 2010. The Origin of Deformation Structures in Periglacial Fluvial Sediments of the Wislok Valley, Southeast Poland. Permafrost and Periglacial Processes 21:301-314.

Swanson, D.K., C.L. Ping, and G.J. Michaelson. 1999. Diapirism in soils due to thaw of ice-rich material near the permafrost table. Permafrost and Periglacial Processes 10:349-367.

Tarnocai, C. 1993. Sampling Frozen Soils, p. 755-765, *In* M. R. Carter, ed. Soil Sampling and Methods of Analysis, 1st ed. Lewis Publishers, Boca Raton, FL.

Tarnocai, C. 1999. The effect of climate warming on the carbon balance of Cryosols in Canada. Permafrost and Periglacial Processes 10:251-263.

Tarnocai, C. 2004. Cryosols of Arctic Canada, p. 95-118, *In* J. M. Kimble, ed. Cryosols: Permafrost-Affected Soils. Springer, Berlin.

Tarnocai, C., and S.C. Zoltai. 1978. Earth Hummocks of the Canadian Arctic and Subarctic. Arctic and Alpine Research 10:581-594.

Tarnocai, C., J.G. Canadell, E.A.G. Schuur, P. Kuhry, G. Mazhitova, and S. Zimov. 2009. Soil organic carbon pools in the northern circumpolar permafrost region. Global Biogeochemical Cycles 23:11.

Van Vliet-Lanoe, B. 1991. Differential Frost Heave, Load Casting and Convection: Converging Mechanisms; a Discussion of the Origin of Cryoturbations. Permafrost and Periglacial Processes 2:123-139.

Vandenberghe, J. 1988. Cryoturbations, p. 179-198, *In* M. J. Clark, ed. Advances in Periglacial Geomorphology. J. Wiley, Chichester, New York.

Vandenberghe, J. 1992. Cryoturbations: A Sediment Structural Analysis. Permafrost and Periglacial Processes 3:343-352.

Walker, A.S., and T.W. Peters. 1977. Soils of Truelove Lowland and Plateau, p. 31-62, *In* L. C. Bliss, ed. Truelove Lowland, Devon Island, Canada: a high arctic ecosystem. University of Alberta Press, Edmonton.

Walker, D.A., H.E. Epstein, W.A. Gould, A.M. Kelley, A.N. Kade, J.A. Knudson, W.B. Krantz, G. Michaelson, R.A. Peterson, C.L. Ping, M.K. Raynolds, V.E. Romanovsky, and Y. Shur. 2004. Frost-boil ecosystems: Complex interactions between landforms, soils, vegetation and climate. Permafrost and Periglacial Processes 15:171-188.

Walker, D.A., H.E. Epstein, V.E. Romanovsky, C.L. Ping, G.J. Michaelson, R.P. Daanen, Y. Shur, R.A. Peterson, W.B. Krantz, M.K. Raynolds, W.A. Gould, G. Gonzalez, D.J. Nicolsky, C.M. Vonlanthen, A.N. Kade, P. Kuss, A.M. Kelley, C.A. Munger, C. Tarnocai, N.V. Matveyeva, and F.J.A. Daniels. 2008. Arctic patterned-ground ecosystems: A synthesis of field studies and models along a North American Arctic Transect. Journal of Geophysical Research-Biogeosciences 113:17.

Washburn, A.L. 1956. Classification of Patterned Ground and Review of Suggested Origins. Geological Society of America Bulletin 67:823-865.

Washburn, A.L. 1980. Geocryology John Wiley & Sons, New York.

Williams, P.J., and M.W. Smith. 1991. The Frozen Earth: Fundamentals of Geocryology Press Syndicate of the University of Cambridge, Cambridge, UK.

Yukon Ecoregions Working Group. 2004. British-Richardson Mountains, p. 111-120, *In* C. A. S. Smith, et al., eds. Ecoregions of the Yukon Territory: biophysical properties of Yukon landscapes. Agriculture and Agri-Food Canada, PARC Technical Bulletin No. 04-01, Summerland, British Columbia.

Zimov, S.A., E.A.G. Schuur, and F.S. Chapin. 2006. Permafrost and the global carbon budget. Science 312:1612-1613.

8. APPENDIX

8.1 Supplementary Organic Carbon Density Diagrams and Profiles

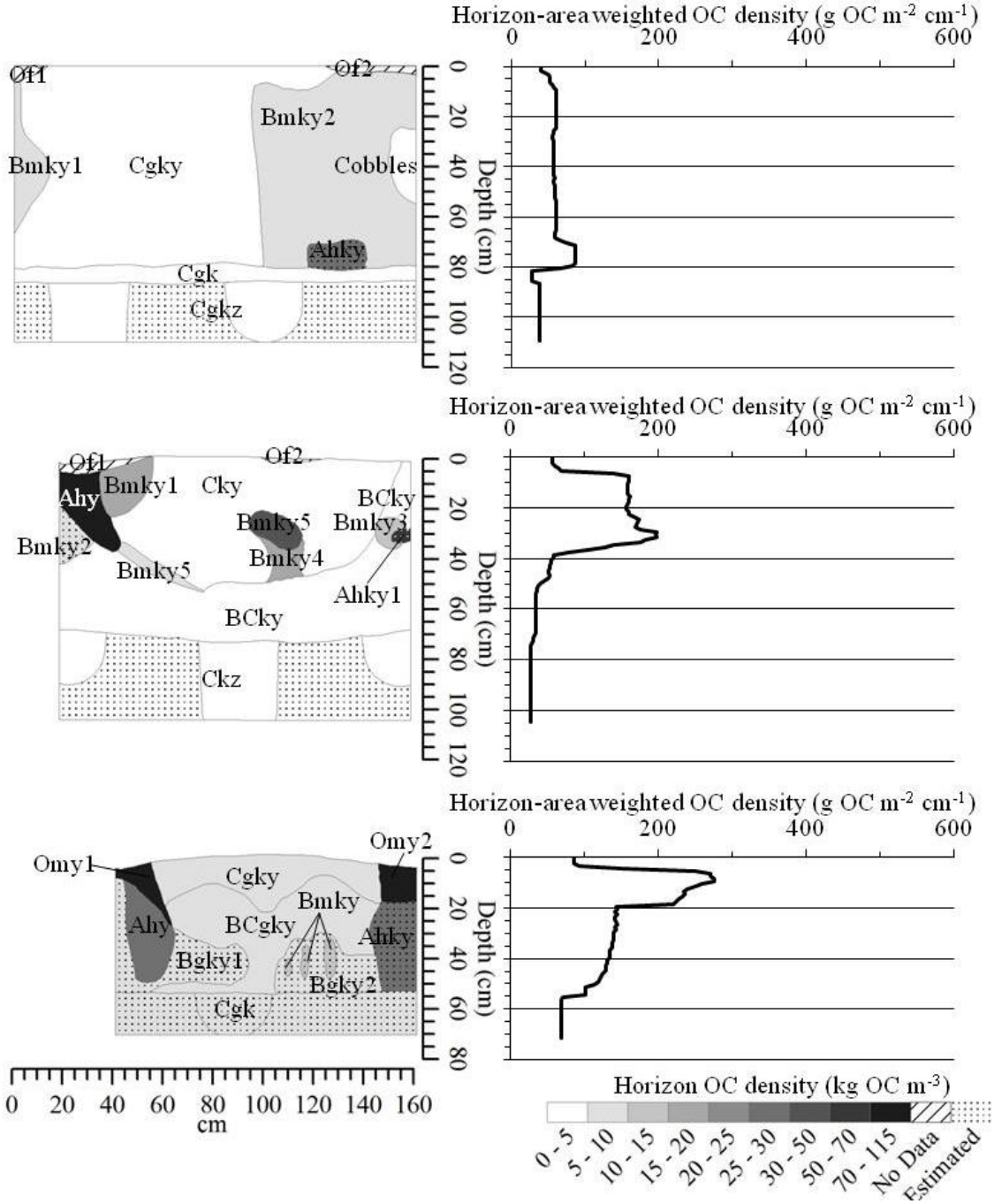

Figure 8.1 OC density diagrams (left) and profiles (right) for the TLTC01 pedon at Truelove Lowland (top), the TLTC02 pedon at Truelove Lowland (middle), and the TLTC04 pedon at Truelove Lowland (bottom). The profiles are created by aggregating the OC densities in the diagrams in 1 cm depth increments. Horizon OC densities are weighted by horizon areas falling within the depth increments when performing the aggregation calculations.

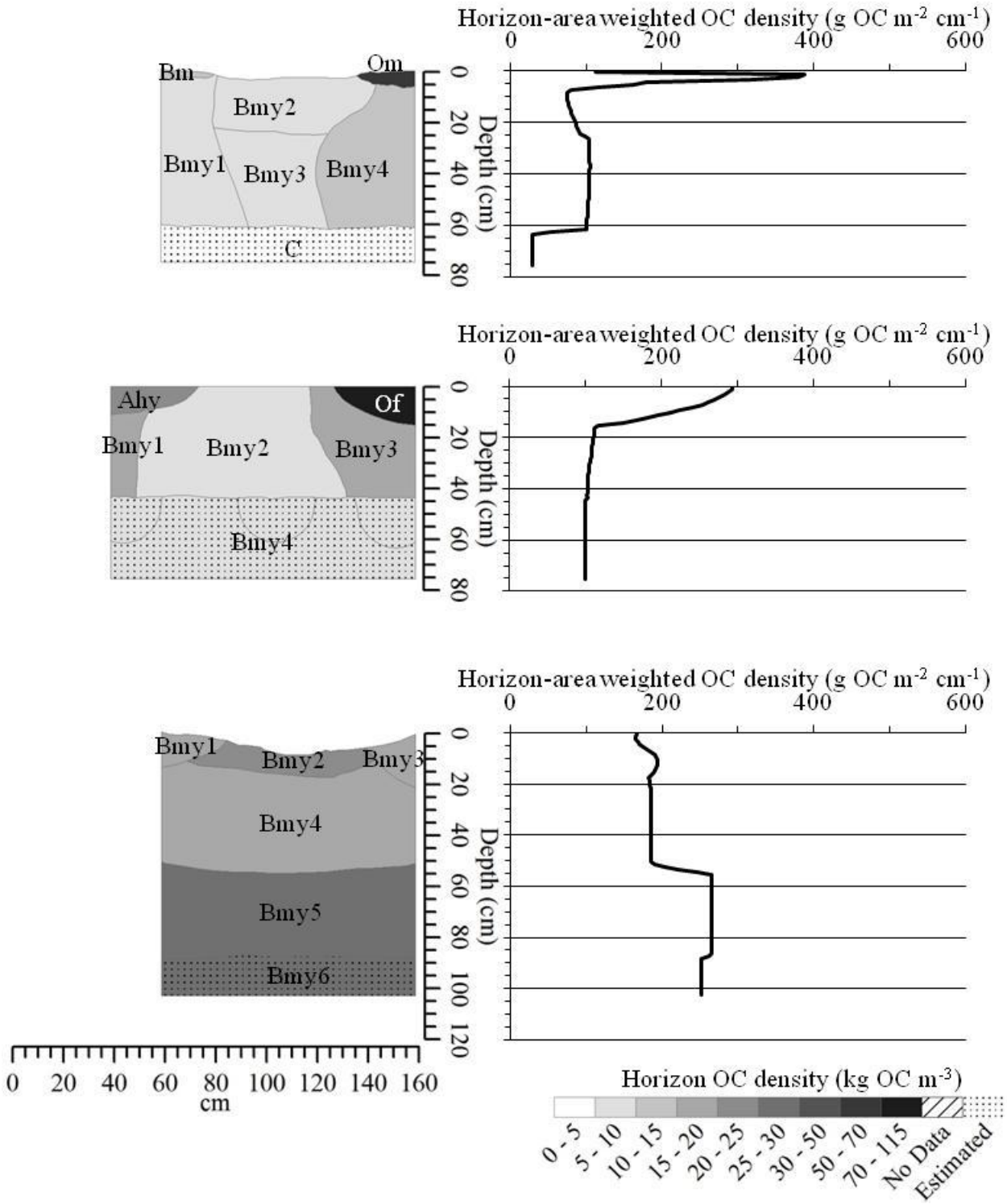

Figure 8.2 OC density diagrams (left) and profiles (right) for the WPTC06 pedon at Wright Pass (top), the WPTC07 pedon at Wright Pass (middle), and the WPTC08 pedon at Wright Pass (bottom). The profiles are created by aggregating the OC densities in the diagrams in 1 cm depth increments. Horizon OC densities are weighted by horizon areas falling within the depth increment when performing the aggregation calculations.

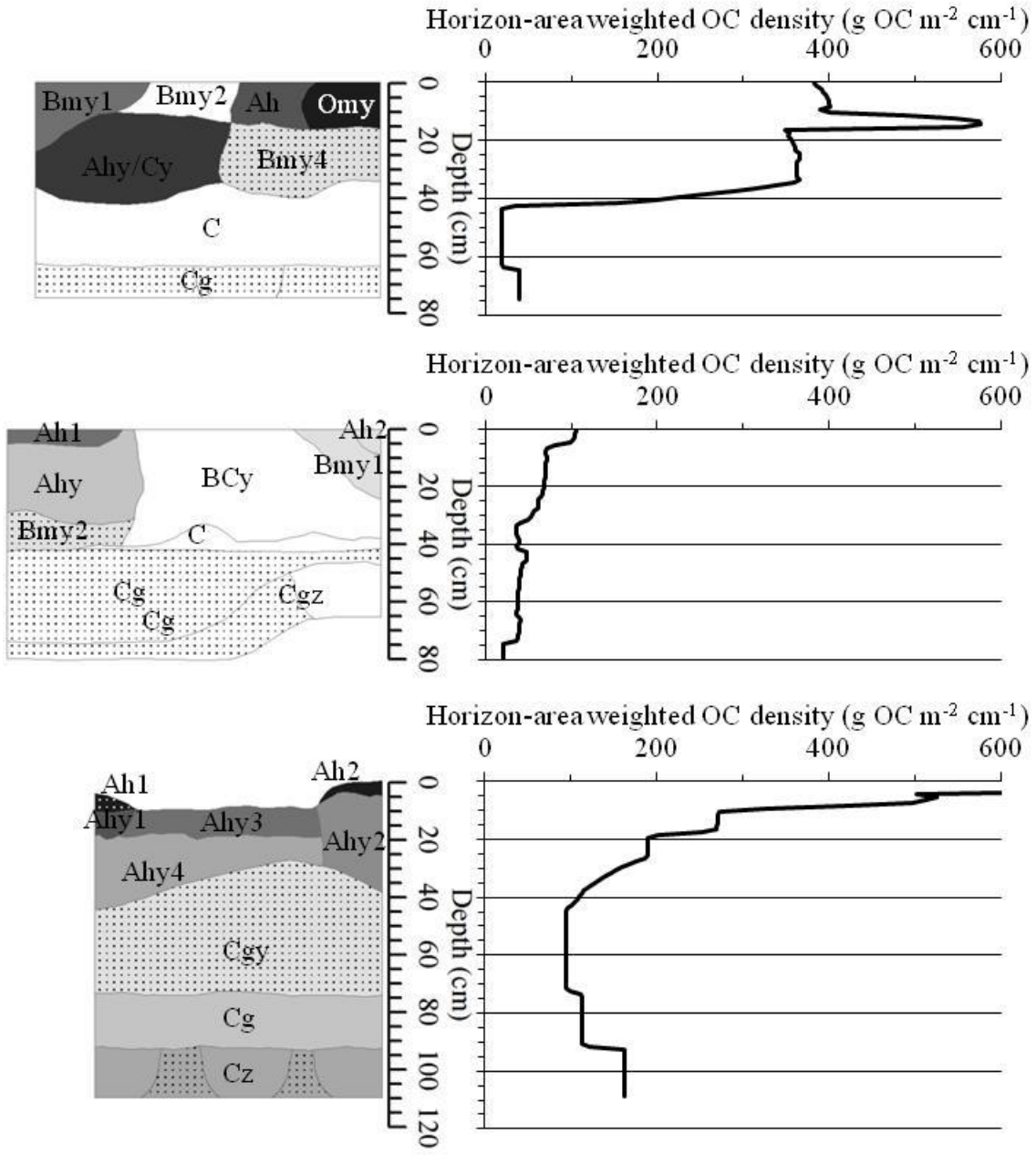

Figure 8.3 OC density diagrams (left) and profiles (right) for the WPTC09 pedon at Wright Pass (top), the WPTC10 pedon at Wright Pass (middle), and the WPTC12 pedon at Wright Pass (bottom). The profiles are created by aggregating the OC densities in the diagrams in 1 cm depth increments. Horizon OC densities are weighted by horizon areas falling within the depth increment when performing the aggregation calculations.

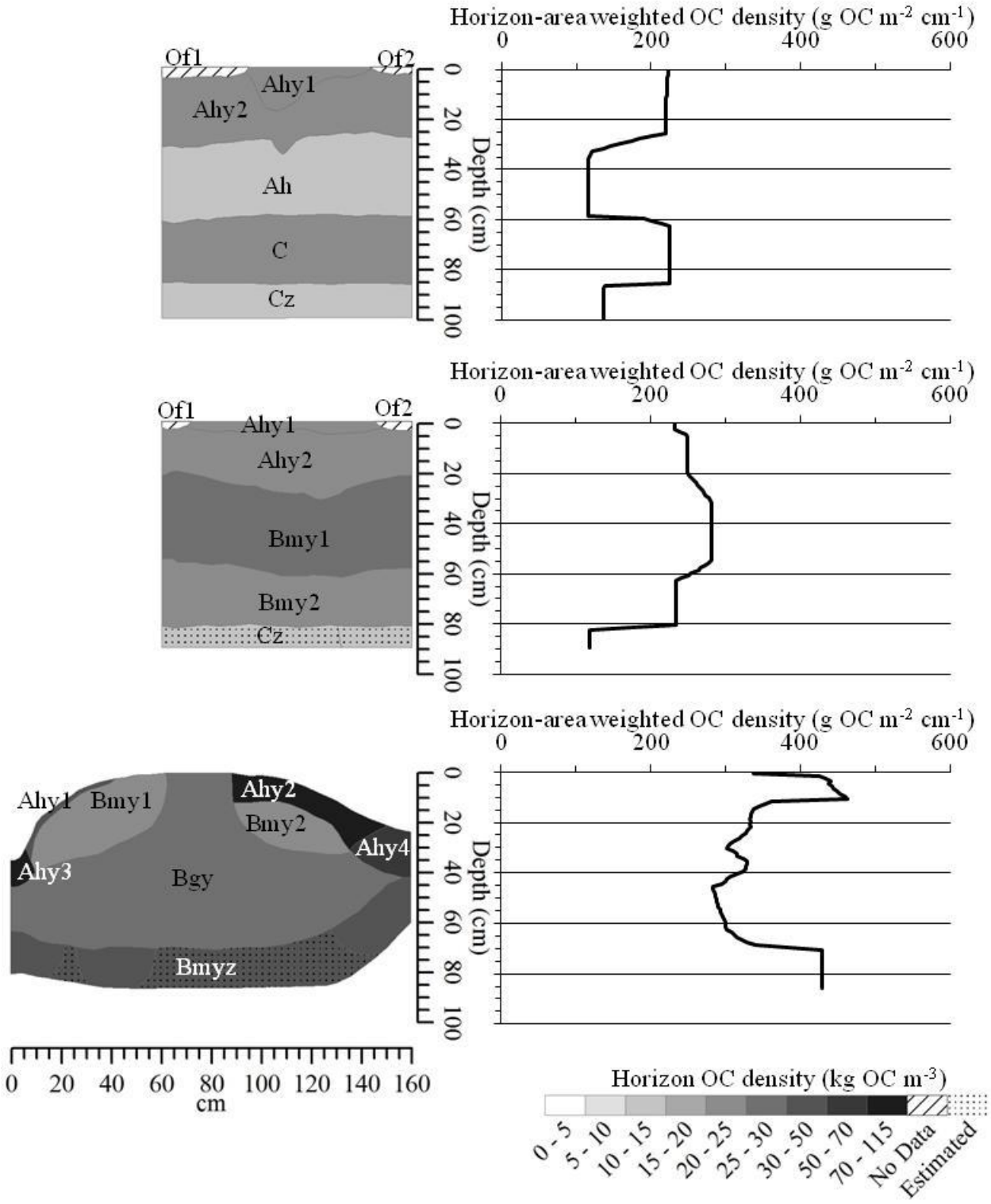

Figure 8.4 OC density diagrams (left) and profiles (right) for the WPTC13 pedon at Wright Pass (top), the WPTC14 pedon at Wright Pass (middle), and the EPTC16 pedon at Eagle Plains (bottom). The profiles are created by aggregating the OC densities in the diagrams in 1 cm depth increments. Horizon OC densities are weighted by horizon areas falling within the depth increment when performing the aggregation calculations.

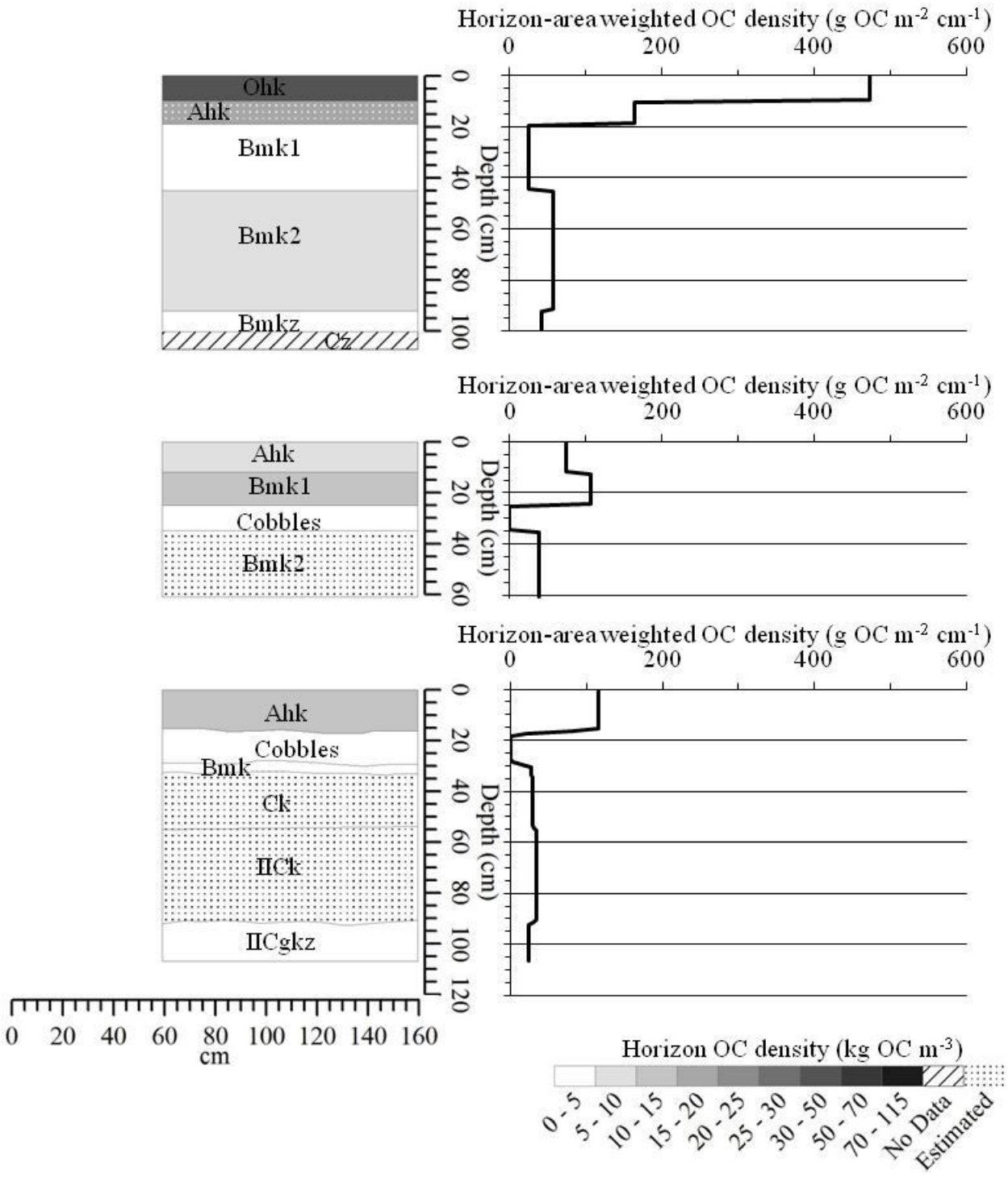

Figure 8.5 OC density diagrams (left) and profiles (right) for the TLSC01 pedon at Truelove Lowland (top), the TLSC02 pedon at Truelove Lowland (middle), and the TLSC03 pedon at Truelove Lowland (bottom). The profiles are created by aggregating the OC densities in the diagrams in 1 cm depth increments. Horizon OC densities are weighted by horizon areas falling within the depth increment when performing the aggregation calculations.

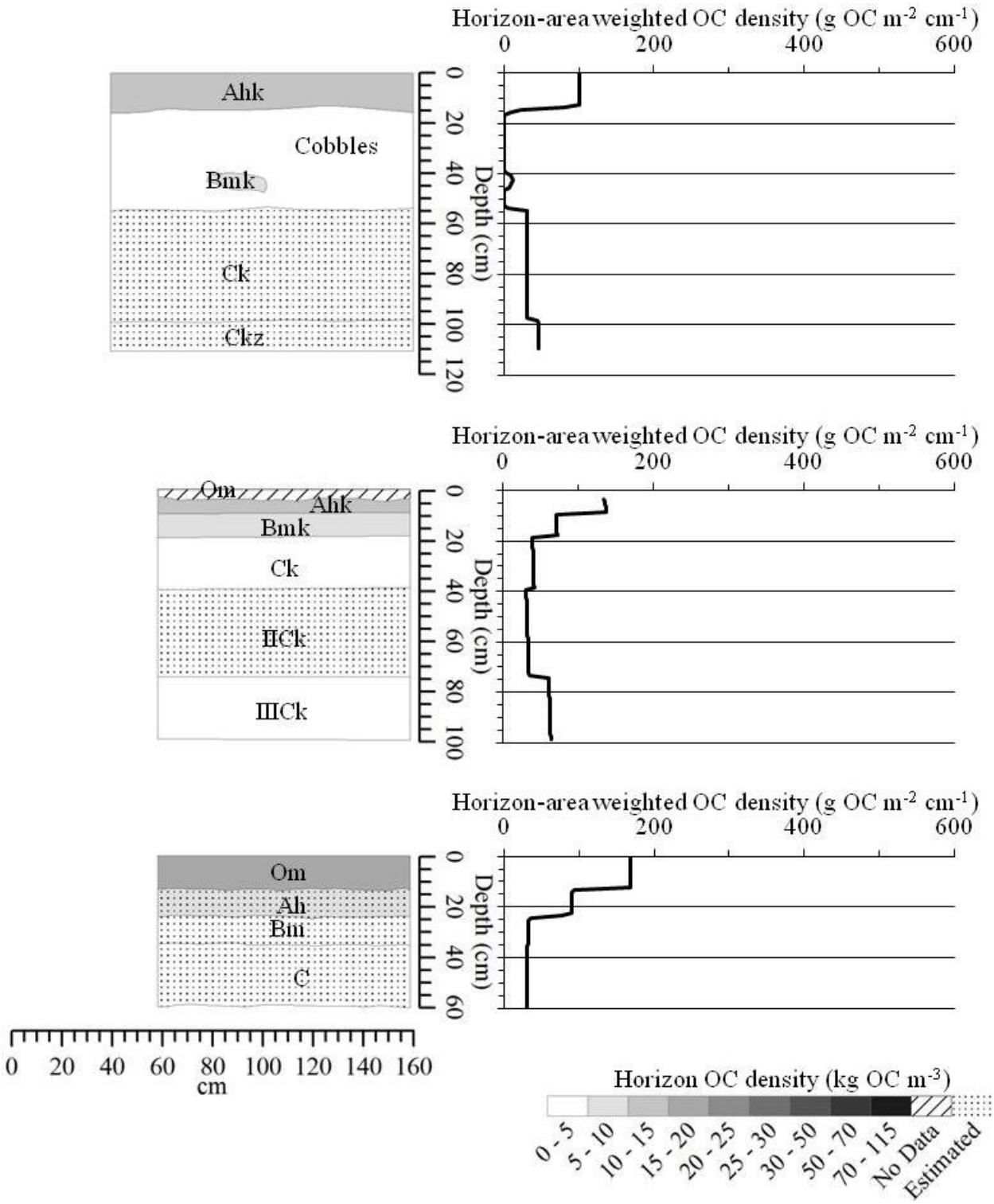

Figure 8.6 OC density diagrams (left) and profiles (right) for the TLSC04 pedon at Truelove Lowland (top), the TLSC05 pedon at Truelove Lowland (middle), and the WPSC06 pedon at Wright Pass (bottom). The profiles are created by aggregating the OC densities in the diagrams in 1 cm depth increments. Horizon OC densities are weighted by horizon areas falling within the depth increment when performing the aggregation calculations.

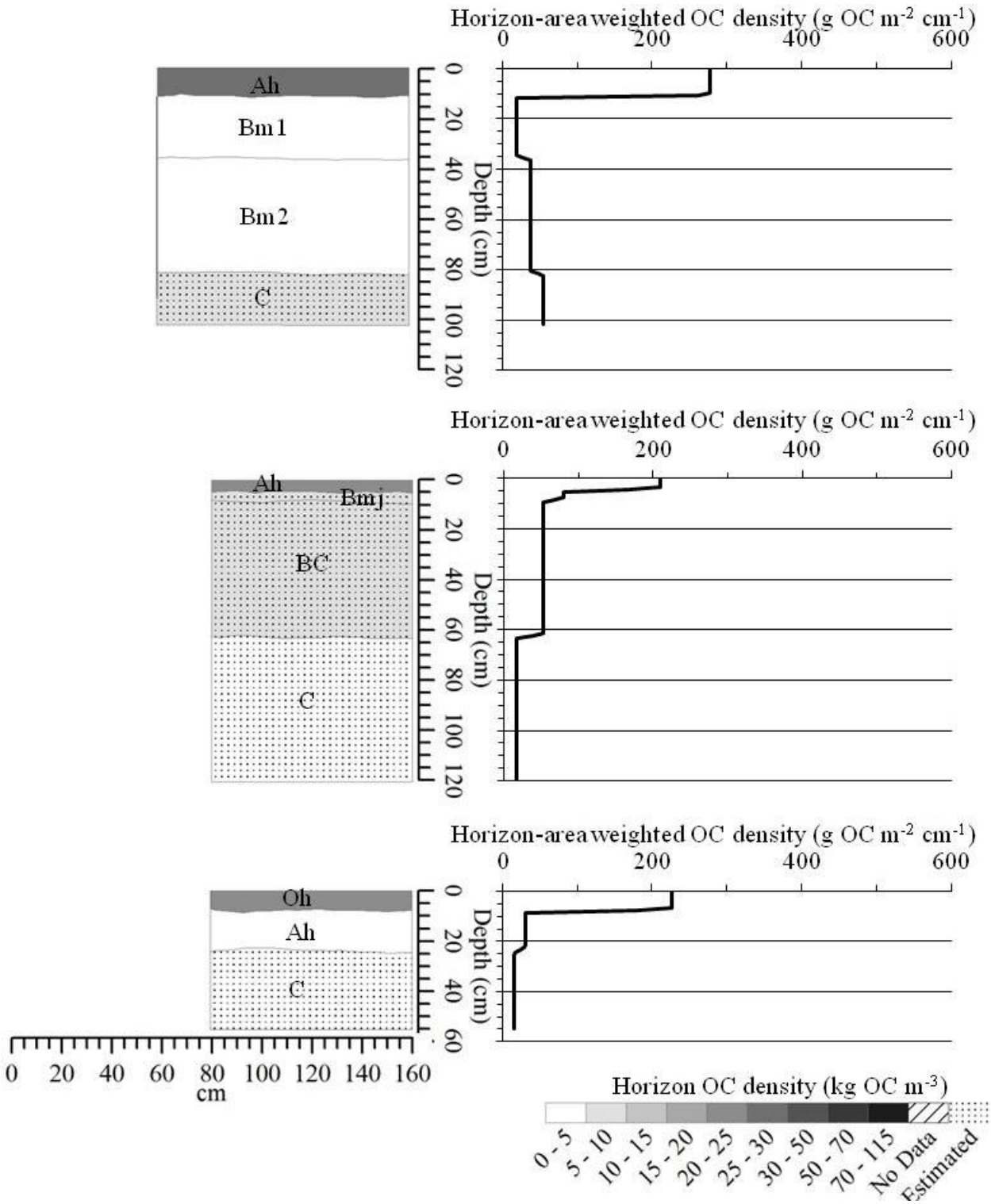

Figure 8.7 OC density diagrams (left) and profiles (right) for the WPSC08 pedon at Wright Pass (top), the WPSC09 pedon at Wright Pass (middle), and the WPSC 12 pedon at Wright Pass (bottom). The profiles are created by aggregating the OC densities in the diagrams in 1 cm depth increments. Horizon OC densities are weighted by horizon areas falling within the depth increment when performing the aggregation calculations.

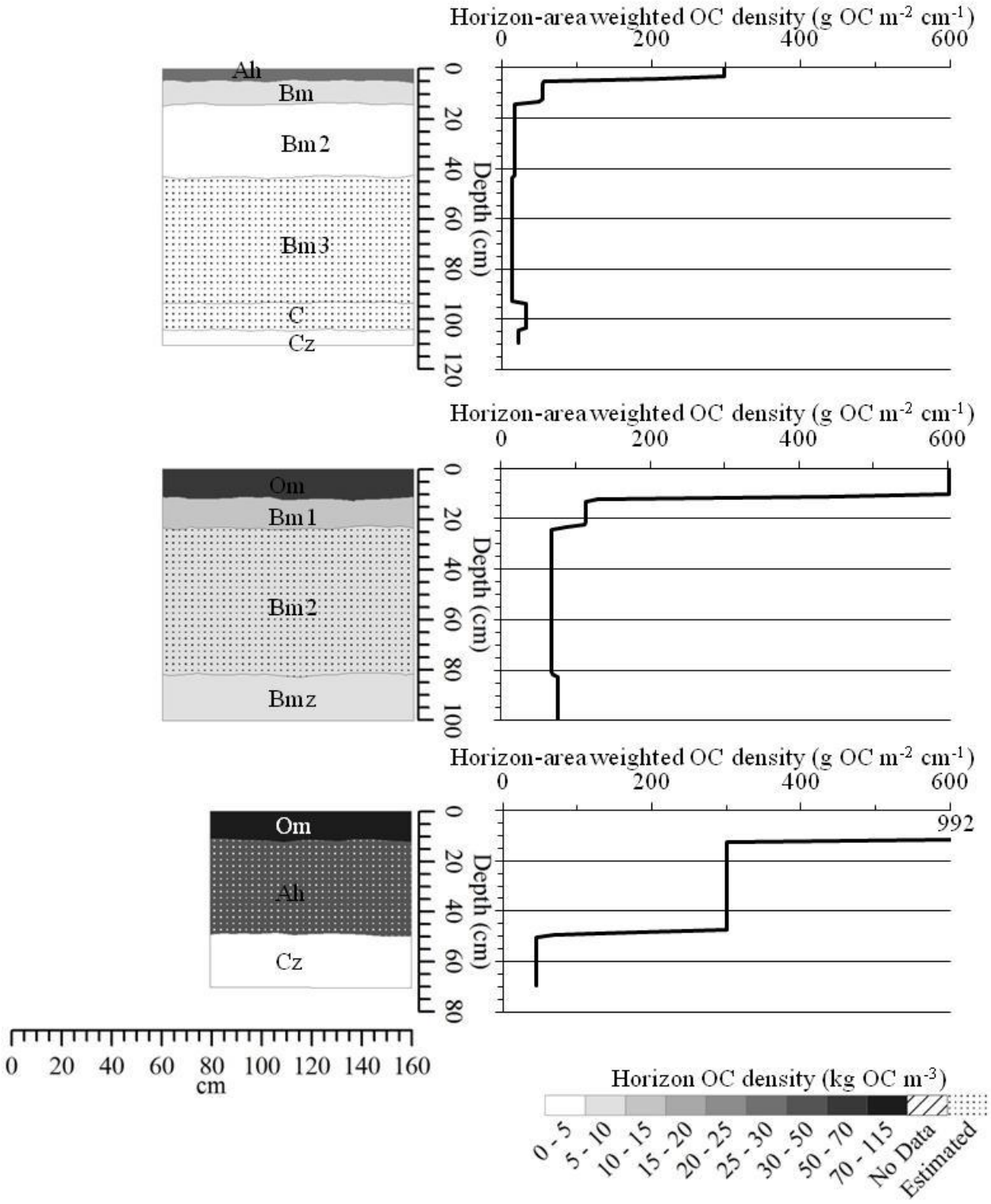

Figure 8.8 OC density diagrams (left) and profiles (right) for the WPSC10 pedon at Wright Pass (top), the WPSC11 pedon at Wright Pass (middle), and the WPSC14 pedon at Wright Pass (bottom). The profiles are created by aggregating the OC densities in the diagrams in 1 cm depth increments. Horizon OC densities are weighted by horizon areas falling within the depth increment when performing the aggregation calculations.

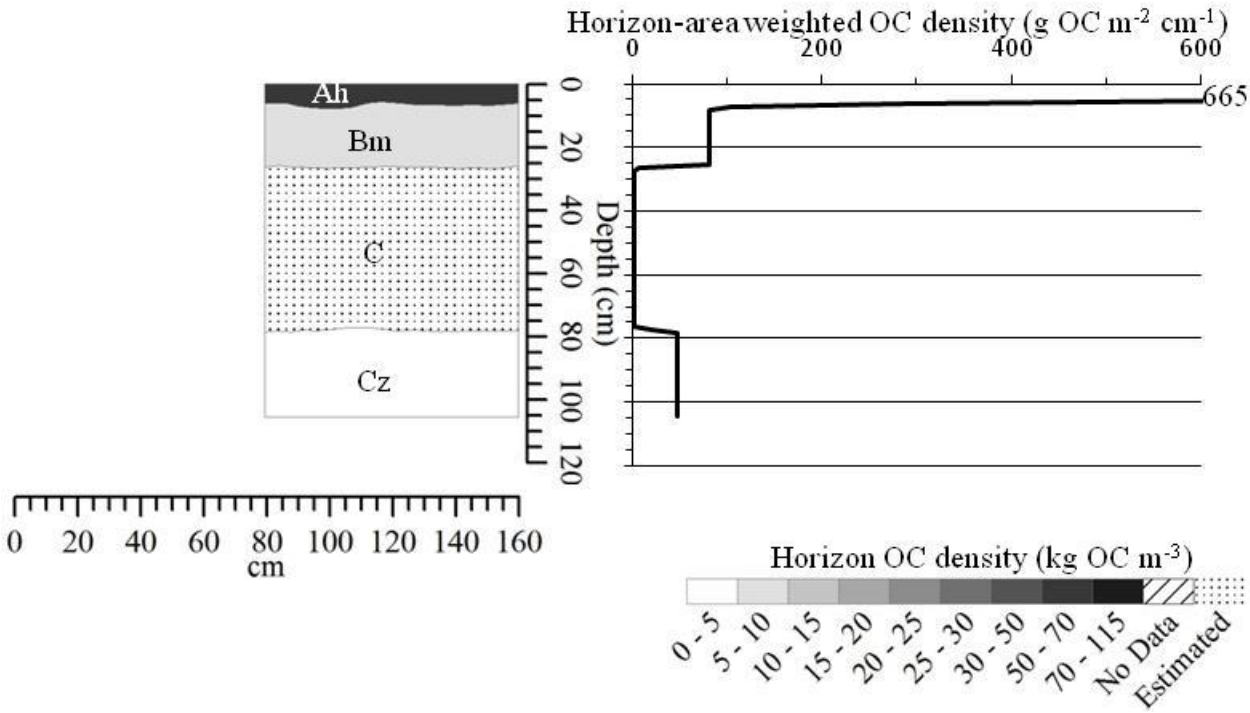

Figure 8.9 OC density diagram (left) and profile (right) for the WPSC13 pedon at Wright Pass. The profile is created by aggregating the OC densities in the diagram in 1 cm depth increments. Horizon OC densities are weighted by horizon areas falling within the depth increment when performing the aggregation calculation.

8.2 Supplementary Organic Carbon Mass Data by Cumulative and Discrete Depth Increments

Table 8.1 Pedon OC masses from cumulative depth increments at Truelove Lowland

Depth (cm)	Organic Carbon Mass (kg OC m^{-2})									
	Static Cryosol Pedons					Turbic Cryosol Pedons				
	TLSC01	TLSC02	TLSC03	TLSC04	TLSC05	TLTC01	TLTC02	TLSC03	TLTC04	TLTC05
0 - 25	6.4	2.3	1.9	1.2	1.7	0.9	2.4	3.9	3.9	3.4
0 - 50	7.2	2.8	2.5	1.2	2.6	1.8	4.3	6.5	6.6	4.3
0 - 75	8.6	-	3.3	1.8	3.5	2.8	4.9	8.1	-	-
0 - 100	10.0	-	4.1	2.4	-	3.5	5.4	-	-	-

Table 8.2 Pedon OC masses from discrete depth increments at Truelove Lowland

Depth (cm)	Organic Carbon Mass (kg OC m^{-2})									
	Static Cryosol Pedons					Turbic Cryosol Pedons				
	TLSC01	TLSC02	TLSC03	TLSC04	TLSC05	TLTC01	TLTC02	TLTC03	TLSC04	TLSC05
0 - 25	6.4	2.3	1.9	1.2	1.7	0.9	2.4	3.9	3.9	3.4
25 - 50	0.8	0.6	0.6	<0.1	0.9	0.9	1.9	2.6	2.8	0.9
50 - 75	1.5	-	0.8	0.5	0.9	1.0	0.6	1.6	-	-
75 - 100	1.3	-	0.8	0.7	-	0.7	0.5	-	-	-

Table 8.3 Pedon OC masses from cumulative depth increments at Wright Pass

Depth (cm)	Organic Carbon Mass (kg OC m^{-2})																	
	Static Cryosol Pedons									Turbic Cryosol Pedons								
	WPSC01	WPSC02	WPSC03	WPSC04	WPSC05	WPSC06	WPSC07	WPSC08	WPSC09	WPTC01	WPTC02	WPTC03	WPTC04	WPTC05	WPTC06	WPTC07	WPTC08	WPTC09
0 - 25	3.2	3.3	3.3	2.7	2.1	8.5	2.8	7.2	19.3	2.4	3.9	3.8	8.6	1.5	1.2	5.3	5.1	6.1
0 - 50	4.0	4.8	4.0	4.3	2.5	10.2	3.3	7.4	28.2	5.0	6.1	8.4	13.2	2.3	2.4	8.6	8.5	13.0
0 - 75	-	6.1	5.0	5.4	2.8	11.8	-	7.4	-	6.6	8.1	14.8	13.8	3.0	3.7	11.1	13.0	19.3
0 - 100	-	-	6.2	5.9	3.3	13.7	-	8.8	-	-	-	21.2	-	-	-	14.3	17.4	-

Table 8.4 Pedon OC masses from discrete depth increments at Wright Pass

Depth (cm)	Organic Carbon Mass (kg OC m^{-2})																	
	Static Cryosol Pedons									Turbic Cryosol Pedons								
	WPSC01	WPSC02	WPSC03	WPSC04	WPSC05	WPSC06	WPSC07	WPSC08	WPSC09	WPTC01	WPTC02	WPTC03	WPTC04	WPTC05	WPTC06	WPTC07	WPTC08	WPTC09
0 - 25	3.2	3.3	3.3	2.7	2.1	8.5	2.8	7.2	19.3	2.4	3.9	3.8	8.6	1.5	1.2	5.3	5.1	6.1
25 - 50	0.8	1.5	0.7	1.6	0.4	1.7	0.5	0.2	9.0	2.6	2.1	4.6	4.6	0.9	1.2	3.3	3.3	7.0
50 - 75	-	1.2	0.9	1.1	0.3	1.7	-	0.1	-	1.6	2.1	6.3	0.6	0.7	1.3	2.4	4.6	6.3
75 - 100	-	-	1.3	0.5	0.5	1.8	-	1.4	-	-	-	6.5	-	-	-	3.2	4.4	-